UC Berkeley
UC Berkeley Electronic Theses and Dissertations

Title
The Role of Lipid Droplets in Cellular Energy Homeostasis and Interorganelle Communication

Permalink
https://escholarship.org/uc/item/657318qg

Author
Nguyen, Truc B.

Publication Date
2019

Peer reviewed|Thesis/dissertation

The Role of Lipid Droplets in Cellular Energy Homeostasis
and Interorganelle Communication

By

Truc B. Nguyen

A dissertation submitted in partial satisfaction of the

requirements for the degree of

Doctor of Philosophy

in

Metabolic Biology

in the

Graduate Division

of the

University of California, Berkeley

Committee in charge:

Professor James A. Olzmann, Chair
Professor Daniel K. Nomura
Professor Roberto Zoncu

Spring 2019

ABSTRACT

The Role of Lipid Droplets in Cellular Energy Homeostasis
and Interorganelle Communication

By

Truc B. Nguyen

Doctor of Philosophy in Metabolic Biology

University of California, Berkeley

Professor James A. Olzmann, Chair

Lipid droplets (LDs) are ubiquitous organelles that play a critical role in lipid homeostasis by regulating the storage and mobilization of fatty acids[1-3]. When nutrient supplies are limited, the fatty acids stored in LDs are transferred to the mitochondria for the generation of energy[1-3]. As starvation persists however, autophagy is triggered to degrade and recycle damaged organelles[4-5]. Autophagy releases FAs into the cytosol to replenishing LDs with new FAs, increasing LD abundance[4-5]. Interestingly, the autophagy-dependent LDs cluster in close proximity to mitochondria, forming membrane contact sites (MCSs)[6-8]. MCSs are areas of close apposition between the membranes of two organelles mediated by tethering forces that arise from protein-protein interaction[8]. However, the identity of a LD-mitochondrial tethering complex and the functional importance of the LD-mitochondrial contacts in FA transfer and energy homeostasis are unknown.

In chapter one, we observed an increase in LD abundance during prolonged nutrient deprivation. Starvation-induced LDs are not required for fatty acid delivery to mitochondria, but instead LDs sequester fatty acids that are released during autophagy to prevent lipotoxic dysregulation of mitochondrial function. In chapter two, we established an inducible heterodimer tethering system to temporally and spatially regulate LD-mitochondrial contact to study the functional importance of the interorganelle contact. Finally, in chapter three we employed proximity-labeling proteomics to identify protein tethers that mediate the close positioning of LDs and mitochondria. Together, our studies advance our understanding of organelle communication in the maintenance of lipid and energy homeostasis.

DEDICATION

I am grateful to have an amazing support system throughout graduate school. I would like to thank my mentors, colleagues, friends, and family for their support, both intellectually and emotionally.

First and foremost, I would like to thank my mentor, Dr. James Olzmann for believing and seeing something in me from the very beginning. Your enthusiasm in research was the reason I came to UC Berkeley, and joining your lab was one of the best decisions I made during graduate school. Thank you for being understanding, supportive, and never giving up on me. Thank you for all the intellectual discussions, for pushing me forward and reminding me to "hang-in there" when things got too difficult. You are truly an amazing scientist, mentor, and friend. I have never met a professor who genuinely cares for their students' success and well-being as much as you had for me during graduate school. I only hope to live up to your expectations and be half the scientist that you are today.

To Drs. Daniel Nomura and Roberto Zoncu: Thank you for your support and guidance over the last few years. Thank you for having confidence in my abilities, and serving on my qualification and dissertation committees. I appreciate our collaborations, and I look forward to working together again in the near future.

To all my labmates and fellow graduate students, former and present: I could not have asked for better colleagues and friends throughout graduate school. Thank you to Clark Peterson for always making me smile and laugh, and for reminding me that there is more to life outside of lab. I will miss your random comments, silly dance, weird and crazy personality. Thank you to Melissa Roberts for all your emotional support the last few years, and for being an awesome baymate.

A special appreciation to Milton To for being there for me since the start and bearing witness to every single step of graduate school. I will miss our lunch dates where we exchanged gossips, complaints, and insults to each other. I will miss your famous one-liners, including "did you try turning it off and on again," and "it's probably fine." Thank you for being my financial advisor, life coach, and close friend. Thank you for spending the time sharing your words of "wisdom" even when you knew I would ignore them. More importantly, thank you for trusting and believing in me even when I doubted my decisions and myself as a scientist. I am glad you are a part of my life, for sharing a birthday with me, and for being the annoying little brother I never had.

To my family – parents, sisters, and brothers-in-law: Your unwavering support, guidance, and advice helped me be the person I am today. Thank you to Tram Nguyen, Tuyen Nguyen, and Hung Pham for urging me to make decisions that were best for me, and encouraging me to fight for my goals. Also, thank you Tuyen for reading and editing my papers.

Finally, to my husband and best-friend, Thao Le: Thank you for your unconditional love, patience, and for listening to all my stories and complaints. No one could deal with my craziness the way you did the last few years. Thank you for taking care of me, and making sure I remember to eat

and sleep. Thank you for driving me to conferences, and lab at random hours in the mornings and evenings to make sure I arrived safely. More importantly, thank you for being an incredible father to our daughter, Annabelle Le, and for picking up the slack whenever I was too tired or busy with graduate school. I am lucky to have you in my life, for your support, and your willingness to embark on any journey I lay out before us.

TABLE OF CONTENTS

LIST OF FIGURES AND TABLES

ACKNOWLEDGEMENTS

INTRODUCTION

Lipid droplets (LDs) are ubiquitous organelles that store neutral lipids (e.g. triacylglycerols and steryl esters)[1-3]. LDs are not a passive sink storing intracellular fatty acids (FAs) as previously believed. Rather, LDs are highly regulated, metabolically active organelles with a wide range of functions. LDs are important for protecting cells from lipotoxicity due to the buildup of excess lipids, such as fatty acids, toxic glycerolipids, and sterols in cell membranes[9-11]. Furthermore, FAs release from LDs though lipolysis or lipophagy (i.e. autophagic digestion of LDs) can be used for energy homeostasis, phospholipid biosynthesis, and lipid signaling molecules[11-15]. Not surprisingly, disrupting lipid storage and utilization have been linked to a variety of neurodegenerative and metabolic diseases, such as atherosclerosis, obesity, and type II diabetes[16]. Thus, a better understanding of LD function and its communication with other organelles will provide novel targets for intervention and prevention of cellular lipotoxicity and lipid-related diseases.

Previous studies identified roles for autophagy in lipid metabolism that may be tissue or condition specific. One particular study demonstrated an upregulation of autophagy during an acute starvation in mouse embryonic fibroblast (MEF) cells that results in FA release from phospholipids within organelle membranes[7]. Surprisingly, these FAs are not directly utilized for mitochondrial β-oxidation but are repackaged into new pools of LDs at the ER membrane[7]. In chapter one, we investigate the nutrient-sensing pathway that regulates autophagy-dependent LD biogenesis and we examine the function of the newly formed LDs.

Organelles can form membrane contact sites (MCSs), which are sites of close organelle membrane apposition that facilitate the efficient exchange of materials[8]. Not surprisingly, LDs form extensive contacts with numerous organelles, including endoplasmic reticulum (ER), Golgi, nucleus, peroxisomes, and mitochondria[17-18]. However, the functions of the LDs at these MCSs are not clearly understood. In chapter two, we developed an inducible heterodimer tethering system to spatially and temporally regulate LD-mitochondrial interaction. This system is a useful tool to study LD functions and the role of interorganelle communication in lipid metabolism.

Currently, it remains to be established what mechanisms underlie the close positioning of LDs and mitochondria. Several proteins have been reported to have a role in LD-mitochondrial contact site formation[19-20]. The most well-studied effector of the LD-mitochondrial interaction is perilipin 5 (PLIN5)[20]. However, it remains to be determined whether PLIN5 directly acts as a LD-mitochondrial tether, or interacts with another mitochondrial protein. In chapter three, we employ a proximity-labeling proteomics to identify protein complexes required for LD-mitochondrial tethering.

CHAPTER ONE

DGAT1-Dependent Lipid Droplet Biogenesis Protects
Mitochondrial Function during Starvation-Induced Autophagy

Introduction

Throughout evolution, organisms have developed mechanisms to monitor and respond to fluctuations in nutrient abundance[21-22]. During prolonged periods of nutrient deprivation, cells initiate global programs to coordinately alter their metabolism, shifting from a reliance on glycolysis to fatty acid (FA) breakdown via mitochondrial β-oxidation for energy[23]. FAs are stored as triacylglycerol (TAG) in lipid droplets (LDs), which are endoplasmic reticulum (ER)-derived organelles that consist of a core of neutral lipids (e.g. TAG and cholesterol esters) encircled by a phospholipid monolayer**Error! Bookmark not defined.**[-3]. LDs serve as dynamic hubs of cellular lipid metabolism, sequestering excess FAs to prevent lipotoxicity[9-13] and providing an "on demand" source of FAs for energy[7, 24-25]. LD-associated neutral lipases (e.g. adipose triglyceride lipase [ATGL]) respond to the metabolic state of the cell and rapidly liberate FAs from the stored TAG for transfer to mitochondria[7, 26].

Under conditions of prolonged starvation, macro-autophagy (herein referred to as autophagy) is upregulated to recycle cellular components and provide constituents for essential processes[4-5]. Autophagy involves a suite of specialized proteins that mediate the biogenesis of the autophagosome, a double-membrane organelle that engulfs portions of the cytoplasm and fuses with the lysosome to enable the degradation of the sequestered cytoplasmic contents**Error! Bookmark not defined.,Error! Bookmark not defined.**. The initiation of autophagy is regulated by numerous signaling pathways that respond to alterations in the levels of nutrients, growth factors, chemokines, and stress[4-5]. Although there are now many examples of selective autophagic degradation, autophagy triggered by nutrient deprivation is relatively nonselective in its delivery of portions of cytoplasm to the lysosome[4-5]. An exception are mitochondria, which undergo morphological changes that prevent their autophagic degradation[27-28].

The breakdown of LDs and the upregulation of autophagy serve complementary roles in supplying the cell with substrates for the generation of energy. Surprisingly, despite evidence of lipolytic degradation of LDs, the abundance of LDs increased in mouse embryonic fibroblasts (MEFs) during combined starvation for amino acids, glucose, and serum in Hank's balanced salt solution (HBSS)[7]. The increase in LDs was not observed in MEFs lacking the critical autophagy gene ATG5, leading to a model in which the autophagic breakdown of membranous organelles releases lipids that are re-esterified and packaged into new LDs[7]. However, the molecular pathways that regulate the biogenesis of autophagy-dependent LDs and the functional explanation for why cells expend energy to package FAs into new LDs during an energy crisis are unknown.

Here, we demonstrate that diacylglycerol acyltransferase 1 (DGAT1) channels FAs into LDs downstream of mTORC1-regulated autophagy during nutrient deprivation. Under these conditions, DGAT1-dependent sequestration of FAs as TAG in LDs protects against lipotoxic disruption of mitochondrial function and promotes cell viability. These data identify a novel and unexplored aspect of the cellular starvation response in which LDs constitute a lipid buffering system that is essential for cellular homeostasis during periods of high autophagy.

Lack of Amino Acids Stimulates Autophagy-Dependent Lipid Droplet Biogenesis

To gain a better understanding of LD dynamics during starvation, we examined LD distribution and abundance in MEFs incubated in complete serum-containing rich medium (CM) or following transfer from CM into HBSS. In contrast to CM, HBSS induced a rapid increase in LD levels that reached a higher steady state level after 16 hr, exhibiting approximately 3.5-fold more LDs than in CM (**Figures 1-1A and 1-1B**). The accumulation of LDs was accompanied by the re-localization of dispersed LDs to a highly clustered distribution (**Figures 1-1A and 1-1C**), and LDs were often observed in close proximity to mitochondria (**Figures 1-1A, and 1-S1A-S1C**). The increase in LDs during starvation also occurred in several cultured human cell lines, including HeLa, Huh7, and U2OS (**Figures 1-S1D-S1G**), suggesting that an increase in LDs is a general cellular response to nutrient deprivation.

HBSS starvation conditions have low concentrations of glucose and lack amino acids and serum. To define the minimal conditions required to induce LD biogenesis, we selectively depleted groups of nutrients (**Figures 1-1D and 1-1E**). Incubation in media lacking glucose or serum resulted in a severe decrease in LDs compared to CM (**Figures 1-1D and 1-1E**), likely due to the degradation of existing LDs and a lack of compensatory LD biogenesis. In contrast, incubation with media lacking amino acids, or just glutamine, increased the pool of LDs, largely phenocopying the effect of HBSS starvation (**Figures 1- 1B, 1-1D, and 1-1E**). Consistent with the importance of autophagy in starvation-induced LD biogenesis, growth in HBSS or in media lacking amino acids induced LC3 and p62 degradation that could be blocked by bafilomycin A1 (BafA1), an inhibitor of V-ATPase and lysosomal acidification (**Figure 1-S2A**). In addition, growth in HBSS or in media lacking amino acids also was found to increase autophagy measured using the GFP-LC3-RFP-LC3ΔG autophagic flux reporter[29] (**Figure 1-S2B**). In contrast, glucose or serum deprivation did not significantly impact LC3 or p62 degradation (**Figure 1-S2A**) or autophagic flux (**Figure 1-S2B**), supporting a correlation between autophagy induction and LD formation. Moreover, the generation of LDs during amino acid starvation was blocked by BafA1 and by the autophagy inhibitor 3-methyladenine (**Figures 1-1F, 1-1G, 1-S3A, and 1-S3B**), but was insensitive to the FA synthase inhibitor TVB-3166 (**Figure 1-1F, G**). These results indicate that amino acid deprivation is sufficient to induce autophagy-dependent LD biogenesis via lipid recycling, in the absence of *de novo* FA synthesis.

mTORC1 Controls Autophagy-Dependent Lipid Droplet Biogenesis During Starvation

Mechanistic target of rapamycin (mTOR) is a nutrient sensitive kinase that, as part of mTOR complex 1 (mTORC1), functions as a master regulator of cell growth and autophagy[30]. Under conditions of sufficient amino acids, the heterodimeric RagA/B-RagC/D GTPases, the Ragulator complex, and the v-ATPase recruit mTORC1 to the surface of lysosomes, where the kinase activity of mTORC1 is turned on (or unlocked)[30] (**Figure 1-2A**). Conversely, in the absence of amino acids, mTORC1 is no longer recruited to the lysosome and is inactive, resulting in the upregulation of autophagy[30].

In agreement with the inhibition of mTORC1 activity during starvation, incubation in HBSS or in media lacking amino acids resulted in the rapid loss of phosphorylated S6 kinase (p-S6K) (**Figures 1-2B and 1-S2A**), a substrate of mTORC1 and a useful reporter of mTORC1 activity, and also a decrease in the phosphorylation of the autophagy initiator kinase ULK1 (p-ULK1 S757) (**Figure 1-S2A**). Inhibition of mTOR with the catalytic inhibitor torin1 was sufficient to increase LD abundance in CM and no further increase was observed during starvation in HBSS (**Figures 1-2C, 1-S3C, and 1-2SD**), a condition in which mTORC1 is already fully inhibited (**Figures 1-2B and 1-S2A**). Torin1 promotion of LD biogenesis was blocked by BafA1 (**Figures 1-S3C and 1-S3D**), indicating a dependence on autophagy. mTORC1 activity and autophagy initiation can be impacted by the AMPK signaling pathway[31-32]. Phosphorylated AMPK (p-AMPK) was absent following 1 hr HBSS starvation and only became apparent after 4 hr HBSS starvation (**Figure 1-2B**), suggesting that AMPK is not functioning upstream of mTORC1 under these conditions. Incubation with the AMPK activator AICAR was insufficient to induce LD biogenesis in complete media, but it had a stimulatory effect during HBSS starvation (**Figures 1-2B and 1-2D**). The AMPK inhibitor compound C (comp. C) had the opposite effect, and decreased LDs during HBSS starvation (**Figures 1-2B and 1-2D**). Thus, inhibition of mTOR is sufficient to induce autophagy-dependent LD biogenesis in the absence of starvation and the extent of LD biogenesis during starvation is modulated by AMPK signaling.

Torin1 inhibits mTOR present in both mTORC1 and mTORC2. To selectively impair mTORC1 activity, we exploited MEFs lacking p18, a subunit of the Ragulator complex that is essential for mTORC1 lysosomal recruitment and activation[33-34] (**Figure 1-2A**). p18 revertant (p18rev) MEFs rescued with strep-tagged p18[33-34] were employed as controls. As in the torin1-treated cells, the p18-/- MEFs exhibited a complete lack of p-S6K, indicating inhibition of mTORC1 (**Figure 1-2E**). Moreover, the p18-/- MEFs displayed high levels of LDs relative to the control p18rev MEFs cells and no further increase was observed during HBSS starvation (**Figure 1-2F**). To determine if mTORC1 inhibition is necessary for LD biogenesis during starvation, we generated MEFs lacking Nprl2 (**Figure 1-S4A**), a subunit of the Gator1 complex that inactivates the Rag GTPases under low amino acid conditions[35] (**Figure 1-2A**). MEFs lacking Nprl2 exhibited decreased starvation-induced inhibition of mTORC1 as evidenced by the persistence of the p-S6K signal during HBSS incubation (**Figure 1-2G**), consistent with the uncoupling of mTORC1 from the nutrient status of these cells. Strikingly, the Nprl2 null cell lines were completely unresponsive to HBSS-induced LD biogenesis (**Figure 1-2H**). Cancer cell lines HCC1500 and SW780, which lack Nprl2 and exhibit decreased mTOR nutrient responsiveness[35] (**Figure 1-S4B**), also showed reduced LD biogenesis during HBSS starvation (**Figures 1-S4C and S4D**). Together, these data demonstrate that inhibition of mTORC1 is necessary and sufficient for autophagy-dependent LD biogenesis.

LD Biogenesis During Starvation Selectively Requires DGAT1

DGAT1 and DGAT2 mediate the final committed step in TAG synthesis, esterifying diacylglycerol (DAG) to yield TAG, which is then packaged into LDs**Error! Bookmark not defined.**[, 36]. Simultaneous inhibition of DGAT1 and DGAT2 abrogates LD biogenesis in adipocytes[36] and

MEFs[37]. To examine the contribution of these two enzymes to LD biogenesis under distinct metabolic states, we treated MEFs with DGAT inhibitors and induced LD biogenesis either with nutrient excess (i.e. oleate supplementation) (**Figure 1-3A**) or nutrient deprivation (i.e. HBSS) (**Figure 1-3B**). In the presence of oleate, LD biogenesis was only partially blocked by treatment with DGAT1 inhibitor T863 (DGAT1i) or DGAT2 inhibitor PF-06424439 (DGAT2i) alone, but it was completely blocked by incubation with both DGAT inhibitors together (**Figure 1-3A**). In contrast, during HBSS starvation, DGAT1i largely blocked LD biogenesis, while DGAT2i had no effect (**Figure 1-3B**). Depletion of the DGAT enzymes using siRNAs also indicated that DGAT1 is preferentially required for starvation-induced LD biogenesis (**Figures 1-S5A-S5C**). Measurements of transcript levels of DGAT1 and DGAT2 revealed that the levels of both transcripts increased during HBSS starvation (**Figure 1-S5D**), indicating that cells upregulate TAG synthesis machinery under these conditions. This result also indicates that the mechanism enabling channeling of FAs selectively into DGAT1-dependent LDs is likely not due to differences in DGAT1 and DGAT2 expression levels, and the mechanism for this selective channeling from the autolysosome remains unclear. LDs are required for autophagy under certain conditions in yeast[13, 38-39] and mammalian cells[40], raising the possibility that DGAT1 inhibition could impact LD biogenesis by disrupting autophagy. However, incubation with DGAT1i had no effect on autophagic flux (**Figure 1-3C**) or the kinetics LC3 and p62 degradation (**Figure 1-3D**) during starvation in HBSS, indicating that the autophagy pathway is intact. Together, these results demonstrate that DGAT1 channels FAs downstream of autophagy into LDs during starvation.

Whether the new pool of starvation-induced LDs is degraded is unknown. Inhibition of DGAT1 provides a useful method to prevent additional LD biogenesis, allowing measurement of the stability and degradation of any existing LDs. Upon shifting MEFs from CM into HBSS starvation media containing DGAT1i (**Figure 1-3E**), the pre-existing pool of dispersed LDs was stable for the first 300 min and then was degraded at a steady rate for the remaining period of the experiment (**Figures 1-3G and 1-3H**). To examine the degradation kinetics of the new pool of autophagy-dependent LDs, we employed a starvation "pulse chase" paradigm (**Figure 1-3F**). In this paradigm, MEFs were briefly starved with HBSS to induce the formation of autophagy-dependent LDs, then DGAT1i was added and the stability of the LDs measured. The autophagy-dependent, clustered LDs were immediately degraded with similar rates as the dispersed LDs (**Figures 1-3G and 1-3H**). The lack of a lag period was likely because the cells had already initiated a starvation response at the beginning of these measurements. Degradation of pre-existing and starvation-induced LDs was blocked by ATGListatin (**Figures 1-S5E and 1-S5F**), an inhibitor of the LD-associated TAG lipase ATGL[41]. These results demonstrate that both the pre-existing dispersed LDs and the newly formed autophagy-dependent LDs are lipolytically degraded during nutrient deprivation.

DGAT1 Impacts Fatty Acid Storage and Channeling to Mitochondria During Starvation
LDs have been reported to form membrane contact sites with mitochondria[7, 15, 20] and we observe LDs in close proximity to mitochondria during HBSS starvation (**Figures 1-1A and 1-S1A-S1C**). One possibility is that LDs could function as a requisite intermediate for the transfer of FAs released by autophagy to mitochondria for breakdown by β-oxidation. If this model is correct, blocking DGAT1-dependent LD biogenesis would reduce FA delivery to mitochondria and their subsequent

conversion into acylcarnitines by mitochondrial carnitine palmitoyltransferase 1 (CPT1), resulting in a decrease in acylcarnitine levels and potentially in an increase in FA flux into non-energy accessible lipid pools (e.g. increase in phospholipids). To test this model, we employed single reaction monitoring (SRM)-based LC-MS steady state lipidomic profiling to analyze the levels of 113 lipids from multiple lipid classes (**Figures 1-4 and 1-S6A-E**). In MEFs incubated in CM, very few lipids were affected by DGAT1 inhibition and TAG levels were unchanged (**Figure 1-S6A-S6E**), indicating that DGAT1 is not required for maintenance of TAG pools in CM. In contrast, DGAT1 inhibition during starvation in HBSS resulted in a number of significant changes in the cellular lipid profile (**Figure 1-4**). The levels of nearly all TAG species measured were significantly decreased (**Figure 1-4A, B**), which correlates well with the importance of DGAT1 in the generation of LDs during HBSS starvation (**Figures 1-3B and 1-S5C**). There was also a large decrease in cholesterol esters and a small increase in cholesterol (**Figures 1-4A, C**), suggesting that impairments in the biogenesis of TAG-rich LDs may impact cholesterol ester synthesis and storage. There were additional small changes in other lipid classes (**Figures 1-4A and 1-4E-I**), including an increase in C16:0 ceramide (1.6-fold) (**Figures 1-4A and 1-4G**), which may reflect cellular stress. Interestingly, there were significant increases in both C16:0 acylcarnitine (3.6-fold) and C18:0 acylcarnitine (2.5-fold) (**Figures 1-4A and 1-4D**), suggesting that FA delivery to mitochondria is not impaired and may increase in the absence of DGAT1 activity.

To more specifically track FA flux, we employed isotopic palmitate tracing (**Figure 1-5**). In these experiments, isotopically-labeled palmitate (d_4-free FA [FFA]) was added at the beginning of the starvation together with vehicle or DGAT1i, and the incorporation of d_4-FFA into lipids tracked by mass spectrometry. We observed incorporation of d_4-FFA into 20 lipids, and incorporation into 7 lipids was statistically altered by DGAT1 inhibition (**Figures 1-5A-5H**). As expected, DGAT1 inhibition reduced d_4-FFA incorporation into TAG species containing C16:0, including C16:0/C16:0/C16:0 TAG and C16:0/C18:1/C16:0 TAG (**Figures 1-5A-5C**). In addition, consistent with our steady state lipidomics data (**Figure 1-4**), we observed increased incorporation of d_4-FFA into C16:0 acylcarnitine (2.3-fold) in DGAT1i-treated cells (**Figures 1-5A and 5D**). These data indicate that the absence of DGAT1 activity disrupts FA channeling into TAG and instead results in FA incorporation into other lipid species, including acylcarnitines. In addition, during an incubation in HBSS with DGAT1i, co-treatment with ATGListatin stabilized TAGs as expected (**Figures 1-S6F-S6J**), but it did not block the increase in acylcarnitines (**Figures 1-S6K and S6L**). Together, these results argue against the model that TAG-containing LDs are a requisite intermediate for FA delivery to mitochondria.

DGAT1-Dependent LD Biogenesis Protects Mitochondrial Function During Starvation
To determine if DGAT1-dependent LDs are important for cellular health under starvation conditions, we analyzed cell viability. Our results indicated that the inhibition of DGAT1, but not DGAT2, significantly increased the percentage of apoptotic cells during HBSS starvation (**Figure 1-6A**). LDs can play cytoprotective roles by sequestering FA and reducing the accumulation of various cytotoxic lipid species. This lipid sequestration function may prevent alterations in ER lipid homeostasis that cause ER stress or prevent the generation of reactive oxygen species (ROS) damaged lipids (e.g. lipid peroxides). However, no changes were observed in cellular levels of

reactive oxygen species (**Figure 1-S7A**) or lipid peroxides (**Figure 1-S7C**) following DGAT1 inhibition during incubations in CM or HBSS. In addition, DGAT1 inhibition in CM or HBSS did not increase ER unfolded protein response (UPR) pathways (**Figures 1-S7D-S7K**), such as IRE1-mediated XBP1 splicing (**Figures 1-S7D and S1E**) or the expression of canonical UPR targets (BiP/GRP78, GRP94, SEL1L, ERDJ4) (**Figures 1-S7H-S7K**). HBSS starvation alone was sufficient to upregulate ATF4 expression (**Figures 1-S7F and S7G**). However, ATF4 induction was unaffected by DGAT1 inhibition (**Figures 1-S7F and S7G**), or PERK inhibition with GSK2606414 (**Figure 1-S7G**). The starvation-induced ATF4 expression likely reflects signaling through the well-characterized, nutrient-responsive GCN2-eIF2α-ATF4 pathway[42], not increased ER stress. Finally, employing the retention using hooks (RUSH) system[43], we found that DGAT1 inhibition did not affect the trafficking of SBP-EGFP-tagged E-cadherin from the ER to the Golgi (**Figure 1-S7L**), indicating that secretory pathway function is not impaired. These data demonstrate that although DGAT1 inhibition during starvation reduces cell viability, it does not cause large increases in ROS or ER stress.

The observed increase in acylcarnitines (**Figures 1-4 and 1-5**) in response to DGAT1 inhibition during starvation could reflect mitochondrial dysfunction. To test whether LD biogenesis impacts mitochondrial function, we measured mitochondrial oxygen consumption and found that DGAT1 inhibition resulted in a significant decrease in the rates of basal mitochondrial oxygen consumption in HBSS starved MEFs, but not MEFs incubated in CM (**Figures 1-6B and 1-6C**). Basal mitochondrial oxygen consumption generally decreased during the HBSS starvation relative to CM (**Figures 1-6B and 1-6C**), but the reduction was more dramatic for DGAT1i-treated MEFs (0.46-fold) compared to the vehicle-treated MEFs (0.80-fold). Furthermore, inhibition of DGAT1 for 16 hr reduced mitochondrial membrane potential in HBSS starved MEFs, but not MEFs incubated in CM (**Figures 1-6D and 1-6E**). In HBSS, mitochondrial membrane potential was maintained for 8 hr and the DGAT1i-induced uncoupling of the mitochondrial membrane potential became evident at the 12 hr and 16 hr time points (**Figures 1-6F and 1-6G**). These reductions in mitochondrial oxygen consumption and membrane potential were not due to a general decrease in the number of mitochondria because the signal from MitoTracker Green FM, which is unaffected by mitochondrial membrane potential, was unaltered by DGAT1 inhibition (**Figures 1-6H-6J**). Although DGAT1 inhibition impacted mitochondrial function, it did not alter the ability of mitochondria to adopt an elongated morphology during starvation (**Figure 1-6K**), a morphology that has been proposed to reduce mitochondrial clearance by autophagy[27-28].

Acylcarnitines exhibited the largest increase in response to DGAT1 inhibition (**Figures 1-4 and 1-5**) and acylcarnitines have been previously suggested to be lipotoxic[44-46]. To explore the possibility that the increase in acylcarnitine levels impacts mitochondrial function we employed the CPT1 inhibitor etomoxir to reduce acylcarnitine levels (**Figures 1-SK and S6L**). Addition of etomoxir alone had no effect on mitochondrial membrane potential during HBSS (**Figures 1-6L and 1-6N**). However, in cells incubated with DGAT1 inhibitor, co-treatment with etomoxir was sufficient to rescue mitochondrial membrane potential (**Figures 1-6M and 1-6N**). Furthermore, addition of palmitoylcarnitine (i.e. C16:0 acylcarnitine) to mitochondria isolated from MEFs was sufficient to depolarize mitochondria (**Figure 1-6O**). Thus, our results indicate that DGAT1-

dependent LDs are required to prevent the accumulation of acylcarnitines, which cause mitochondrial dysfunction during periods of prolonged nutrient deprivation.

Conclusion

In this study, we examined the biogenesis and function of LDs during nutrient deprivation. Our data support a model (**Figure 1-7**) in which mTORC1-regulated autophagy degrades membranous organelles, releasing FAs that are selectively channeled by DGAT1 into new LDs. The biogenesis of LDs under these conditions is necessary to sequester FAs in TAG-rich LDs, preventing acylcarnitine accumulation and subsequent mitochondrial dysfunction. These data identify a novel aspect of the cellular response to starvation and reveal a role for LDs as a lipid buffering system that protects against lipotoxicity during autophagy. These findings underscore the high degree of crosstalk between autophagy, the ER, LDs, and mitochondria that is essential to maintain lipid and energy homeostasis during nutrient deprivation.

In agreement with the importance of autophagy in the formation of LDs**Error! Bookmark not defined.**, uncoupling the canonical mTORC1 signaling pathway from nutrient status by disrupting the Gator1 complex strongly blocked LD biogenesis during starvation. Interestingly, mTORC1 inhibition was sufficient to induce autophagy-dependent LD biogenesis in CM. This finding indicates that autophagy-dependent LD biogenesis is not limited to nutrient deprivation conditions and suggests that LD biogenesis is a general protective response to high levels of autophagy, which may be relevant to particular cancers, during development and aging, or following rapamycin treatment[47]. LDs may play a similar role to prevent lipotoxicity during the selective autophagic degradation of the ER (i.e. ERphagy) or mitochondria (i.e. mitophagy), which would be predicted to release FAs. It is worth noting that mTORC1 integrates a wide variety of nutrient, chemokine, and stress signals, and the alteration of mTORC1 activity could explain reported LD increases during diverse stress conditions, including proteasome inhibition[48] and ER stress[49-50]. Indeed, the sestrin proteins inhibit mTORC1 in response to tunicamycin-induced ER stress through their association with the Gator2 complex[51], providing a mechanism connecting cellular stress with mTORC1 inhibition, autophagy, and possibly LDs.

The biogenesis of starvation-induced LDs specifically required DGAT1, but not DGAT2. Differences in the structure and distribution of DGAT1 and DGAT2 suggest that the two enzymes serve unique functions[52-53]. In contrast to the ER-resident polytopic DGAT1, DGAT2 adopts a hairpin structure and is able to traffic to the surface of LDs, where it facilitates local TAG synthesis and LD expansion[52]. DGAT1 mediates the formation of small LDs, and it was suggested that these LDs may function to protect the ER from accumulating lipotoxic intermediates[52]. Our data are in agreement with a protective role for LDs, and emerging findings suggest a role for DGAT1-dependent LDs in mitigating lipotoxicity under multiple conditions, including high fat diet conditions[54], models of lipotoxic cardiomyopathy[55-57], incubation with exogenous saturated fatty acids[11, 54], and during periods of high autophagic flux (this work). In each of these examples, DGAT1 is likely playing a conceptually similar role, sequestering FA as TAG in LDs and preventing the accumulation of a cytotoxic lipid species. However, the cytotoxic lipid species and the resulting downstream cellular dysfunctions may differ. For example, the addition of exogenous palmitate to CHO cells caused apoptosis associated with ceramide generation and ER stress

induction[11]. The addition of exogenous saturated FAs to macrophages resulted in altered ER phospholipid composition, upregulation of the IRE1 ER stress pathway, and activation of the NLRP3 inflammasome and secretion of pro-inflammatory cytokines[58]. In mouse models of lipotoxic cardiomyopathy, DGAT1 protected against lipotoxicity associated with the accumulation of DAG and ceramide in cardiomyocytes[55-57]. In contrast to these examples, DGAT1 inhibition in MEFs during starvation-induced autophagy was not associated with large changes in DAG or ceramide and also was not associated with increases in ROS or ER stress. Instead, autophagy-associated lipotoxicity was associated with acylcarnitine accumulation and mitochondrial dysfunction. Whether the lipotoxic disruption of mitochondrial function occurs in other models of lipotoxicity (e.g. exogenous saturated fatty acid addition or high fat diet) remains to be determined. However, it is interesting to note that mitochondrial breakdown of FAs and LD sequestration of FAs may serve complementary roles in preventing lipotoxicity by reducing the levels of FFA. Thus, DGAT1-dependent LDs broadly mitigate lipotoxicity, but the cytotoxic lipid species and the downstream cellular dysfunction likely differ depending on the initiating cellular insult and cell type.

DGAT1 inhibition during starvation resulted in an increase in acylcarnitines, a small increase in ceramide, and no increase in other potentially cytotoxic lipids such as DAGs and FFA. Reducing acylcarnitine levels with the CPT1 inhibitor etomoxir largely rescued mitochondrial membrane potential, implicating acylcarnitines as the cytotoxic culprit under these conditions. In addition, acylcarnitine disrupted the membrane potential of purified mitochondria *in vitro*, indicating that acylcarnitines are able to directly uncouple mitochondria. Our finding are consistent with previous suggestions that high concentrations of acylcarnitines may be cytotoxic and may disrupt mitochondrial function[59-61]. This may be particularly relevant in the heart, which derives a large portion of its energy from fatty acid oxidation. Indeed, it is noteworthy that acylcarnitine accumulation is associated with fatty acid oxidation diseases and ischemia[59-61]. In addition, improvements in cardiac function in a mouse model of cardiomyopathy were associated with reduced acylcarnitines, but not reductions in DAG, TAG, or ceramide, leading to the proposal that the accumulation of acylcarnitines may be lipotoxic in the heart[61]. Interestingly, N-acyl amino acids were also recently shown to act as direct mitochondrial uncouplers[62], raising the possibility that this may be a common property of fatty acid derivatives. Acylcarnitines are capable of disrupting membrane integrity *in vitro*[63-64], but whether mitochondrial uncoupling by acylcarnitine in cells is due to direct disruption mitochondrial membrane integrity or involves association with mitochondrial proteins is unclear at this time. In addition, due to their interrelationship, mitochondrial dysfunction and the accumulation of acylcarnitines could result in a positive feedback loop that further increases toxicity.

We observed that the autophagy-dependent pool of LDs was lipolytically degraded by the LD-associated lipase ATGL during nutrient deprivation; and together, our data suggest that these LDs mediate two distinct functions during starvation – to protect against lipotoxicity and then to serve as a lipolytically regulated source of FAs. The autophagy-dependent LDs clustered in close proximity to mitochondria and LD-mitochondrial contacts have been proposed to function as sites for FA transfer[7, 20]. This model is attractive because the membrane contact sites could enable channeling of FAs efficiently into the β-oxidation pathway, reducing the danger of

lipotoxicity due to cytoplasmic passage of FFAs. The ER makes extensive contacts with organelles throughout the cell[65-66], facilitating organelle-to-organelle lipid exchange and acting as an organizing scaffold for organelle events, such as mitochondria[67] and endosomes[68] fission. LDs are ER-derived organelles that form extensive contacts with the ER[52, 69-70] and the ER is also known to contact mitochondria[71]. It is possible that ER serves as an organizer of LD-mitochondrial contacts and thereby organizes a protected pathway for FA channeling to mitochondria from autolysosomes. However, the identity of a LD-mitochondrial tethering complex, the role of the ER in organizing LD-mitochondrial interactions, and the functional importance of these organelle contact sites in FA transfer and energy homeostasis remain to be determined.

Emerging findings indicate multiple modes of crosstalk between LDs and autophagy. For example, in liver cells a selective autophagic pathway termed lipophagy degrades LDs and inhibition of autophagy in liver cells results in LD accumulation[14-15]. Lipophagy does not appear to play a role during nutrient deprivation in our cell types, since LDs decrease following inhibition of autophagy. In addition, we found that LD degradation in MEFs during starvation was inhibited by ATGListatin, and it was previously shown that LD degradation upon starvation was prevented by siRNA-depletion of the LD-associated lipase ATGL[7], consistent with the dominance of the LD lipolytic pathway. LDs have also been suggested to be required for autophagy, either by supplying lipids for autophagosome biogenesis or by sequestering lipids that disrupt ER homeostasis and impair autophagosome biogenesis[14, 38-40]. However, under our conditions, autophagic flux and degradation of autophagy substrates (e.g. LC3 and p62) was unaffected by the loss of DGAT1-dependent LDs. Thus, it is likely that nature of the LD-autophagy relationship is cell type and context specific.

Together, our findings demonstrate that DGAT1-dependent LD biogenesis protects against lipotoxic mitochondrial damage and that LDs are integrally involved in the coordinated, adaptive response to nutrient deprivation. These finding raise the possibility that LDs are more widely involved as protective lipid buffering systems in cellular stress responses, especially those involving altered mTORC1 signaling and upregulation of autophagy. Future research examining the mechanism of mitochondrial dysfunction under these conditions will be important to achieve a comprehensive understanding of the organelle crosstalk underlying cellular lipid and energy homeostasis.

Materials and Methods

Cell Culture
MEFs, U2OS, HeLa, HEK293T/17, and Huh7 cells were cultured in DMEM containing 4.5 g/L glucose and L-glutamine (Corning) supplemented with 10% fetal bovine serum (FBS; Thermo Fisher Scientific and Gemini Bio Products) at 37°C and 5% CO_2. HCC1500 cells (ATCC) were cultured in RPMI-1640 (ATCC) supplemented with 10% FBS at 37°C and 5% CO_2. SW780 (ATCC) cells were cultured in Leibovitz's L-15 (ATCC) supplemented with 10% FBS at 37°C in the absence of CO_2. Unless specified, starvation conditions consisted of growth in Hank's Balancing Salt Solution (HBSS) (Invitrogen) for 16 hr. For deprivation of amino acids, cells were cultured in

DMEM (D9800-13, US Biological) supplemented with 4.5g/L glucose, and 10% FBS. For low glucose, high glucose, and glutamine starvation, DMEM (A1443001, Life Technologies) was supplemented with 10% FBS, 4 mM glutamine (Thermo Fisher Scientific), and 1 g/L glucose (low glucose conditions) or 4.5 g/L (high glucose) accordingly.

Plasmids and Reagents

CRISPR sequences targeting exon 2 and 3 of mouse Nprl2 were designed using the online-available CRISPR design tool developed by the Zhang laboratory (http://crispr.mit.edu/). The seed sequences preceding the protospacer adjacent motif (PAM) are the following: Nprl2 gRNA #1, Exon 2, 1-5': *CACCG*GAGCAGCTTTGTATCCAACG and 2-5': *AAAC*CGTTGGATACAAAGCTGCTCC. Nprl2 gRNA #2, Exon 3, 1-5': *CACCG*ATGGCGAAACCCGTCAATGT and 2-5': *AAAC* ACATTGACGGGTTTCGCCATC. Nucleotides in italics show the overhangs necessary for incorporation into the restriction enzymatic site BbsI of LentiCRISPR-v2 vector expressing Cas9 and the sgRNA (kindly provided by Dr. Joseph Napoli, UC Berkeley). Lentiviruses were produced in 293T/17 cells. MEF cells were infected and selected with 3 µg/mL puromycin and successful disruption of Nprl2 expression confirmed by RT-qPCR. The pMRX-IP-GFP-LC3-RFP-LC3ΔG plasmid[29] was a gift from Dr. Noboru Mizushima (University of Tokyo, Addgene plasmid # 84572). The Str-KDEL_SBP-EGFP-E-cadherin plasmid[43] was a kind gift from Gaelle Boncompain (Institut Curie).

Plasmid transfections were performed using X-tremeGENE HP (Roche) transfection reagent according to the manufacturer's instructions. siRNAs were obtained from Sigma Aldrich and transfected using Lipofectamine RNAiMAX (Thermo Fisher Scientific) according to the manufacturer's instructions.

Reagents employed in this study, and their concentrations, include: 250 nM Bafilomycin A1 (Sigma Aldrich), 1 µM TVB-3166 (3-V Biosciences), 250 µM AICAR (Cell Signaling), 10 µM Compound C (Torcis), 250 nM torin1 (Torcis), 20 µM T863 (DGAT1i; Sigma Aldrich), 10 µM PF-06424439 (DGAT2i, Sigma Aldrich), 1 µM GSK2606414 (PERKi; EMD Millipore), 200 µM oleate (Sigma Aldrich), 100ng/mL rapamycin (Sigma Aldrich), 250 nM oligomycin (Agilent Technologies), 250 nM FCCP (Agilent Technologies), 100 nM rotenone/antimycin (Agilent Technologies), 5 µg/mL tunicamycin (Cayman Chemical), 100 µM etomoxir (Cayman), and 20 µM ATGListatin (EMD Millipore Corporation).

Fluorescence Microscopy

Cells grown on poly-L-lysine-coated coverslips were incubated in the presence or absence of 200 µM oleate for 16 hr. For the last 30 minutes of treatment, 100 nM of MitoTracker Orange CMTMRos was added to the cells. Cells were then washed with PBS, fixed for 15 min in PBS containing 4% (wt/vol) paraformaldehyde, and washed again with PBS. LDs (10 µg BODIPY 493/403; Thermo Fisher Scientific) and nuclei (100 mg DAPI; Thermo Fisher Scientific) were stained by incubating with staining buffer [PBS and 1% (wt/vol) bovine serum albumin] for 1 hr at room temperature. Cells were subsequently washed with staining buffer and mounted in Fluoromount G (Southern Biotech). Stained cells were analyzed by Deltavision Elite widefield epifluoresence deconvolution microscope with either a 40× air objective or a 60× oil immersion

objective. The area of stained LDs was quantified from three independent experiments (average of 50 cells per experiment) using ImageJ[82] and mean ± SEM was determined. Statistical significance was evaluated using the Student t test with a p-value < 0.05.

For live-cell imaging, 5 X 10^4 cells were seeded on Nunc LabTek II chambered coverglass. MitoTracker Orange CMTMROS was added to cells for 30 min at 37°C, cells were washed with HBSS, and LDs were stained with 1ug BODIPY 493/503. Prior to imaging, chemical inhibitors were added to cells. Cells were incubated at 37C in a 5% CO2 humidified chamber and images were taken every 10 min for 18 hr using a Deltavision Elite widefield epifluoresence deconvolution microscope with a 60x oil immersion objective. To analyze the proximity of mitochondria and LDs, images were taken every 5 sec for 3 min. Relative LD proximity to mitochondria was calculating by measuring the distance from the center of the LD to the center of the nearest mitochondrion in ImageJ[82].

Immunoblotting
Cells were washed in PBS and lysed in 1% SDS. Protein amounts were normalized using bicinchoninic acid (BCA) Protein Assay (Thermo Fisher Scientific). Proteins were separated on 4-20% polyacrylamide gradient gels (Bio-Rad) and transferred onto low fluorescence PVDF or nitrocellulose membranes (Bio-Rad). Membranes were washed in PBS + 0.1% Tween-20 (PBST) and blocked in 5% (wt/vol) dried nonfat milk in PBST for 30 min to reduce non-specific antibody binding. Membranes were incubated for at least 2 hr in PBST containing 1% bovine serum albumin (BSA) (Sigma Aldrich) and primary antibodies. Following washing in PBST, membranes were incubated with fluorescent secondary antibodies were diluted in 1% BSA in PBST at room temperature for 1 hr. All immunoblots were visualized on a LI-COR imager (LI-COR Biosciences).

The following antibodies were used: anti-pS6K (Thr389, 108D2; Cell Signaling), anti-S6K (Cell Signaling Technology, Inc.), anti-pAMPK (Thr172; Cell Signaling Technology, Inc.), anti-GAPDH (EMD Millipore), anti-LC3β (Sigma), anti-p62 (Enzo Life Sciences, Inc.), anti-pULK1 (Ser757, D7O6U; Cell Signaling Technology, Inc.), anti-ULK1 (D8H5; Cell Signaling Technology, Inc.), anti-ATF4 (Proteintech Group, Inc.). All IRDye680 and IRDye800 conjugated secondary antibodies for immunoblotting were obtained from Li-COR Biosciences.

Lipidomics
Lipidomics experiments were performed as described previously[37, 73-74]. MEFs seeded (5 X 10^6 cells) in a 60 mm dish were incubated in CM or HBSS. Cells were treated with DGAT1 inhibitor for 16 hr and etomoxir for the last 4 or 8 hr of starvation, where indicated. For isotopic analysis of palmitate incorporation MEFs were starved in HBSS and incubated with d_0-palimate acid or (7,7,8,8-d_4)-palmitic acid (10 μM in 0.1% BSA) together with vehicle or DGAT1 inhibitor for 16 hr. Cells were washed twice in PBS, collected by centrifuged at 500 x g, and cell pellets frozen at -80°C until lipid extraction.

Lipids were extracted from cells in a 2:1:1 chloroform:methanol:phosphate-buffered saline solution with inclusion of internal standards (10 nmoles of dodecylglycerol and 10 nmoles of pentadecanoic acid). The organic layer was collected and aqueous layer was acidified with 0.1%

formic acid and re-extracted in chloroform. The organic layers were combined and dried down under a stream of nitrogen. Dried extracts were resolubilized in chloroform and 10 µl was injected onto an Agilent 6400 triple quadrupole (QQQ)-liquid chromatography-mass spectrometry (LC-MS) instrument. Metabolites were quantified by integrating the area under the curve. This value was normalized to internal standards and the levels calculated based on external standard curves with representative lipids standards. In cases in which a there was a background peak for the isotopic d_4-lipid in the d_0-C16:0 treated group, we subtracted the average of the background form both d_0- and d_4-C16:FFA groups.

Viability Assay
MEF cells were seeded (2 X 10^5 cells) and upon adherence, cells were incubated in CM or HBSS and treated with DGAT1 inhibitor for 16 hr. Floating cells in the media were collected and adherent cells were trypsinized. Cells were pelleted by centrifugation at 500 x g for 5 min, washed in PBS, and stained with the Annexin V-FITC apoptosis Detection Kit I (BD Pharmingen), which includes Annexin V-FITC and propidium iodide, according to manufacturer protocol. Fluorescence was analyzed using a BD Biosciences LSRFortessa and the percentage of cell death quantified using FlowJo Software.

Flow Cytometry Measurement of Mitochondrial Membrane Potential and ROS in Cells
MEF cells (2 X 10^5) were seeded and upon adherence, cells were incubated in CM or HBSS and treated with DGAT1 inhibitor or etomoxir for the time-points indicated. Cells were trypzinized and pelleted by centrifugation at 500 x g for 5 min, washed with PBS. For mitochondria membrane potential, cells were stained with 100 nM MitoTracker Orange CMTMRos and MitoTracker Green FM (Thermo Fisher Scientific) for 30 min. Data was acquired by the BD BIOsciences LSRForetessa using the PE-Tx-Red YG and FITC channel and quantified by FlowJo Software. A minimum of 10,000 cells were analyzed per condition.

To measure ROS production, cells were incubated with 5 µM MitoSOX Red (mitochondrial superoxide indicator), CellROX Deep Red Reagent (oxidative stress indicator), or BODIPY 581/591 C11 (lipid peroxidation sensor) (Thermo Fisher Scientific) for 30min at 37°C. Cells were then analyzed by flow cytometry and data were collected from the PE-Tx-Red YG (MitoSOX, C11-BODIPY), APC (CellROX) and FITC (BODIPY 581/591 C11) channels.

Analysis of Autophagic Flux using the GFP-LC3-RFP-LC3ΔG Reporter
pMRX-IP-GFP-LC3-RFP-LC3ΔG plasmid[29] was obtained from Addgene and retrovirus produced in 293T/17 cells. Infected MEFs were selected with 3 µg/mL puromycin and expressing cells were isolated using the BD Bioscience Influx Sorter. Cells were starved, treated accordingly for 16 hr, and flow cytometry data was acquired using the BD Biosciences LSRFortessa FITC and PE-Tx-Red YG channels. The ratio of GFP to RFP for individual cells was quantified using FlowJo Software.

Mitochondrial Respiration Measurements
Mitochondrial activity was determined using the Seahorse Flux Analyzer XF24 according to the manufacturer's instructions. Briefly, 5 X 10^4 cells were seeded on Seahorse 24-well plates. After 24 hr, cells were incubated in HBSS for 16 hr in the presence or absence indicated treatments.

The OCRs were average from three independent experiments and normalized by cell number. Samples were mixed (3 min), time delayed (2 min), and measured (3 min). Oligomycin (250 nM), FCCP (250 nM), and rotenone / antimycin (100 nM) were injected at the indicated time points. The mean ± SEM was determined and statistical significance was evaluated using the Student t test with a P value < 0.05.

Analysis of the Membrane Potential of Isolated Mitochondria
Mitochondria were isolated from four p150 (15 cm) plates of MEFs via a previously described differential centrifugation protocol[75]. Briefly, PBS from previous washes was replaced with filtered mitochondrial isolation buffer (MIB) [50 mM KCl, 110 mM Mannitol, 70 mM Sucrose, 0.1 mM EDTA (pH 8.0), 5 mM Tris-HCl (pH 7.4), and Protease Inhibitors (Calbiochem)] and cells were homogenized by five passes through a 27.5-gauge needle. JC-9 (3,3'-Dimethyl-α-naphthoxacarbocyanine iodide) (Thermo Fisher Scientific) was added [final 10 µM] (except for the "unlabeled mitochondria" control) and the stained mitochondria then aliquoted into Eppendorf tubes. Tubes were then centrifuged at 200 x g for 5 min at 4° C. The supernatant was removed and transferred to new tubes, which were subsequently spun at 800 x g for 10 min at 4° C. The supernatant from these tubes was spun once more at 12,000 x g for 10 min at 4º C. Finally, this supernatant was removed and mitochondria pellets were resuspended in filtered MIB and kept on ice. Three technical replicates were completed for every biological replicate performed. Tubes containing mitochondria then had palmitoyl-DL-carnitine (AC) added to different final concentrations (0 µM, 10 µM, 25 µM, 50 µM, 100 µM) after which samples were incubated on ice for ~30 min and then analyzed by flow cytometry (LSR Fortessa Analyzer). Once all "polarized" samples were run, valinomycin [final 12 µM] was added to these set-aside tubes for 3-5 min and then mitochondria were re-analyzed. JC-9 dye, similar to JC-1 dye, is incompatible with CCCP and FCCP, therefore valinomycin was used to depolarize mitochondria[75-78]. All "depolarized" sample controls were analyzed in this manner. A tube containing filtered MIB and JC-9 alone was included in these spins to use as a dye-alone control during all experiments. An additional tube with lysate, but no JC-9 dye, was also included in the spins to control for "unlabeled mitochondria". Tubes with MIB and AC alone at [10 µm, 25 µm, 50 µm, 100 µm] were also run after ~30 min on ice.

Data was acquired using an LSR Fortessa Analyzer using the forward scatter (FSC), side scatter (SSC, "Granularity") (488 nm/10), FITC ("Green channel") (525 nm/50 with a 500 nm Long Pass filter), and PE-Tx-Red YG ("Red channel") (610 nm/20 with a 600nm Long Pass filter) filters. Although all data points were recorded, lasers and acquisition settings were calibrated to nullify any signal from unlabeled mitochondria or aggregates of JC-9 dye, valinomycin, or palmitoyl-DL-carnitine (AC) in the fluorescent channels used. For all experiments, only singlets (or single mitochondria) were used when creating any plots or performing any statistical analyses. FlowJo v10 was used to process the data. With respect to mitochondrial morphology measurements, mitochondrial diameter was determined by extrapolating from forward scatter (FSC) data acquired using standard beads from Duke Standards (NIST Traceable Polymer Microspheres, catalog #3K-400, 3K-700, and 3K-1000). Mitochondria diameter (nm) = y = 123.08*(FSC)^0.244, R^2 = 0.998, Residual sum of squares (RSS) = 467.31. This is an established use of FSC to approximate mitochondrial size[79-81]. Notably, AC suspended alone in MIB is autofluorescent in

the Green channel, which made ratiometric determination of membrane potential (e.g. Red /Green fluorescence) a poor predictor of this quality, especially with depolarized mitochondria. Importantly, AC was not autofluorescent in the Red channel, so to normalize the amount of Red JC-9 aggregates (an indicator of membrane potential) we divided this value by the calculated diameter of mitochondria.

RT-qPCR and RT-PCR
RNA from cells was harvested using TRIzol (Thermo Fisher Scientific) according to manufacturer's protocol. Synthesis of cDNA from total RNA was performed using High Capacity cDNA Reverse Transcription Kits (Applied Biosystems). Primers were order from Integrated DNA Technologies and used in conjunction with 2X SYBR master mix (Bio-Rad), and a 3-step amplication repeated 40X on CFX96 thermocycler (Bio-Rad). RT-qPCR primers used in this study are listed in Table S4.

The expression of spliced and full length XBP-1 was determine by RT-PCR with oligonucleotide sense primer: 5'-AAACAGAGTAGCAGCTCAGACTGC-3' and anti-sense primer: 5'-AAACAGAGTAGCAGCGCAGACTGC-3'. Amplified PCR products were resolved on a 2.5% agarose gel, visualized using a Gel Doc imaging system (Bio-Rad), and the density of each band was quantified using ImageJ[82].

Analysis of Secretory System Function using the Retention using Selective hooks (RUSH) Reporter System
The RUSH system to analyze secretory function was previously described[43]. MEF grown in DMEM with 10% dialyzed FBS (Life Technologies) were transfected with the Str-KDEL_SBP-EGFP-E-cadherin plasmid using Fugene 6 (Promega) according to manufacturer's protocol. Transfected cells grown on coverslips were incubated in CM or in HBSS for 16hr in the presence of DMSO or DGAT1 inhibitor. 40 µM biotin (Sigma) was added for 0 or 60 min to induce release of the SBP-EGFP-E-cadherin fusion reporter. Cells were fixed for 15 min in PBS containing 4% (wt/vol) paraformaldehyde, washed with PBS, and coverslips mounted in Fluoromount G (Southern Biotech). Transfected cells were imaged using a Deltavision Elite widefield epifluoresence deconvolution microscope with a 60× oil immersion objective.
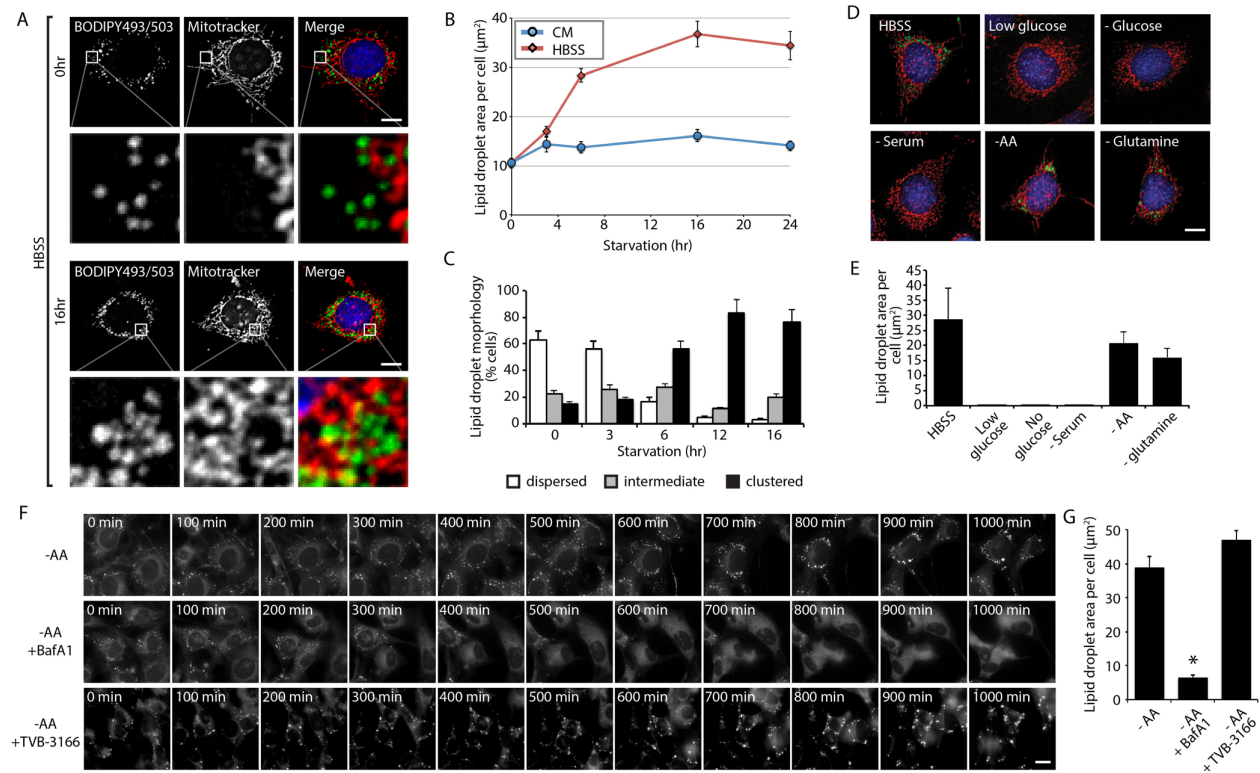
Figures

Figure 1-1. Lack of amino acids is sufficient to induce autophagy-dependent lipid droplet biogenesis

(A-C) MEFs were grown in CM or HBSS for the indicated times, fixed, and analyzed by fluorescence microscopy. *(A)* LDs were stained with BODIPY 493/503 (green), mitochondria with MitoTracker Orange CMTMRos (red), and nuclei with DAPI (blue). *(B)* The abundance of LDs was quantified during incubations in complete media (CM) or HBSS. *(C)* The percentage of cells with dispersed, intermediate, or clustered LDs were quantified after incubating in HBSS for the indicated times. *(D and E)* Cells deprived of the indicated groups of nutrients for 16 hr were fixed, the distribution of LDs (green) and mitochondria (red) analyzed by fluorescence microscopy *(D)*, and the LD area per cell quantified *(E)*. *(F)* A time-lapse montage of BODIPY 493/503-stained LDs in live cells during amino acid deprivation in the presence and absence of bafilomycin A1 (BafA1) or FA synthesis inhibitor TVB-3166. *(G)* Quantification of LD area following a 16 hr amino acid starvation with the indicated treatments (as in panel F). All graphical data are quantified as mean ± SEM. An asterisk indicates a significant difference ($p < 0.05$, *t* test) based on n = 50 cells from three independent biological replicates. In the micrographs, white boxes indicate the magnified regions. Scale bars = 10 μm.

See also Figure S1, Figure S2, Figure S3
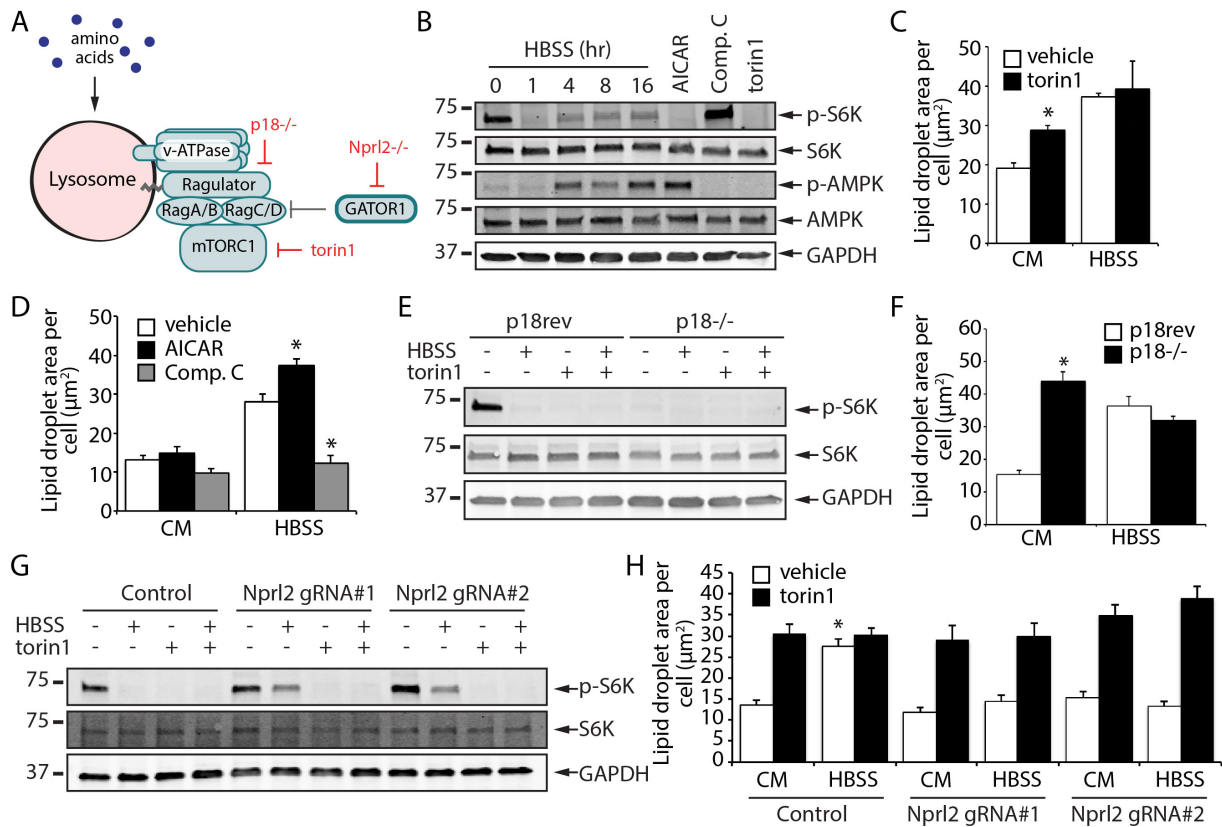
Figure 1-2. mTORC1-regulated autophagy impacts lipid droplet biogenesis during nutrient deprivation

(A) A model illustrating methods to control mTORC1 activity by using the small molecule torin1 or by deletion of the Ragulator subunit p18 or the Gator1 subunit Nprl2. *(B)* Immunoblot analysis of S6K and AMPK phosphorylation in MEF cells incubated in HBSS for the indicated times or treated with the designated compounds for 16 hr. *(C and D)* MEFs were treated as indicated for 16 hr, fixed, and LDs stained with BODIPY 493/503. Stained MEFs were imaged and the area of LDs was quantified. *(E and F)* p18-/- rev and p18-/- MEFs were treated as indicated for 16 hr and analyzed either by immunoblotting *(E)* or by quantifying LD area after fixation and staining with BODIPY 493/503 *(F)*. *(G and H)* Control and Nprl2 KO MEFs were treated as indicated for 16 hr and analyzed by immunoblotting *(G)* or by quantifying LD area after fixation and staining with BODIPY 493/503 *(H)*. All graphical data are quantified as mean ± SEM. An asterisk indicates a significant difference ($p < 0.05$, *t* test) based on n = 50 cells from three independent biological replicates.

See also Figure S2, Figure S3, and Figure S4.
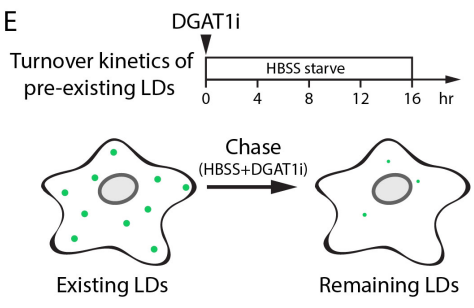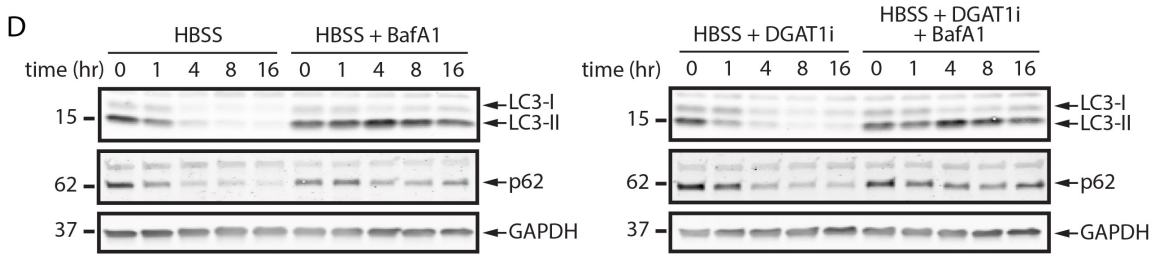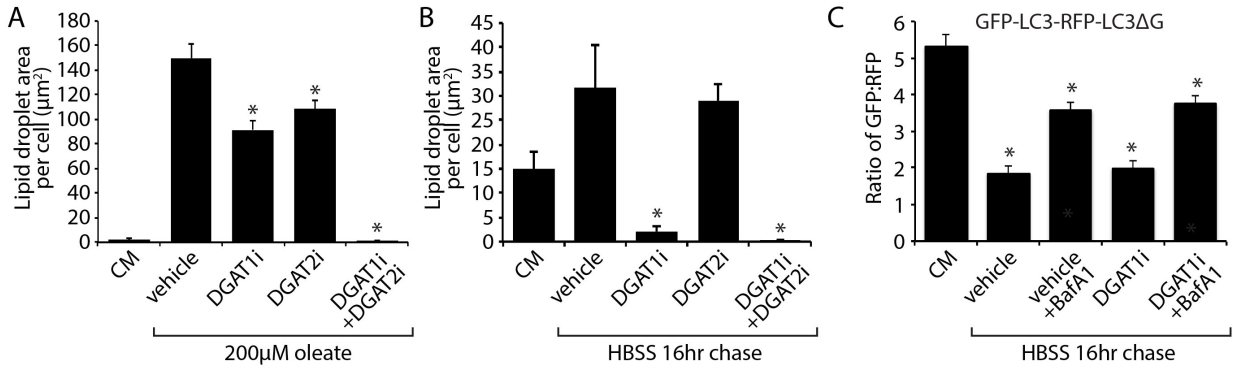
Figure 1-3. DGAT1 channels autophagy released lipids into new lipid droplets that are degraded during nutrient deprivation

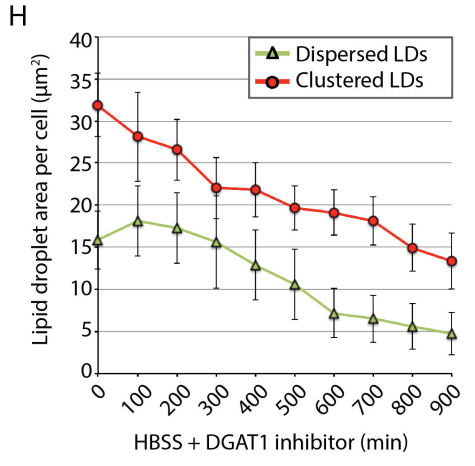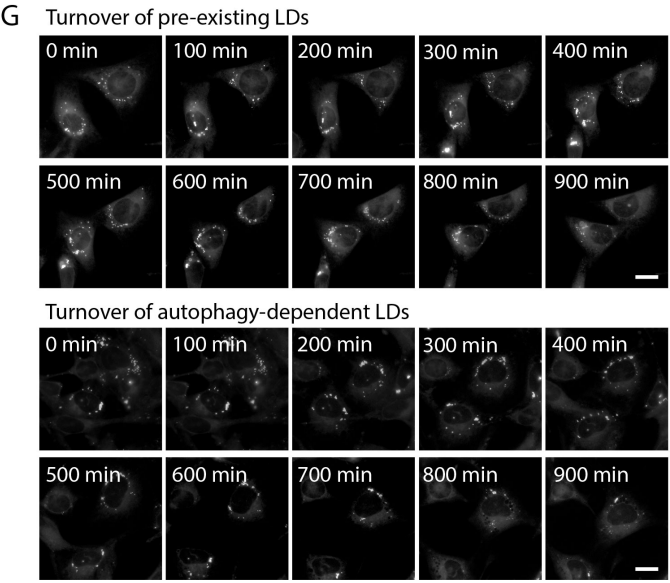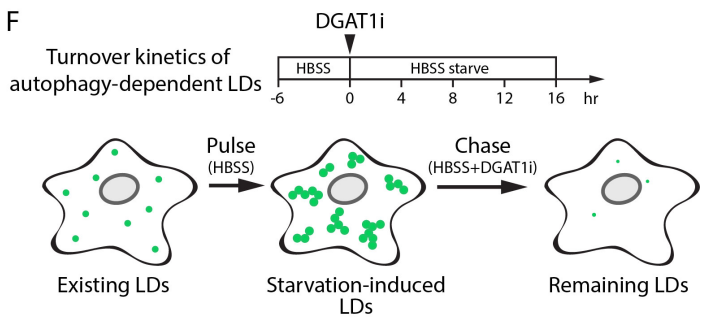*(A and B)* LD biogenesis was induced in MEFs by incubation with 200 µM oleate in CM *(A)* or by starvation in HBSS for 16 hr *(B)*. MEFs were treated with DGAT1 and/or DGAT2 inhibitors (DGAT1i and DGAT2i) as indicated. Cells were fixed, BODIPY 493/503-stained LDs imaged by fluorescence microscopy, and the abundance of LDs quantified. *(C)* MEFs stably expressing a GFP-LC3-RFP-LC3ΔG autophagy flux reporter were incubated in CM or HBSS and treated with DGAT1 and/or DGAT2 inhibitors as indicated. Following a 16 hr incubation, the GFP:RFP ratio was measured by flow cytometry and the fold change in the GFP:RFP ratio quantified (n=3; mean ± SEM). *(D)* Immunoblot analysis of MEFs starved in HBSS and treated with vehicle, DGAT1i, and/or BafA1. *(E)* Illustration of the chase paradigm to visualize the stability of pre-existing, dispersed LDs. DGAT1i is added together with HBSS and the amount of BODIPY493/503-stained LDs present in live cells imaged and quantified over 16 hr. *(F)* Illustration of the pulse-chase paradigm to visualize the stability of starvation-induced, clustered LDs. Following a 6 hr HBSS (pulse) to induce autophagy-dependent LD biogenesis, DGAT1i is added and the amount of BODIPY493/503-stained LDs present in live cells imaged and quantified over 16 hr. *(G)* Time-lapse montage of dispersed and clustered LD degradation in live cells treated according to the paradigms in panels *E* and *F*. *(H)* Quantification of the turnover kinetics of dispersed and clustered LDs treated and imaged as in panel *G*. All graphical data are quantified as mean ± SEM. For the quantified microscopy images, an asterisk indicates a significant difference (p < 0.05, *t* test) based on n = 50 cells from three independent biological replicates.

See also Figure S5.
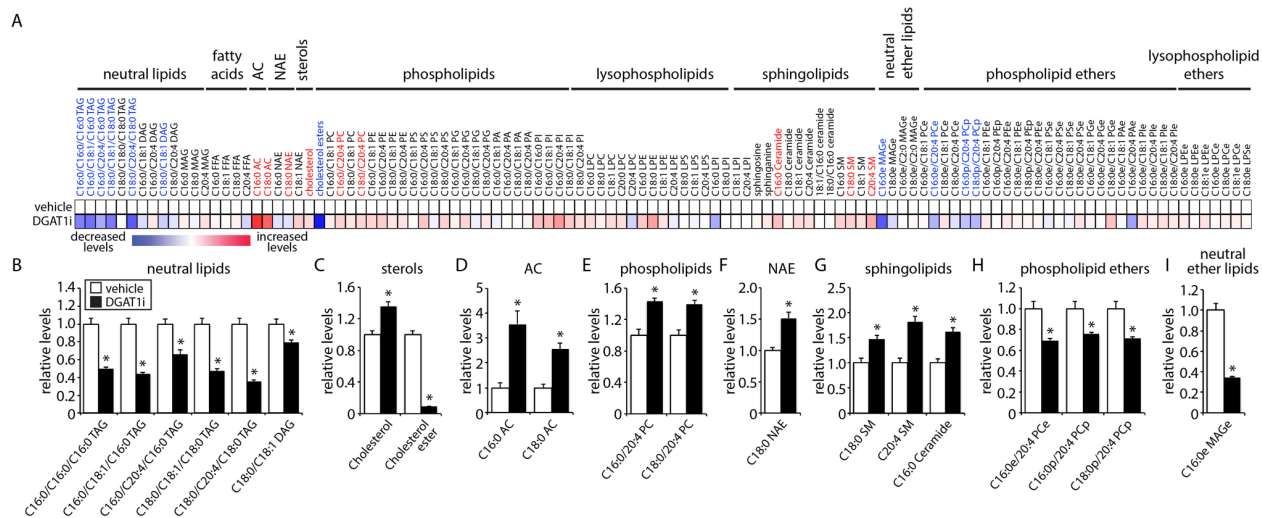
Figure 1-4. DGAT1 impacts fatty acid channeling and sequestration in TAG during nutrient deprivation

(A-I) MEFs were starved in HBSS in the presence of vehicle or DGAT1i for 16 hr. *(A)* Heatmap of metabolomic alterations organized by lipid class. Significantly altered lipids are indicated in blue (significantly decreased) and red (significantly increased). *(B-I)* Quantification showing the relative levels of significantly altered lipids (p < 0.01, *t* test) (n = 4-5).

See also Figure S6.
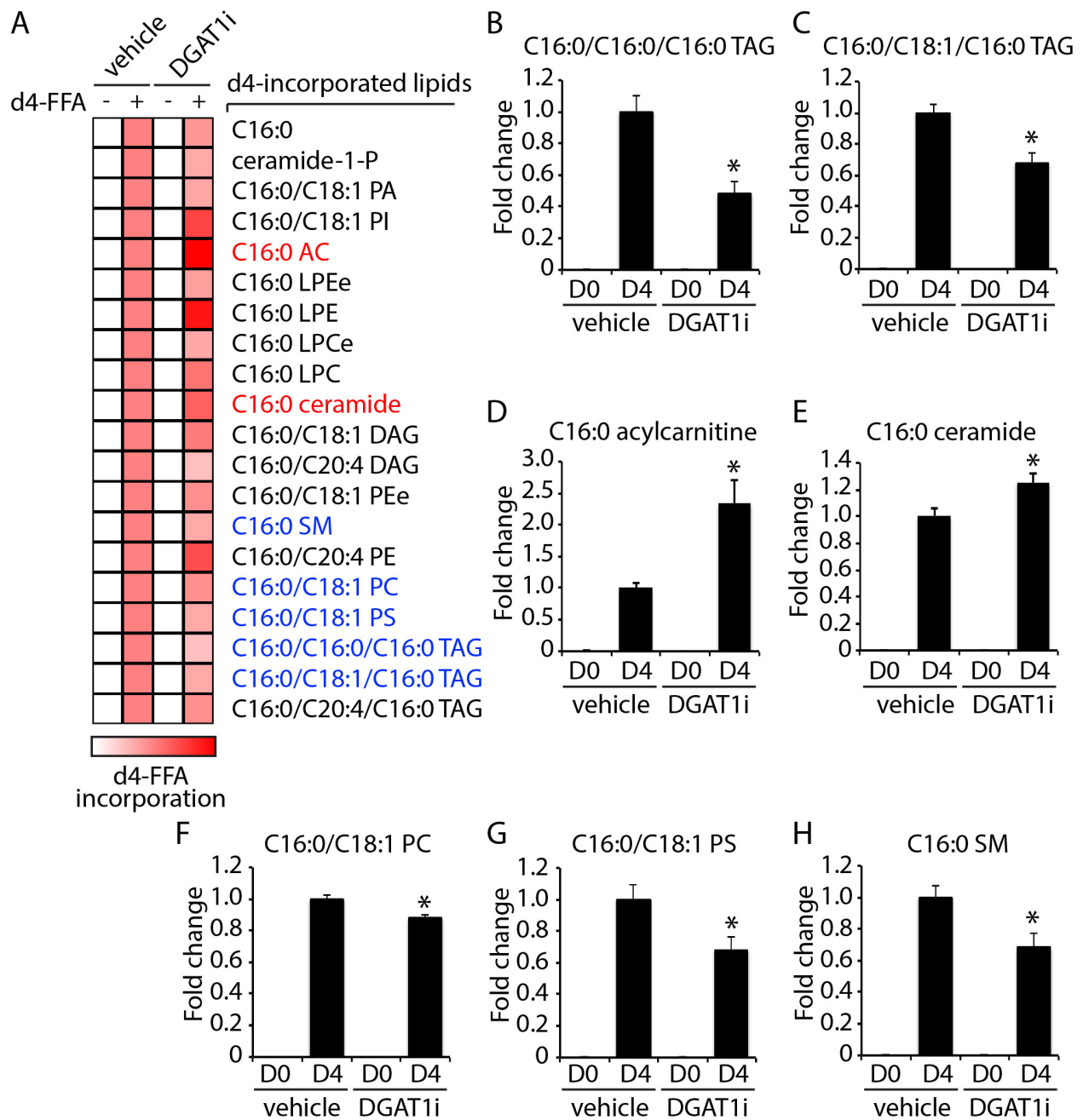
Figure 1-5. Analysis of fatty acid channeling during nutrient deprivation using isotopic palmitate tracing

(A-H) MEFs were starved for 16 hr in HBSS in the presence of either d_0-C16:0 or d_4-C16:0 FFA complexed with 0.5% BSA. Cells were also treated with vehicle or DGAT1i as indicated. *(A)* Heatmap showing the relative levels of lipids with significant incorporation of d_4-C16:0 FFA. Lipids that were significantly altered by treatment with DGAT1i are indicated in blue (significantly decreased) and red (significantly increased). *(B-H)* Quantification showing the relative levels of lipids significantly altered by treatment with DGAT1i ($p < 0.01$, *t* test) (n =5).

See also Figure S6.
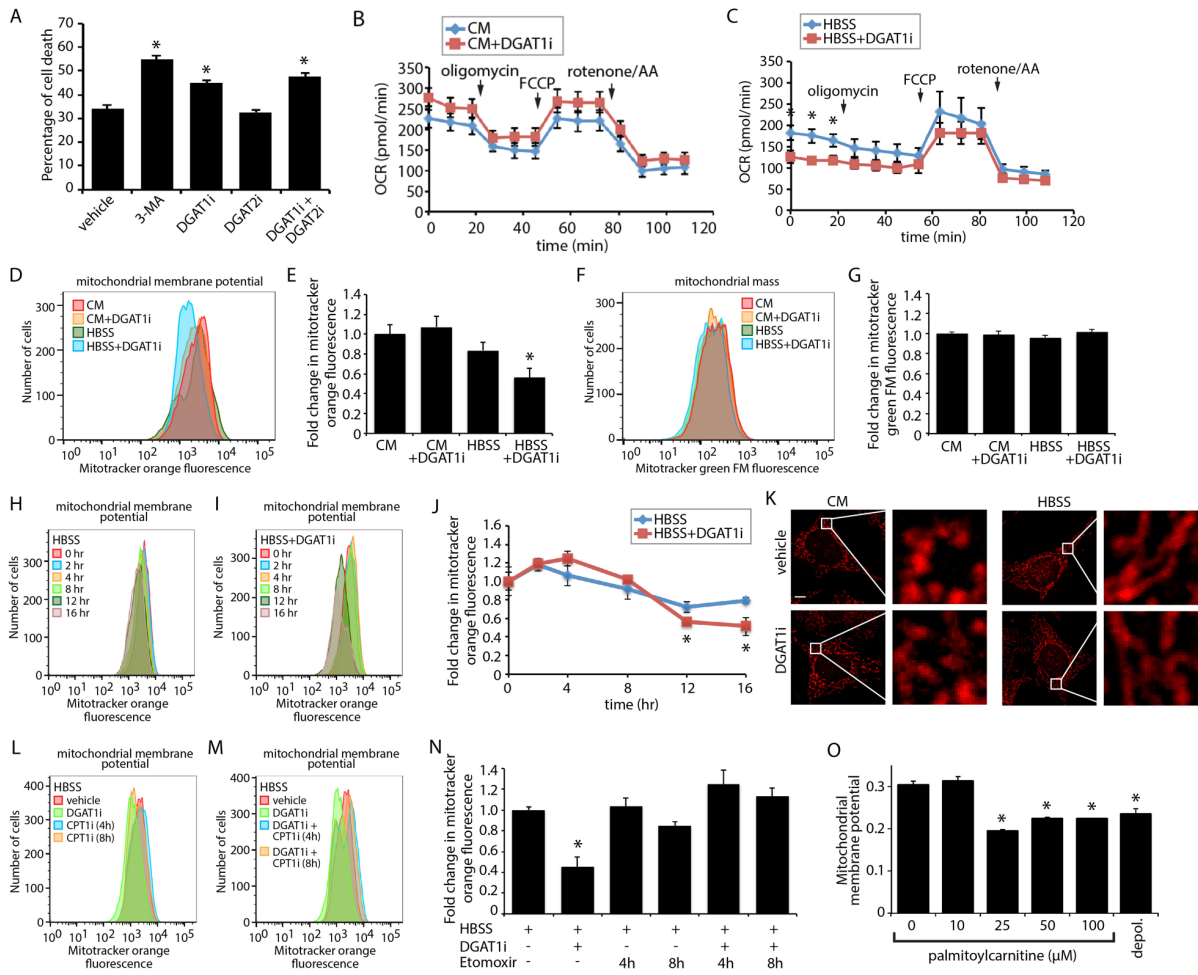
Figure 1-6. DGAT1-dependent LD biogenesis protects mitochondrial function during starvation
(A) MEFs were treated as indicated during a 16 hr HBSS starve. Cells were stained with propidium iodide and annexin-V, and the percentage of cell death measured by flow cytometry. *(B and C)* Oxygen consumption rates (OCR) were measured for MEFs incubated in CM *(B)* or HBSS *(C)* together with vehicle or DGAT1i for 16 hr. Oligomycin, FCCP, and rotenone/antimycin were added at the indicated time points. *(D and E)* Flow cytometry histograms *(D)* and the corresponding quantification of mean fluorescent intensity (n=3) *(E)* of MEFs stained with MitoTracker Orange CMTMRos following incubation in CM or HBSS together with vehicle or DGAT1i for 16 hr. *(F-H)* Flow cytometry histograms *(F and G)* and the corresponding quantification of mean fluorescent intensity (n=3) *(H)* of MEFs stained with MitoTracker Orange CMTMRos following treatment with vehicle or DGAT1i during an HBSS starvation for the indicated times. *(I and J)* Flow cytometry histograms *(I)* and the corresponding quantification of mean fluorescent intensity (n=3) *(J)* of MEFs stained with MitoTracker Green FM following incubation in CM or HBSS together with vehicle or DGAT1i for 16 hr. *(K)* MEFs were incubated in CM or HBSS for 16 hr in the presence or absence of DGAT1i. Mitochondria stained with MitoTracker Orange CMTMRos (red) were visualized by fluorescence microscopy. In the micrographs, white boxes indicate the magnified regions. Scale bars = 10 μm. *(L-N)* Flow cytometry histograms *(L and M)* and the corresponding quantification of mean fluorescent intensity (n=3) *(N)* of MEFs stained with MitoTracker Orange CMTMRos following treatment with vehicle, DGAT1i, and CPT1i (etomoxir) as indicated during an HBSS starvation for 16 hr. CPT1i was added for the final 4 hr or 8 hr of the experiment where indicated. *(O)* Mitochondria isolated from MEFs were stained with JC-9 and then incubated with increase concentrations of palmitoylcarnitine for 30 min. JC-9 fluorescence and mitochondrial diameter were measured by flow cytometry and the normalized mitochondrial membrane potential determined. The background value of depolarized mitochondria (depol.) was determined by incubation with valinomycin. All graphical data are quantified as mean ± SEM (n=3). An asterisk indicates a significant difference ($p < 0.05$, *t* test).
See also Figure S6 and Figure S7.
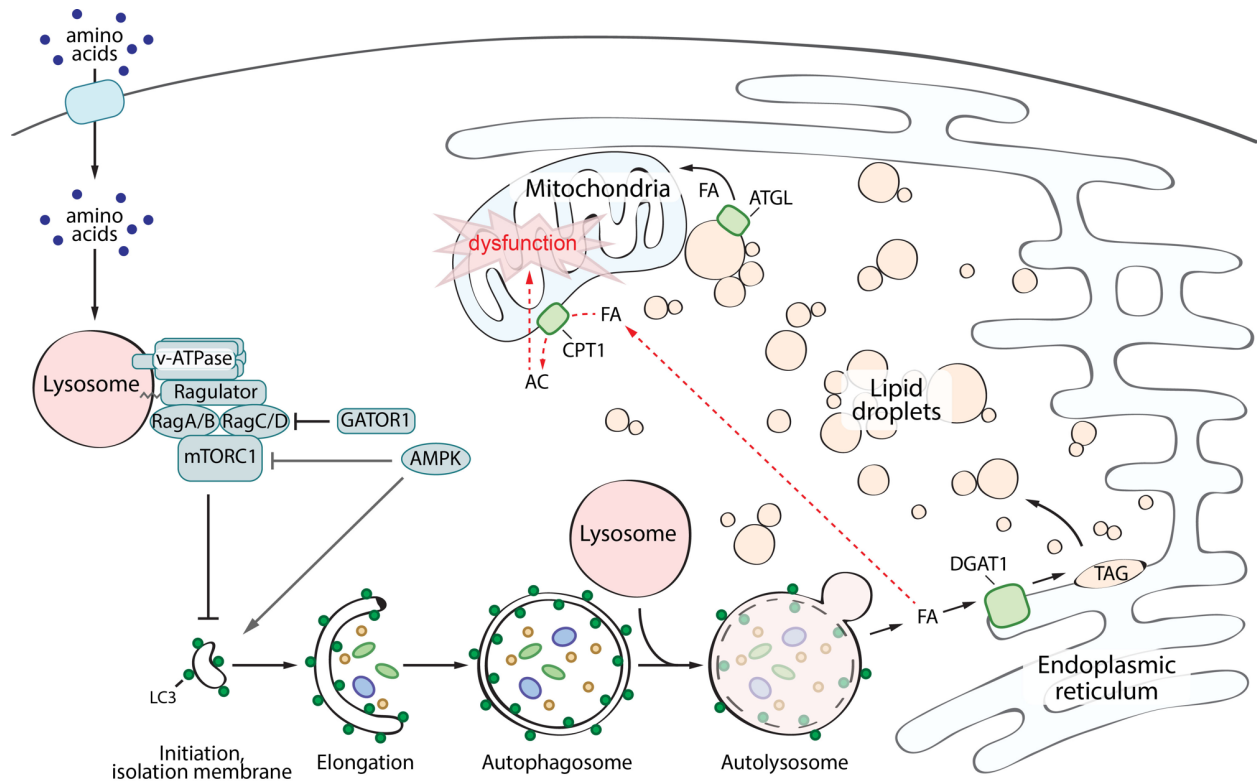
Figure 1-7. DGAT1-dependent lipid droplet biogenesis prevents lipotoxicity during starvation-induced autophagy

In the presence of sufficient amino acids, mTORC1 is recruited to the lysosome and activated through the actions of the Rag GTPases, the Ragulator complex, and the V-ATPase. Active mTORC1 inhibits the initiation of autophagy. In the absence of amino acids, mTORC1 is inactive and autophagy is upregulated. This pathway can be modulated by the Gator1 complex and AMPK signaling. Autophagic degradation of membranous organelles releases FAs that are selectively channeled into DGAT1-dependent LDs, which form clusters of LDs in close proximity to mitochondria. These new LDs are degraded by ATGL-mediated lipolysis, presumably supplying FAs to mitochondria for energy. These LDs also sequester FA in TAG, preventing acylcarnitine accumulation, which leads to mitochondrial dysfunction.

Supporting Information Figures
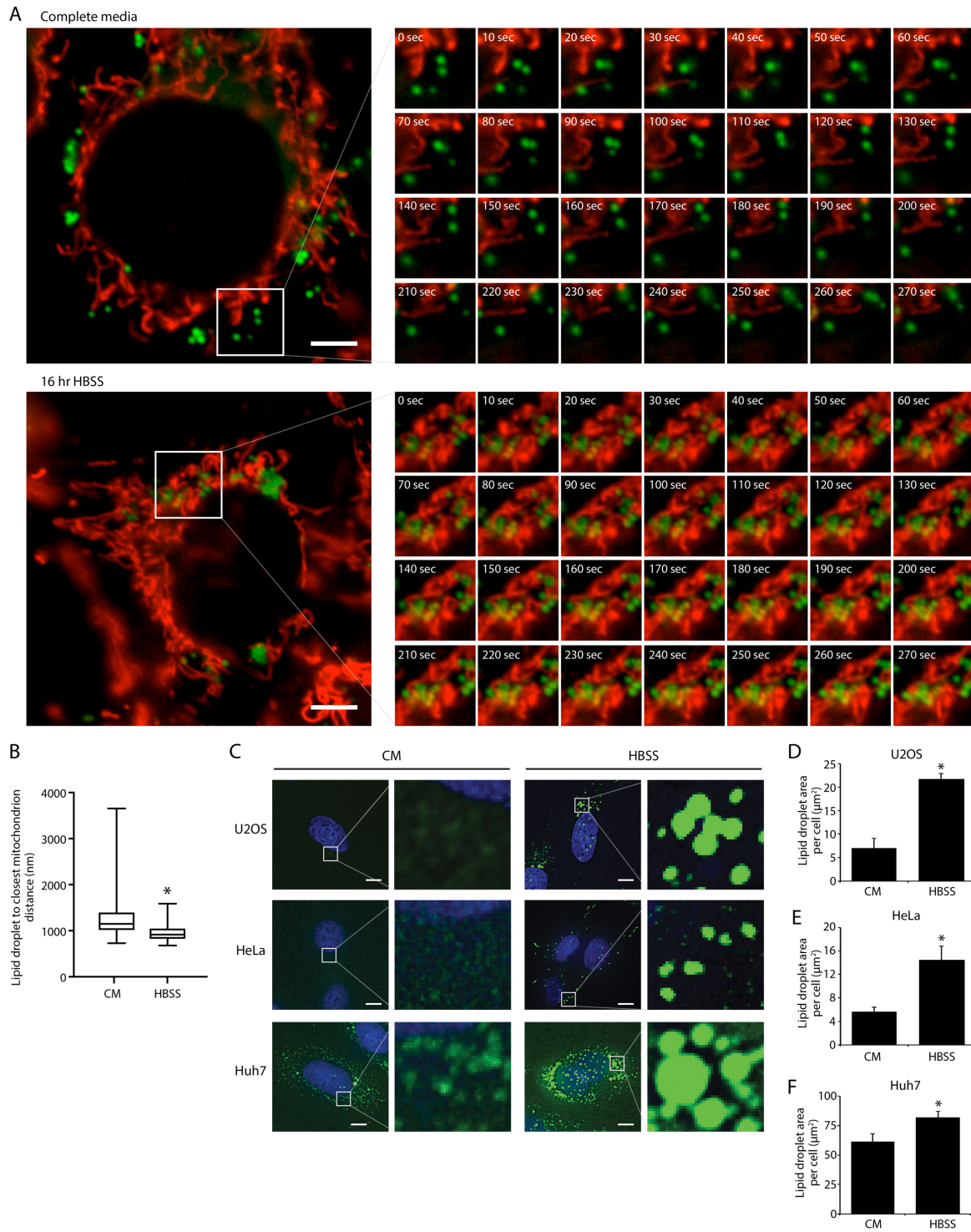
Figure S1-1. Starvation induces LD biogenesis in various cell types

(A) Representative images of LDs in living cells stained with BODIPY 493/503 (green) and mitochondria stained with mitotracker (red) in MEFs following 16 hr incubation in CM or HBSS. Time-lapse imaging of LDs and mitochondria in the boxed region is shown. *(B)* Images of live cells incubated in CM or HBSS for 16 hr and stained as in panel A were acquired and the distance from the center of a LD to the center of the closest mitochondrion was measured in 10 cells per condition (245 LDs in CM and 306 LDs in HBSS). *(C)* U2OS, HeLa, and Huh7 cells incubated in CM or HBSS were fixed and analyzed by fluorescence microscopy. LDs were stained with BODIPY 493/503 (green) and nuclei with DAPI (blue). *(D-F)* The abundance of LDs was quantified from U2OS (*D*), HeLa (*E*), and Huh7 (*F*) treated as in panel *C*. All graphical data are quantified as mean ± SEM. An asterisk indicates a significant difference ($p < 0.05$, *t* test) based on measurements from 10 cells in panel B or 50 cells from three independent biological replicates in panels D, E, and F. Scale bars = 10 μm.
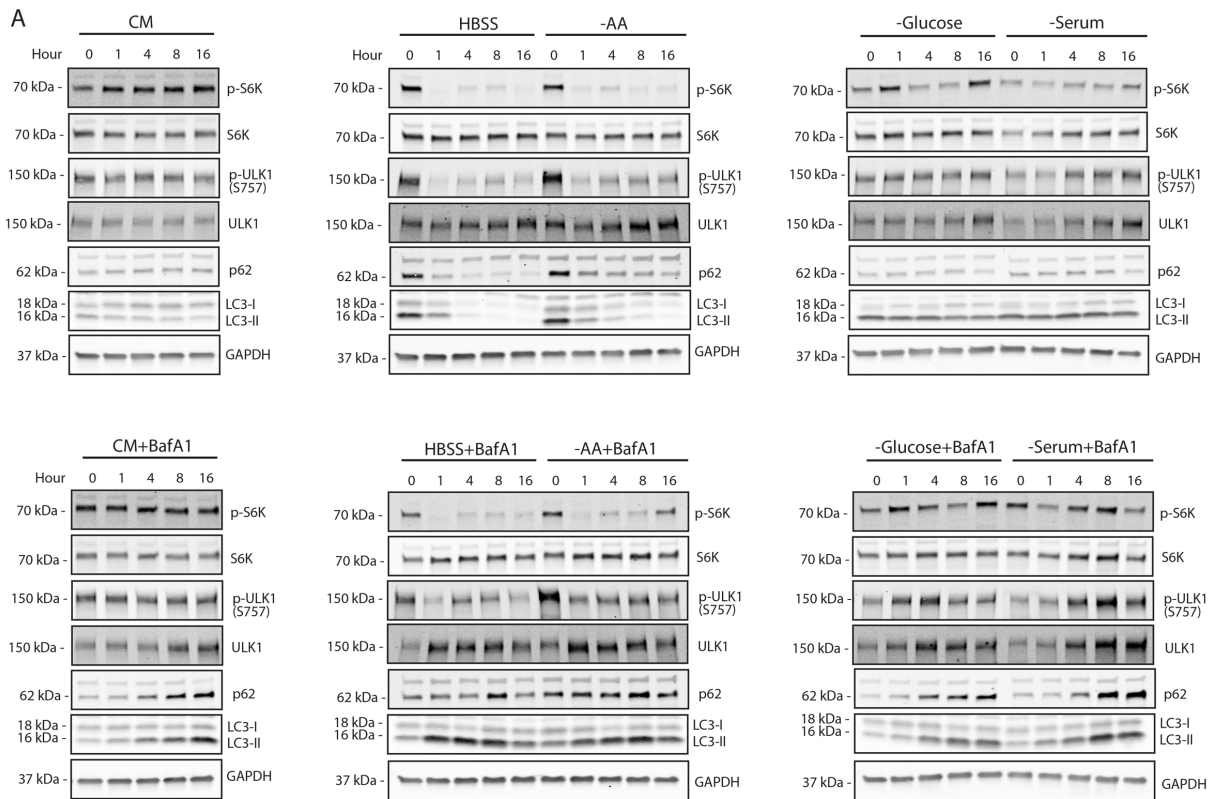
Figure S1-2. Amino acid deprivation induces autophagy

(*A*) Immunoblot analysis of LC3 and p62 degradation kinetics, mTORC1 activity (p-S6K and pULK), and autophagy initiation (p-ULK1) in MEFs incubated in the indicated media (CM, HBSS, -AA, -Glucose, -Serum) in the presence or absence of BafA1 for the indicated times. (*B*) MEFs stably expressing a GFP-LC3-RFP-LC3ΔG autophagy reporter were incubated in the indicated media in the presence and absence of BafA1 for 16 hr. The GFP:RFP ratio was measured by flow cytometry. All graphical data are quantified as mean ± SEM (n=3). An asterisk indicates a significant difference (p < 0.05, *t* test) based on three independent biological replicates.
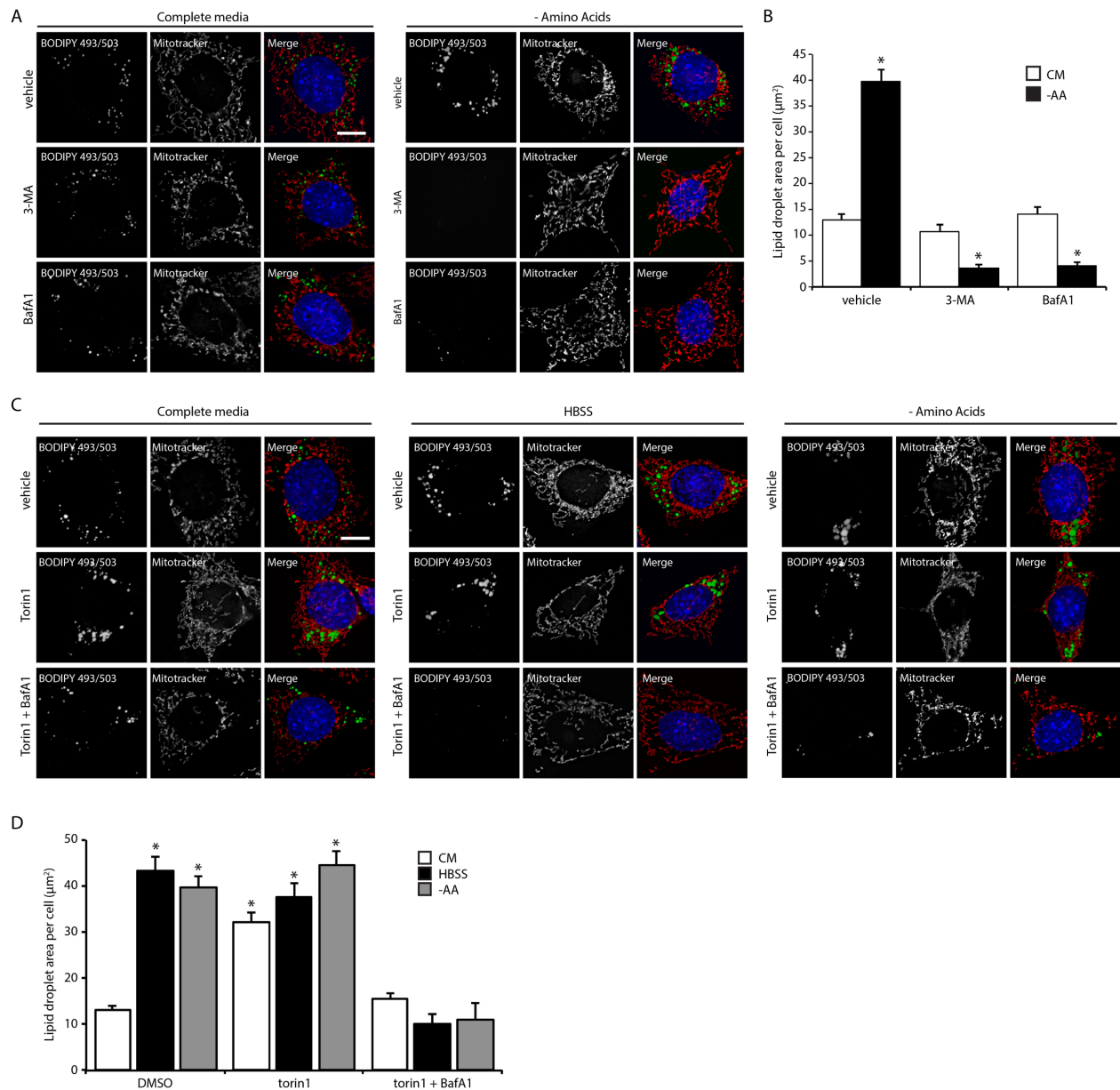
Figure S1-3. The role of mTOR and autophagy in LD biogenesis

(*A*) Fluorescence microscopy of MEFs incubated in CM or media lacking amino acids for 16 hr. MEFs were co-incubated with vehicle, BafA1, and 3-methyladenine (3-MA) as indicated and fixed. LDs were stained with BODIPY 493/503 (green), mitochondria with mitotracker (red), and nuclei with DAPI (blue). (*B*) The abundance of LDs was quantified from cells treated as in panel A. (*C*) Fluorescence microscopy of MEFs incubated in CM, HBSS, or media lacking amino acids for 16 hr. MEFs were co-incubated with vehicle, torin1, and torin1 + BafA1 as indicated and fixed. LDs were stained with BODIPY 493/503 (green), mitochondria with mitotracker (red), and nuclei with DAPI (blue). (*D*) The abundance of LDs was quantified from cells treated as in panel C. Scale bars = 10 μm. All graphical data are quantified as mean ± SEM. An asterisk indicates a significant difference (p < 0.05, *t* test) based on n = 50 cells from three independent biological replicates.
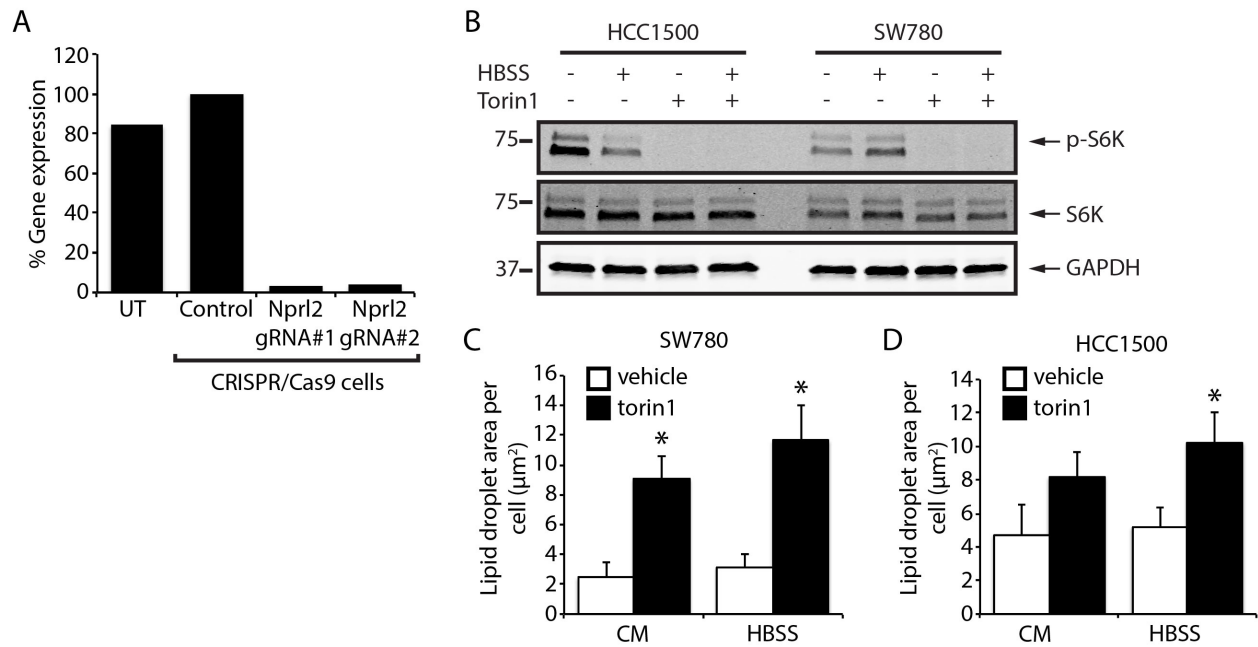
Figure S1-4. Constitutively active mTORC1 prevents starvation-induced LD biogenesis
(A) RT-qPCR gene validation of CRISPR/Cas9 disruption of the Nprl2 gene. *(B)* Immunoblot analysis of HCC1500 and SW780 cells incubated in CM or HBSS in the presence or absence of torin1 for 16 hr. *(C and D)* LDs in fixed cells were stained with BODIPY 493/503. Quantification of LD area of SW780 *(C)* and HCC1500 *(D)* cells treated as indicated for 16 hr. All graphical data are quantified as mean ± SEM. An asterisk indicates a significant difference (p < 0.05, *t* test) based on n = 50 cells from three independent biological replicates.
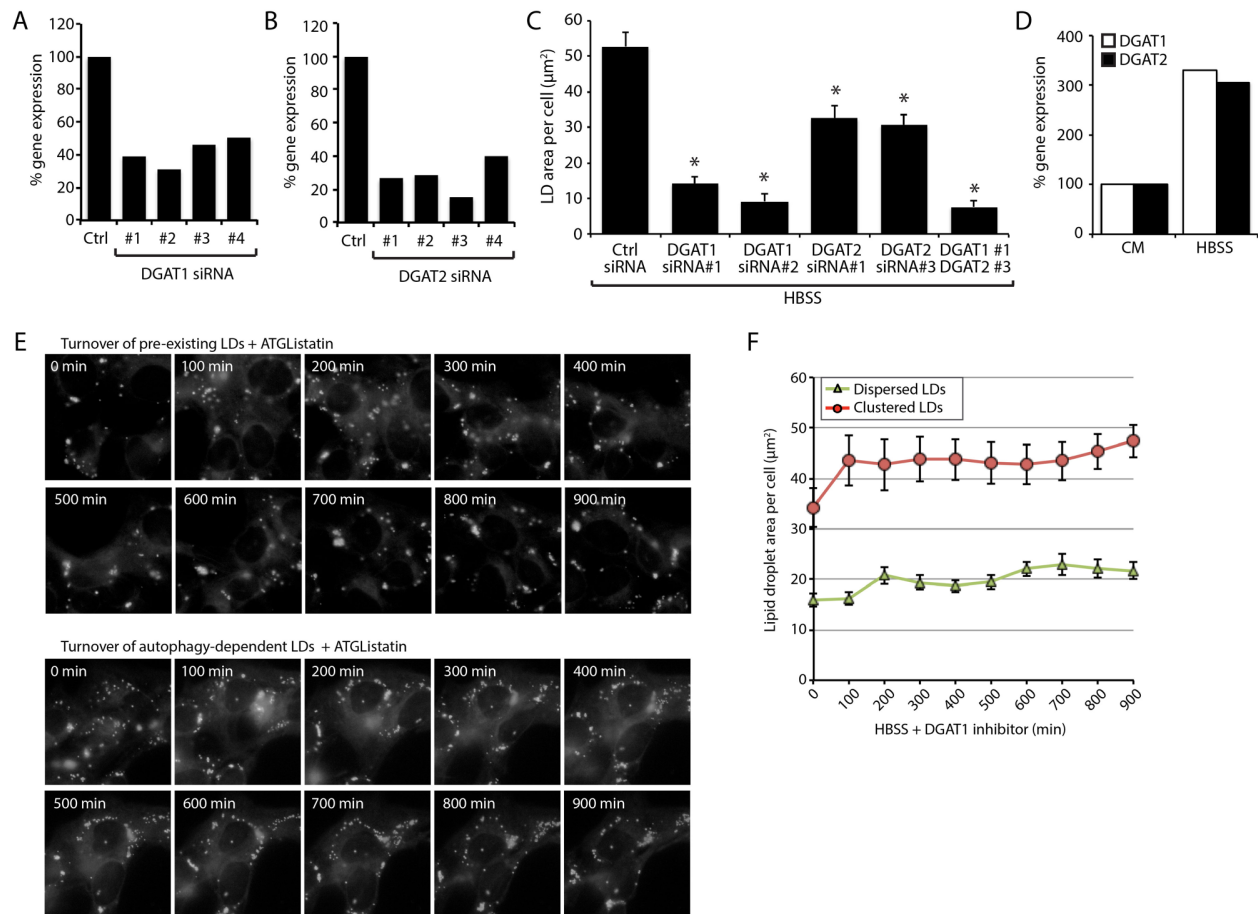
Figure S1-5. DGAT1 knockdown prevents LD biogenesis during starvation
(A and B) RT-qPCR validation of siRNA-mediated knockdown of DGAT1 *(A)* and DGAT2 *(B). (C)* Quantification of LD area in DGAT1 and DGAT2 knockdown MEFs starved in HBSS for 16 hr, fixed, and stained with BODIPY 493/503. *(D)* RT-qPCR of DGAT1 and DGAT2 expression levels in CM and HBSS for 16 hr. Scale bars = 10 μm. *(E)* Time-lapse montage of BODIPY 493/503 stained LDs in living cells illustrating the impact of 40 μM ATGListatin on the turnover of pre-existing LDs and autophagy-dependent LDs during HBSS starvation treated according to the paradigms in Figure 3E,F. (*F*) Quantification of LD abundance from cells in panel *G*. Graphical data for LD area are quantified as mean ± SEM. An asterisk indicates a significant difference (p < 0.05, *t* test) based on n = 50 cells from three independent biological replicates.
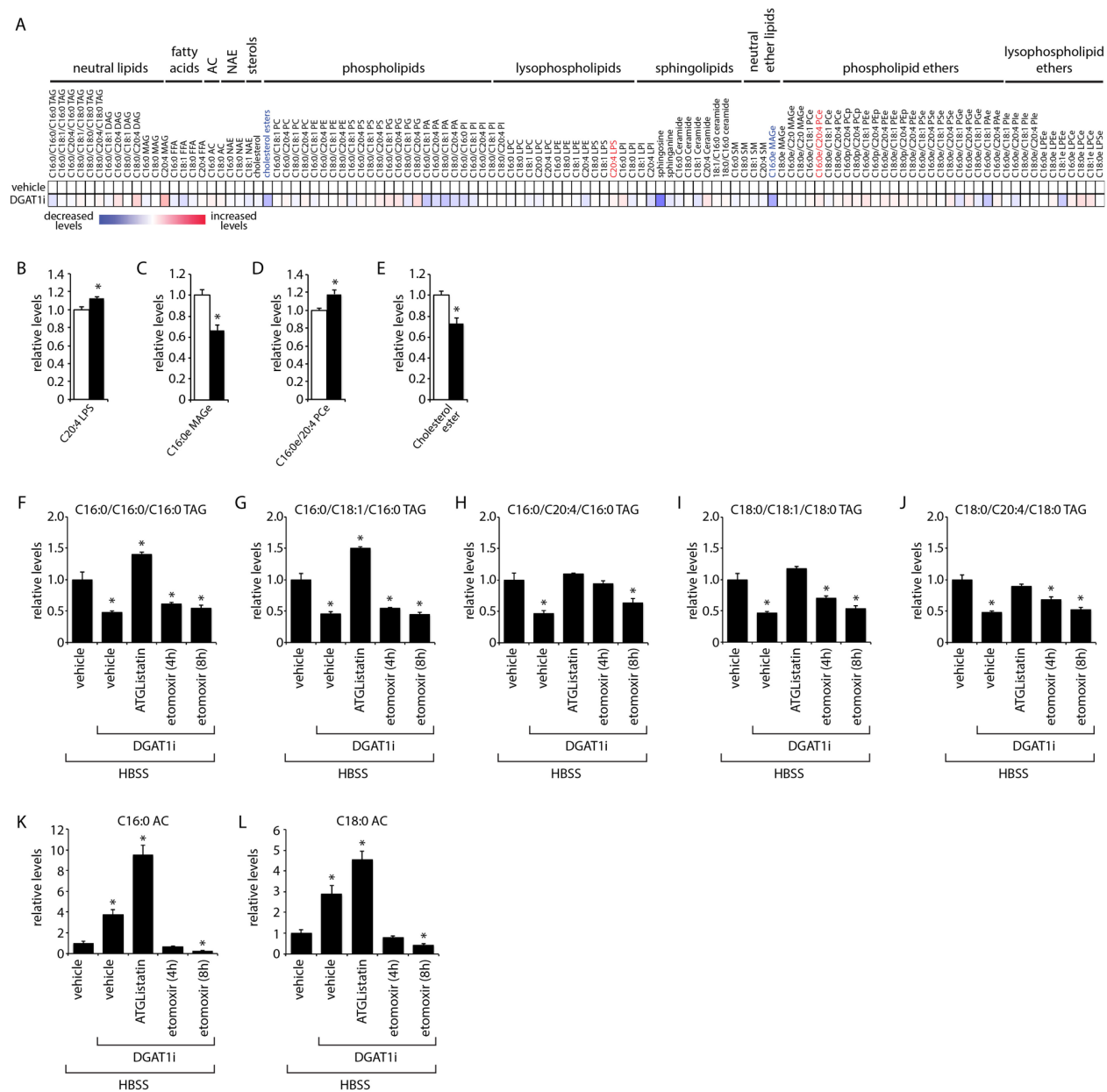
Figure S1-6. Lipidomic profiling by DGAT1 inhibition in complete media
(A) Heatmap of metabolomic alterations in MEFs incubated in CM in the presence or absence of DGAT1 inhibitor. Significantly altered lipids are indicated in blue (significantly decreased) and red (significantly increased). *(B-E)* Quantification showing the relative levels of significantly altered lipids. (*F-L*) The relative levels of TAGs and ACs were measured in HBSS starved MEFs incubated with DGAT1i and the indicated treatments. Asterisk indicates a significant difference relative to the vehicle control (p < 0.01, *t* test) (n= 4-5).
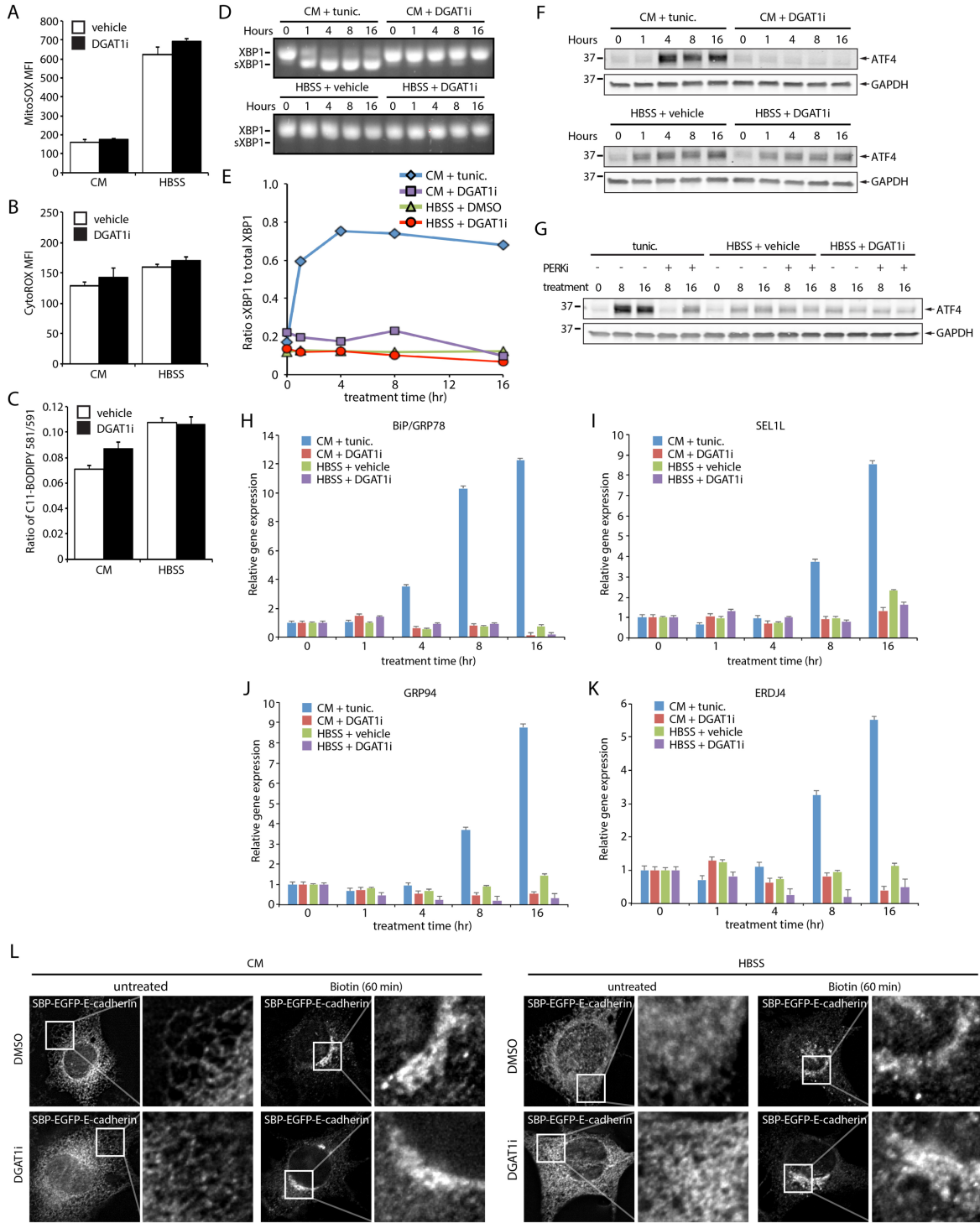
Figure S1-7. Analysis of ROS and ER stress during DGAT1 inhibition

(A-C) MEFs incubated in CM or HBSS were treated with vehicle or DGAT1i as indicated. Following a 16 hr incubation, MEFs stained with MitoSOX (*A*), CytoROX (*B*), or C11-BODIPY 581/591 (*C*) were analyzed by flow cytometry. Mean fluorescence levels (n=3; mean ± SEM) are displayed. (*D, E*) MEFs were incubated as indicated and XBP1 splicing evaluated by RT-PCR (*D*). The ratio of spliced XBP1 (sXBP1) to total XBP1 was quantified (*E*). (*F, G*) MEFs were incubated as indicated and ATF4 levels measured by immunoblotting. PERKi indicates co-incubation with 1 μM of the PERK inhibitor GSK2606414. (*H-K*) MEFs were incubated as indicated and the relative expression levels of BiP/GRP94 (*H*), SEL1L (*I*), GRP94 (*J*), and ERDJ4 (*K*) measured by RT-qPCR (n=3; mean ± SEM). (*L*) The retention using selective hooks (RUSH) system was employed to assess secretory system function. MEFs were transfected with a plasmid encoding Streptavidin-KDEL fusion protein (ER luminal hook) and streptavidin-binding protein (SBP)- and EGFP-tagged E-cadherin (reporter). Following incubations with CM or HBSS and DMSO or DGAT1i, 40 μM biotin was added for 60 min to release the reporter and allow for trafficking to the Golgi. The distribution of SBP-EGFP-E-cadherin (reporter) was visualized in fixed cells by fluorescence microscopy. A 4x zoom image of the boxed region is shown.

Supporting Information Tables

Table S1-1. RT-qPCR primers employed in this study

Gene	Direction	Primer sequence	Experiment
BiP/GRP78	Forward	GTCCAGGCTGGTGTCCTCTC	Figure S7H
BiP/GRP78	Reverse	GATTATCGGAAGCCGTGGAG	Figure S7H
SEL1L	Forward	GGTGTGCCACAACCTATGACT	Figure S7I
SEL1L	Reverse	TGGCTCTTCCTATTGCTTCCA	Figure S7I
GRP94	Forward	TCGTCAGAGCTGATGATGAAGT	Figure S7J
GRP94	Reverse	GCGTTTAACCCATCCAACTGAAT	Figure S7J
ERDJ4	Forward	CTCCACAGTCAGTTTTCGTCTT	Figure S7K
ERDJ4	Reverse	GGCCTTTTTGATTTGTCGCTC	Figure S7K
DGAT1	Forward	TCCGTCCAGGGTGGTAGTG	Figure S5A,C,D
DGAT1	Reverse	TGAACAAAGAATCTTGCAGACGA	Figure S5A,C,D
DGAT2	Forward	GCGCTACTTCCGAGACTACTT	Figure S5B-D
DGAT2	Reverse	GGGCCTTATGCCAGGAAACT	Figure S5B-D
Nprl2	Forward	CAGCTTTGTATCCAACGAGGAG	Figure S4A
Nprl2	Reverse	GCTGCTCGATCACCTTCAAG	Figure S4A

CHAPTER TWO

Temporal Control of Lipid Droplet-Mitochondrial
Contacts using Inducible Heterodimeric Tethers

Introduction

Lipid droplets (LDs) are dynamic and complex organelles that switch between periods of growth and consumption[83]. These processes are highly regulated by cellular metabolism and nutrient availability. Fatty acids (FAs) are stored in LDs when nutrients are plentiful, and are mobilized for energy production or for phospholipid synthesis during starvation[83]. The breakdown of triacylglycerols (TAGs) require the release of FAs from LDs through TAG hydrolysis by lipases, a process termed lipolysis. TAGs can also be hydrolyzed by selective degradation of LDs by autophagy, also known as lipophagy. Free FAs transferred to the mitochondria are metabolized by β-oxidation and the citric acid cycle to yield large amounts of ATP.

LDs sequester neutral lipids to prevent lipotoxicity and oxidative stress**Error! Bookmark not defined.**[, 9-13]. Thus, the cell must possess a mechanism to directly "hand over" free FAs between the storage and oxidation compartments to avoid high concentrations of cytotoxic FAs. One possible solution is mediated by the formation of membrane contact sites (MCSs). MCSs are regions where organelles are held in close apposition to facilitate the efficient exchange of lipids, metabolites, and ions[65, 84]. Contact sites between LDs and other organelles, including endoplasmic reticulum (ER), peroxisomes, mitochondria, and lysosomes (vacuoles in yeasts) have been previously observed[83-85]. Proteins that interact with two organelles directly, or form as part of a protein complex help to establish and maintain organelle associations are known as protein "tethers"[83-85]. For most of LD contact sites however, the identification of the tethering proteins, their mechanisms of regulation, and their functions remain unknown.

LDs have shown to form extensive contacts with the mitochondria in various tissues, including brown adipose tissue (BAT)[86], heart[87], and type I skeletal muscle[88]. In starved mammalian cells, FAs trafficked to the mitochondria are directly delivered from LDs and not from free cytosolic pools**Error! Bookmark not defined.**. During excess exercise, a condition that requires pronounced fat dependent ATP production, the skeletal muscle display rows of alternating LDs and mitochondria[88]. Thus, LD-mitochondrial contact may allow efficient and rapid delivery of FAs. This prevents replying on diffusion of FAs, and the potential accumulation of toxic lipids in the cytosol. Furthermore, LD-mitochondrial contacts may ensure that FAs are used for energy production, rather than fluxing into other lipid pools such as phospholipids for membrane biosynthesis during starvation or exercise.

A recent study suggested an alternative model[89]. The authors segregated mitochondria bound LDs from cytoplasmic mitochondria and found that LD-associated mitochondria have reduced β-oxidation, increased ATP synthesis capacities, and maintain a distinct protein composition due to low fusion-fission dynamics[89]. Interestingly, LD-associated mitochondria supported LD expansion and increases ATP synthase-dependent TAG synthesis, rather than oxidation of lipids. Discrepancies between studies may be partially explained by different approaches used to isolate the mitochondria[89]. Consistent with previous studies however, Benador et al. (2018) suggested that LD expansion may prevent muscle and liver injury from lipotoxicity during nutrient excess conditions, such as obesity[89]. Due to its diverse functions, in the regulation of intracellular lipid and energy metabolism, it is not surprising that abnormalities in LD biogenesis and degradation

are involved in many pathological and physiological conditions. Some examples include neutral lipid storage disease, atherosclerosis, and obesity[16]. Thus, a better understanding of the function of LD-mitochondrial contacts may be important for developing new therapies for lipotoxic tissue injury and insulin resistance.

A system in which LD-mitochondrial association can be regulated will help resolve its function. A chemical-inducible dimerization system for example, allows spatial and temporal manipulation of target molecules within the cell, which allows determination of interactions and pathways that would otherwise be difficult to study[90]. The development of chemically regulated heterodimerizers has been influenced by the discovery of the mechanism of action of rapamycin, an inhibitor of the protein kinase mTORC1[90-93]. Within a cell, rapamycin binds to FKBP12, a 12 kDa cytosolic protein. Only then will the FKBP-rapamycin complex bind to FRB, 11 kDa domain of mTOR, rendering mTORC1 enzymatically inactive[90-93]. Thus, two proteins fused to FKBP and FRB are brought into close proximity in the presence of rapamycin[90-93]. The FKBP-FRB complex forms rapidly, and tightly in the presence of rapamycin, with high affinity for both proteins[90-93].

Rapamycin is an immunosuppressant that inhibits TORC1, an important protein kinase involved in cell growth, proliferation, and regulation of autophagy[93]. Therefore, application of rapamycin in cell culture may have pleiotropic effects. Rapamycin analogs (so-called rapalogs) were created to abolish binding to endogenous FRB[92]. The region where rapamycin normally binds to the endogenous FRB domain of TOR was modified by a bulky substituent[92]. To restore the dimerizing potency, the FRB domain was mutated (T2098L) to accommodate the rapalog by enlarging the binding pocket[92]. As a result, rapalog does not inhibit TORC1 but still readily induces dimerization of FKBP and the mutated FRB domain[92]. Raplog is applied for only a short time to minimize the broad effects initiated by its endogenous proteins[92]. The interaction is rapid, on a timescale of seconds to minutes, and is irreversible[92]. Cross-linking different membrane-bound organelles via FRB and FKBP was previously used to activate and inhibit small GTPase signaling pathways[91]. FBR-FKBP heterodimer system was also used to study the ER-mitochondrial junction, which was found to be important for calcium signaling between the two organelles[94]. Here we developed an inducible tethering of organelles with synthetic heterodimers (iTOSH) system that can be used to study the function of LD-mitochondrial contacts.

Inducible Tethering of Organelles with Synthetic Heterodimers (iTOSH) System in HeLa Cells

For labeling and functional characterization of LD-mitochondrial interface, we coupled the LD and OMM target sequences with two components of the FKBP-FRB heterodimerization system (**Figure 2-1A**). Here, FRB was fused to either a functionally inactive adipose triglyceride lipase (FRB-ATGL*) or perilipin 2 (FRB-PLIN2), both of which localized to LDs (**Figure 2-1B**). Tandem FKBP domains were fused to the TOM20 signal sequence (tom20ss-tdFKBPP), which targets to the mitochondria (**Figure 2-1B).** Yellow fluorescent protein was also fused to each of the heterodimer domains to test cytosolic protein recruitment (YFP-FRB and YFP-FKBP, **Figure 2-1B).** Western blot analysis confirms the expected molecular weights of all fusion proteins (**Figure 2-1C and 2-1E).**

We next confirmed that the FRB and FKBP domains can dimerize with the addition of rapalog. Following 30 min rapalog induction, YFP-FRB and YFP-FKBP were recruited to tom20-tdFKBP and FRB-PLIN2, respectively (**Figure 2-2A and 2-2B)**. This indicates that the FRB and tdFKBP domains are functional and can heterodimerize and recruit a cytosolic binding partner. To verify that the inducible heterodimer system is capable of inducing interorganelle tethering, we co-expressed tom20ss-tdFKBP and FRB-PLIN2 proteins in cervical cancer HeLa cells and analyzed their localization by immunofluorescence. With the addition of rapalog, the mitochondria were recruited and wrapped around FRB-PLIN2 coated LDs (**Figure 2-2C)**.

Fatty Acid Trafficking in Starved MEF Cells

During starvation, cells generate ATP by β-oxidation and oxidative phosphorylation in the mitochondria. This requires the transfer of FAs stored in LDs to mitochondria. To track FA flux from LDs to mitochondria during starvation, we utilized BODIPY558/568 C_{12} (Red-C12). Red-C12 is a saturated FA analog composed of 12-carbons and a BODIPY fluorophore with an overall length equivalent to an 18-carbon FA. Red-C12 was previously shown to incorporate into LDs, and used to study lipid trafficking in mouse embryonic fibroblast (MEF) cells**Error! Bookmark not defined.**. In the pulse-chase assay, MEF cells were incubated with 1 µM of Red-C12 for 16 hr. Excess amounts of Red-C12 were then washed out and replaced with either complete media (CM) or Hank's Balancing Salt Solution (HBSS) for 0, 3, 6, 12, 16 hr. After the indicated time points, the mitochondria were stained with MitoTracker Green FM and imaged live by fluorescence microscopy. During nutrient replete conditions, Red-C12 accumulated in LDs and was not transported to the mitochondria (**Figure 2-S1A, CM)**. In contrast, cells starved in HBSS showed a loss of Red-C12 signal from LDs and re-distributed to mitochondria after 16 hr of starvation (**Figure 2-S1A, HBSS**). The transfer of FAs was detectable even after 3 hr of starvation (**Figure2-S2B**), and near-complete overlap of Red-C12 with MitoTracker Green FM occurred after 16 hr of starvation (**Figure 2-S2B**). Previous studies confirmed that Red-C12 does not label other organelles**Error! Bookmark not defined.**. Furthermore, the amount of esterified Red-C12 was found to decrease with time during starvation, while the amount of free Red-C12 increases as analyzed by thin-layer chromatography**Error! Bookmark not defined.**. Inhibition of the mitochondrial FA importer, CPT1, with etomoxir partially blocked LD-to-mitochondria transfer of FAs**Error! Bookmark not defined. (Figure 2-S2C)** and breakdown of products Red-C12**Error! Bookmark not defined.**. These results indicate that FAs are transferred from LDs to mitochondria, and that Red-C12 is a substrate for β-oxidation during starvation.

Studies suggest that LD-mitochondrial contacts promote efficient transfer of FAs during starvation**Error! Bookmark not defined.**. If our hypothesis is correct, the time it takes to completely transfer Red-C12 from LDs to the mitochondria should decrease when we induce LD-mitochondrial tethering using the iTOSH system. We first confirmed that Red-C12 trafficking can be traced in wild-type HeLa cells. As expected, Red-C12 accumulated in LDs during nutrient replete conditions (**Figure 2-S1D)**. However, Red-C12 did not re-distribute to the mitochondria after 16 hr of HBSS starvation but remained in LDs (**Figure 2-S1D)**. U2OS cells also do not readily undergo lipolysis and transfer FAs from LDs to mitochondria during starvation (**Figure 2-S1E)**. It

is possible that these cells do not have similar lipolytic machineries as MEF cells to remove the BODIPY558/568 fluorophore covalently bound to the FA tail. Another possibility is that cancer cells, unlike MEF cells, rely on glycolysis rather than oxidative phosphorylation for ATP production, a process known as the Warburg effect[95]. In order to use Red-C12 to measure fatty acid flux, we decided to regenerate the iTOSH system in MEF cells.

Fatty Acids Trafficking in Starved MEF Cells Expressing the iTOSH System

For live cell imaging analysis, we generated stably expressing eGFP-FRB-PLIN2 and tom20ss-tdFKBP-BFP in MEF cells under a Tet-On, doxycycline (DOX)-inducible system **(Figure 2-1B)**. The addition of DOX for 48 hr induced eGFP-FRB-PLIN2 and tom20ss-tdFKBP-BFP expression (**Figure 2-3A).** eGFP-FRB-PLIN2 localized to LD-positive LipidTox, while tom20ss-tdFKBP-BFP colocalized to MitoTracker Orange CMTMRos (**Figure 2-3B).** Incubating the cells with rapalog, induced the recruitment of tom20ss-tdFKBP-BFP to eGFP-FRB-PLIN2 (**Figure 2-3C**), confirming FRB-FKBP heterodimerization.

Time-lapse microscopy was used track the localization of Red-C12 in MEF cells expressing the iTOSH system. Yellow arrows indicate a cell expressing both positive for eGFP-FRB-PLIN2 and tom20-tdFKBP-BFP. Prior to starvation, only eGFP-FRB-PLIN2 positive cells contained Red-C12 while non-positive cells did not accumulate Red-C12 **(Figure 2-3D)**. We observed an increase abundance of LDs over the course of starvation, which is consistent with previous studies that suggest autophagy-dependent LD biogenesis during HBSS starvation**Error! Bookmark not defined.**ˉ**Error! Bookmark not defined.**. Interestingly, cells expressing eGFP-FRB-PLIN2 retained Red-C12 (**Figure 2-3D**). It is possible that overexpressing PLIN2 is stabilizing LDs[96], or preventing LD turnover by crowding out endogenous proteins that are required to facilitate lipolysis and FA transfer[97]. Another possibility is that LD-mitochondrial contact in HeLa cells promote LD expansion rather than FA transfer[89].

Conclusion

Organelles are highly dynamic entities that interact and disengage from each other. Through these physical contacts, the organelles communicate to fulfill a specific function. Three types of functions are suggested: 1) the specific bidirectional transport of molecules such as various ions, lipids, amino acids, $Ca^{2+,}$ and metals[98-100]; 2) the transmission of signaling information or remodeling activities, such as organelle biogenesis, dynamics, inheritance, positioning, fission, and autophagy[101-106]; and 3) the position of enzymes to regulate their activity[105,107-108]. Hence, it is becoming evident that organelles are highly interconnected and that there are multiple functions for these physical associations at contact sites.

Contact sites are way for LDs and other organelles to communicate, contributing to their function in cellular metabolism[109-112]. For example, LDs needs to tightly communicate with the ER to coordinate lipid storage and synthesis. LDs also interact with other organelles to optimize

utilization of stored lipids under conditions of nutrient stress. However, the metabolic decision that results in LDs associated with mitochondria, peroxisomes, or induction of lipophagy is not fully understood. The function and regulation may depend on the cell type or metabolic conditions.

LDs are also involved in other cellular events other than lipid storage, ranging from protein degradation, sequestration of transcription factors, enzymes, chromatin components to generate lipid ligands for certain nuclear receptors[113]. Furthermore, LDs can be hijacked by various pathogens including viruses, bacteria, and parasites. Hepatitis C virus for example, was shown to hijack LDs for proliferation and assembly of capsid proteins[114]. Thus, our current understanding of LD function in organelle communication is still at its early stages. It is possible that LDs play other important functions at these contact sites that have yet to be explored.

LDs associated with mitochondria have been observed as early as 1959[115], but the function of the contact was unclear. Only recently did studies suggest that the physical interaction allows FAs released from LDs to be quickly taken up by juxtaposed mitochondria**Error! Bookmark not defined.**, and to prevent lipotoxicity**Error! Bookmark not defined.**. A more recent study demonstrated that the LD-mitochondrial contact facilitates LD expansion rather than breakdown[89]. However, the interaction is transient, where the two organelles engage in kiss-and-run events. A more stable contact can be achieved though starvation, cold exposure, or exercise depending on the cell type. Still, these perturbations are not fast, precise, and cannot be applied at desired time points. Here, we generated an iTOSH system that enables inducible, quick-onset, and specific perturbation of LD-mitochondrial contact in living cells.

In this system, the FRB and FKBP heterodimers were anchored to LDs and mitochondrial proteins. The addition of rapalog induced the formation of the FRB-FKBP complex, crosslinking the two membrane-bound organelles of the same cell together. This resulted in a striking morphological change, in which the typical tubular structure of the mitochondria overlapped and formed rings around LDs. We also tested other combinations of the anchor units and found that cytosolic proteins can be recruited to LDs or mitochondria. However, finer characterization will be required to examine the functional importance of the contact site.

The iTOSH system is useful for studying cases where membranes from different organelles are naturally tethered already. A similar strategy was used to study the ER-mitochondrial junction that is important for recruiting Ca^{2+} stored from the ER into the mitochondrial matrix[116]. This approach was also used to examine the ER-plasma membrane junction during Ca^{2+} release[117]. By varying the linker length, the authors demonstrated that space is required between the ER protein STIM1 and the plasma membrane Ca2+ channel Orai1[117]. These studies would have been difficult to achieve without the use of a chemically-inducible system.

A widely used method to detect interorganelle contact sites in live cells employs a fluorescent protein, such as split-GFP[118] or split-venus[119]. Each of the GFP fragments for example, are attached to known components at the contact site[118]. If the organelles interact, the GFP fragments will spontaneously assemble with each other to form a complete β-barrel structure of

GFP and emit GFP fluorescence[118]. This is a useful tool to detect pre-exiting organelle contact sites, but the tethering proteins has to be known. Furthermore, the system is irreversible which can perturb the physiological organelle-contact sites[118]. The size assembly of split-GFP signals for example, was found larger than those typically found at ER-mitochondrial contact sites and affected organelle morphology[118]. The split-GFP probes could also function as an artificial tethering protein between the organelles, and the expression levels of the probes can affect the visualization of organelle contact sites.

The iTOSH system resolves some of these issues. First, it can be used to study the function of interorganelle contact without knowing the identification of the tethering proteins. This is assuming that the organelles being studies are known to form contacts. Second, the iTOSH system can be regulated with rapalog, preventing adaptations at the contact sites. One limitation when using rapamycin or rapalog is its irreversibility, as the small molecules cannot be released from their binding proteins. It would therefore be beneficial to have a photo-destructible version that would allow transient heterodimer system that would mimic patterns observe in intact cells. Nevertheless, the iTOSH system can be used to complement prevailing perturbation methods to offer additional information regarding spatiotemporal dynamics and crosstalk between LDs and other organelles.

Materials and Methods

Cell Culture
MEFs, U2OS, HeLa, and HEK293T/17 cells were cultured in DMEM containing 4.5 g/L glucose and L-glutamine (Corning) supplemented with 10% fetal bovine serum (FBS; Thermo Fisher Scientific and Gemini Bio Products) at 37°C and 5% CO_2.

Fluorescence Microscopy
Cells grown on poly-L-lysine-coated coverslips were incubated in the presence or absence of 200 µM oleate for 16 hr. For the last 30 minutes of treatment, 100 nM of MitoTracker Orange CMTMRos or MitoTracker Green FM (Thermo Fisher Scientific) were added to the cells and incubated at 37°C. To induce FRB-FKBP heterodimerization, cells were treated with 250 nM rapalog (Clontech) during the mitochondria staining. Cells were then washed with PBS, fixed for 15 min in PBS containing 4% (wt/vol) paraformaldehyde, and permeabilized for 30 min with 0.1% triton diluted in staining buffer [PBS and 1% (wt/vol) bovine serum albumin]. Primary antibodies were incubated with staining buffer for 2 hr at room temperature. Cells were washed with staining buffers, and incubated with Alexa Fluor antibodies or 10 µg BODIPY 493/503 (Thermo Fisher Scientific) in staining buffer for 1 hr at room temperature. Cells were subsequently washed with staining buffer and mounted in Fluoromount G (Southern Biotech). Stained cells were analyzed by Deltavision Elite widefield epifluorescence deconvolution microscope with either a 40× air objective or a 60× oil immersion objective.

Fluorescent FA Pulse-Chase Experiments

2.5-5 X 10^4 cells were seeded on Nunc LabTek II chambered coverglass. Cells were incubated in DMEM complete media (CM) containing 1 μM BODIPY 558/568 C_{12} (Red-C12, Life Technologies) for 16 hr. Cells were washed three times with CM, incubated for 30 min to allow the fluorescent lipids to incorporate into LDs, and then chased for the time points indicated in CM or Hank's Balancing Salt Solution (HBSS; Invitrogen) in the presence or absence of various drugs. Mitochondria was labeled with 100 nM MitoTracker Green FM (Life Technologies) in the presence or absence of 250 nM rapalog for 30 min at 37°C prior to imaging live using the Deltavision Elite widefield epifluorescence deconvolution microscope with either a 40x air objective or 60x oil immersion objective. For time-lapse microscopy, cells were incubated at 37°C in a 5% CO2 humidified chamber and images were taken every 10 min for 16-24 hr with a 60x oil immersion objective.

Image Processing, Analysis, and Statistics
Image brightness and contrast were adjusted by ImageJ[82] and Adobe Photoshop CS. To quantify the fluorescence intensity of Red-C12 in mitochondria, we made a mask using the Mitotracker channel and the mean fluorescence intensity in the Red-C12 channel was calculated across the entire mask.

Plasmids and Reagents
Plasmids were generated using traditional restriction enzyme and ligation protocols. MEF TetR expression lines were generated by infection with pLenti CMV TetR Blast virus (716-1) (Addgene plasmid #17492) and treated with 10 μg/mL polybrene followed by selection in media containing 4 μg/mL blastidicin (Thermo Fisher Scientific). MEF TetR cells were subsequently infected with pLenti CMV/TO Puro DEST (670-1) or Hygro DEST virus (693-2) (Addgene plasmids #17293 and #17291) containing the FRB-FKBP fusion constructs and expressing cells were selected by FACS sort.

Plasmid transfections were performed using Fugene 6 (Promega) or X-tremeGENE HP (Roche) transfection reagent according to the manufacturer's instruction. Lentiviruses were produced in HEK293T/17 cells.

Reagents employed in this study, and their concentrations, include: 200 μM oleate (Sigma-Aldrich), 0.1% fatty-acid free BSA (Sigma-Aldrich), doxycycline (Sigma-Aldrich), 100 μM etomoxir (Cayman), and 50 μM orlistat (Sigma-Aldrich).

Immunoblotting
Cells were washed in PBS and lysed in 1% SDS. Protein amounts were normalized using bicinchoninic acid (BCA) Protein Assay (Thermo Fisher Scientific). Proteins were separated on 4-20% polyacrylamide gradient gels (Bio-Rad) and transferred onto low fluorescence PVDF or nitrocellulose membranes (Bio-Rad). Membranes were washed in PBS + 0.1% Tween-20 (PBST) and blocked in 5% (wt/vol) dried nonfat milk in PBST for 30 min to reduce non-specific antibody binding. Membranes were incubated for at least 2 hr in PBST containing 1% bovine serum albumin (BSA) (Sigma Aldrich) and primary antibodies. Following washing in PBST, membranes

were incubated with fluorescent secondary antibodies were diluted in 1% BSA in PBST at room temperature for 1 hr. All immunoblots were visualized on a LI-COR imager (LI-COR Biosciences).

The following antibodies were used: anti-S-tag (EMD Millipore), anti-HA-tag (Proteintech Group, Inc), anti-GFP (Proteintech Group, Inc), anti-α-tubulin (Cell Signaling Technology, Inc), anti-GAPDH (EMD Millipore). All IRDye680 and IRDye800 conjugated secondary antibodies for immunoblotting were obtained from Li-COR Biosciences.
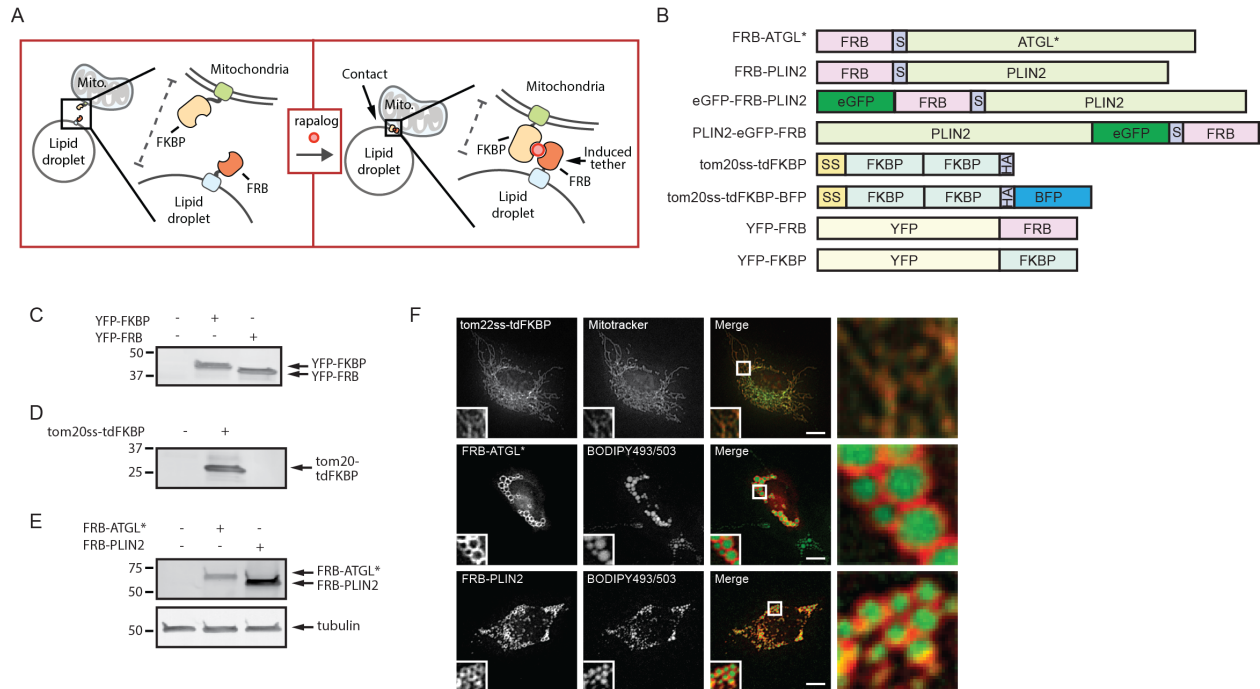
Figures

Figure 2-1. Inducible lipid droplet-mitochondria tethers and subcellular localization in HeLa cells.
(A) FKBP and FRB domains were fused to a mitochondrial and LD proteins, respectively. The addition of 250 nM rapalog, induces FKBP and FRB heterodimerization to promote LD-mitochondrial tethering. This system allows spatial and temporary control of inter-organelle contacts. *(B)* FRB and FKBP constructs used in this study. (*C-E*) Western blot analysis confirmed protein expression of FRB and FKBP constructs. *(F)* Transient transfected FRB and FKBP constructs treated with 200 µM oleate to induce LD biogenesis, and localization were analyzed by immunofluorescences. Cells were co-stained with either MitoTracker Orange CMTMRos (red) or BODIPY493/503 (green) to label the mitochondria or LDs, respectively. White boxes indicate where images were enlarged. Scale bars represent 10 µm.
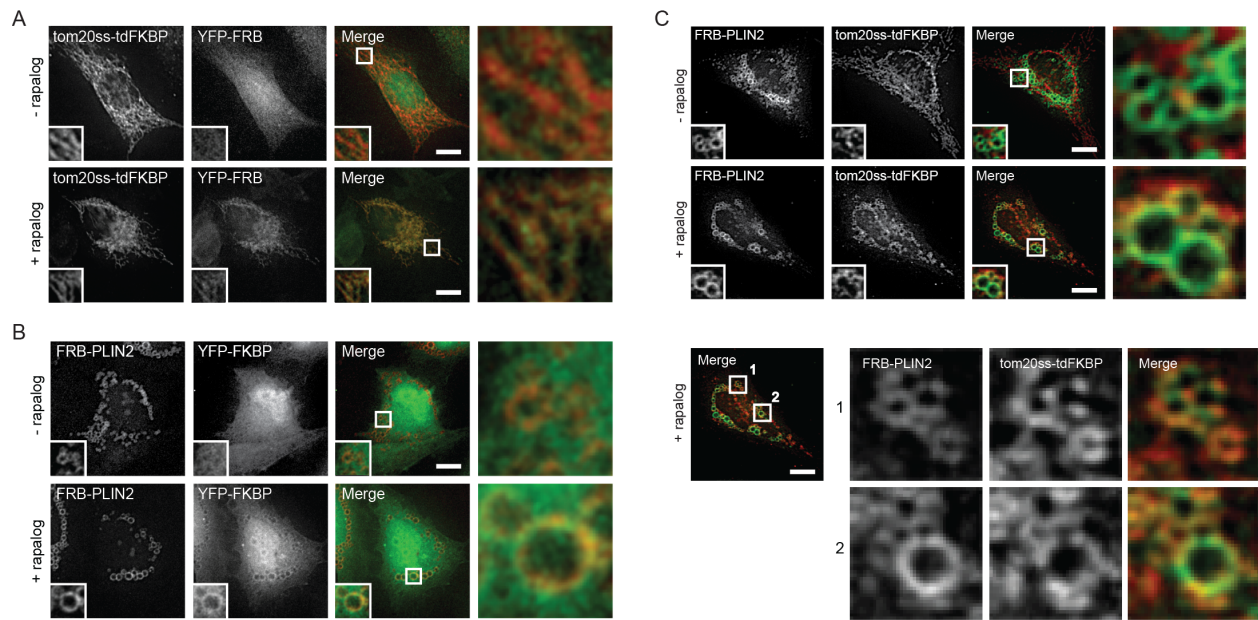
Figure 2-2. Inducible recruitment of heterodimer fusion proteins in HeLa cells

(A) Cells cotransfected with tom20ss-tdFKBP and YFP-FRB, *(B)* FRB-PLIN2 and YFP-FKBP, or *C)* FRB-PLIN2 and tom20ss-tdFKBP. (*A-B*) Cells were treated with 200 µM oleate overnight. Cells were subsequently incubated with 250 nM rapalog for 30 min, fixed, and analyzed by immunofluorescence microscopy using antibodies against *(A)* HA-tag (red), *(B)* S-tag (red), or *(C)* S-tag (green) and HA-tag (red). White boxes indicate where images were enlarged. Scale bars represent 10 µm.
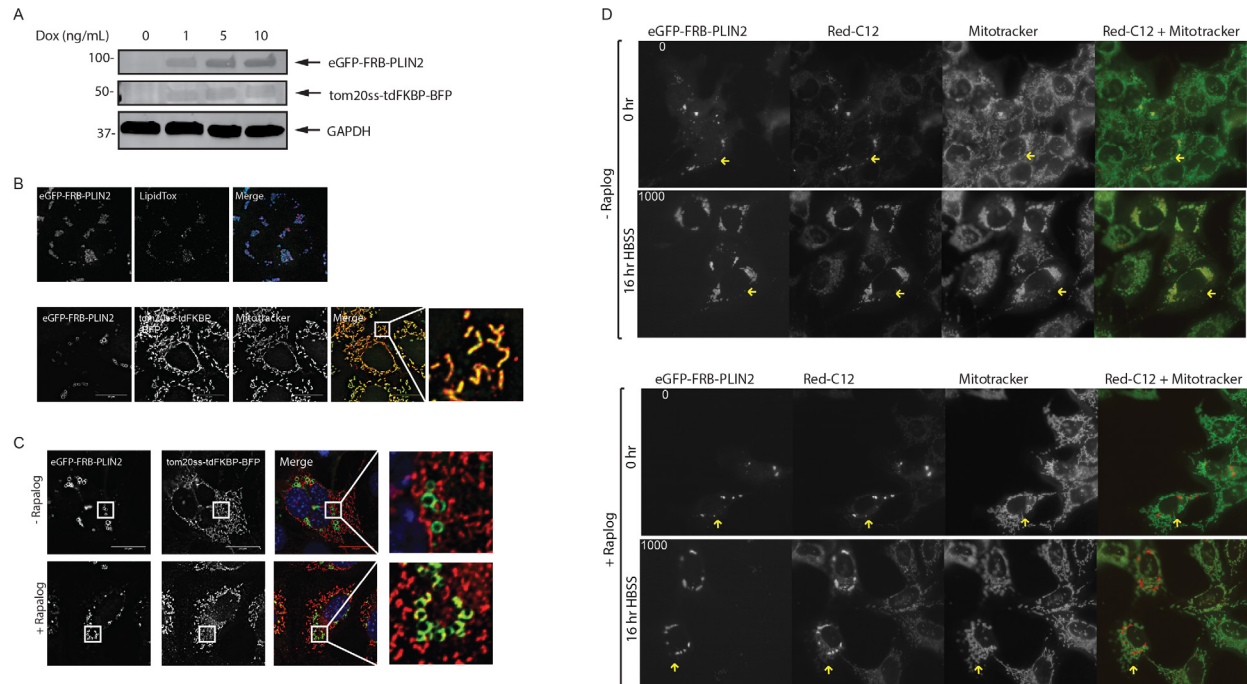
Figure 2-3. Inducible recruitment of heterodimer fusion proteins in MEF cells
(A) Cells were incubated with DOX for 48 hr and 200 μM oleate for 16 hr. Protein expression of heterodimer fusion proteins analyzed by Western blot. *(B-C)* Cells were incubated with 1 ng/mL DOX for 48 hr and 200 μM oleate for 16 hr. *(B)* Colocalization of heterodimer proteins costained with either LipidTox (red) or MitoTracker Deep Red (Red), and analyzed by fluorescence microscopy. BFP was difficult to visualize using the Deltavision microscope, so an antibody against HA-tag was used to image tom20ss-tdFKBP-BFP (green). *(C)* Cells incubated with 250 nM rapalog for 30 min, fixed, and analyzed by immunofluorescence microscopy using antibodies against HA-tag (red). Nucleus stained with DAPI (blue). *(D)* Cells were incubated with 1 ng/mL DOX for 48 hr, 1 μM Red-C12 for 16 hr, and 250 nM rapalog and MitoTracker Deep Red (green) for 30 min. Cells were then washed and replaced with HBSS at the start of the time-lapse movie. Images were taken every 10 min. Yellow arrows indicate cells that are positive for both eGFP and BFP. White boxes indicate are where image was enlarged. Scale bars represent 10 μm.

Supporting Information Figures

49
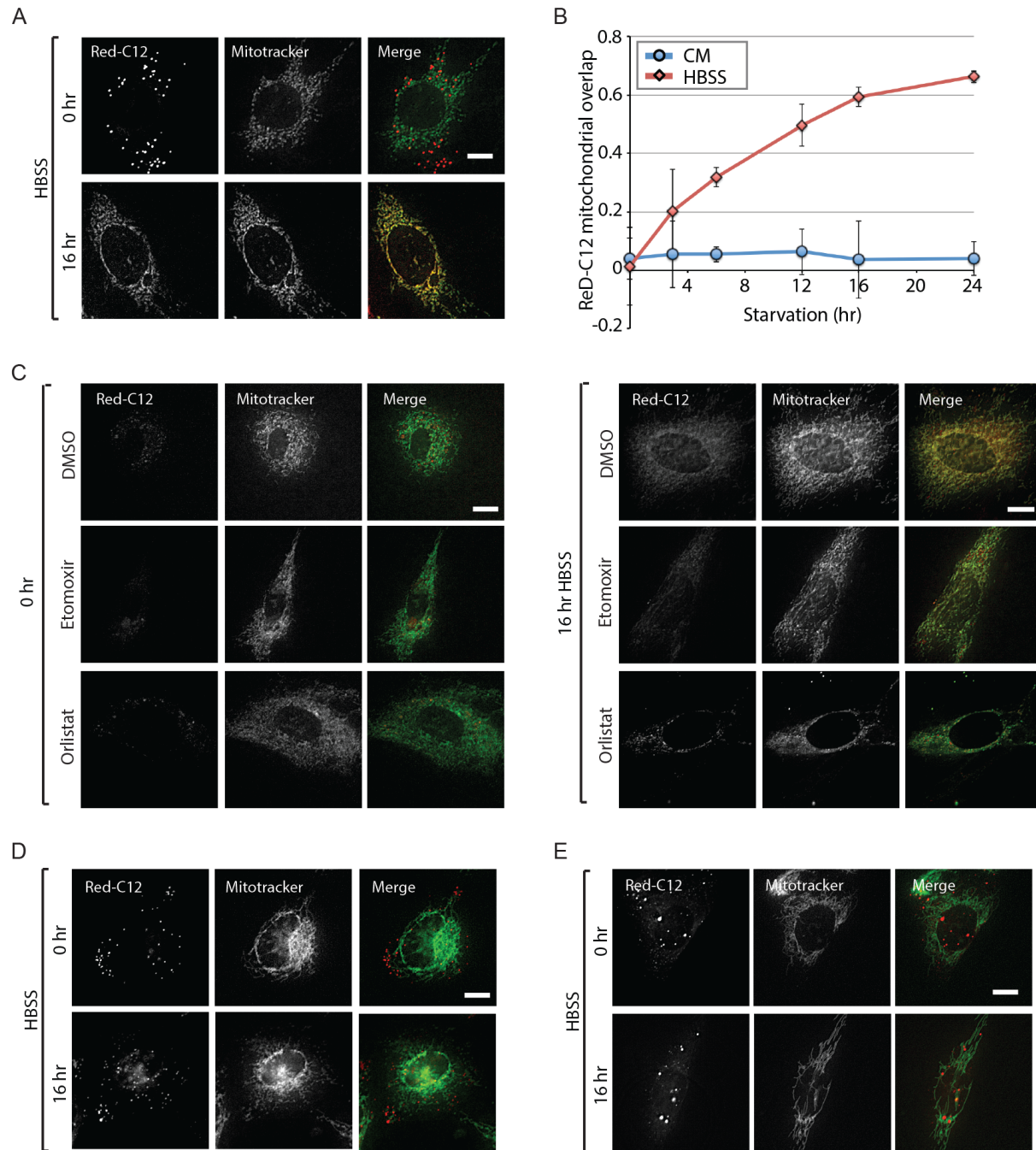
Figure S2-1. Fatty acid trafficking in cells

(A-E) Cells were treated with BODIPY558/568 C_{12} (Red-C12) overnight for 16 hr. Mitochondria were labeled with MitoTracker Green FM for 30 min prior to imaging the cells live by fluorescence microscopy. *(A)* MEF cells were washed and incubated in complete media (CM) or HBSS for 16 hr. *(B)* Relative cellular localization of Red-C12 was quantified by Pearson's coefficient analysis. *(C)* MEF cells were washed and treated with 100 µM etomoxir or 50 µM orlistat during the HBSS starvation for 16 hr. *(D)* Fatty acid flux in HeLa and *(E)* U2OS cells. Data are expressed as means ± SEM. Scale bars represent 10 µm.

CHAPTER THREE

A Proximity Labeling Strategy to Identify
LD-Mitochondrial Tethering Proteins

Introduction

Lipid droplets (LDs) communicate with other organelles to fulfill their numerous functions in cellular physiology. However, the unique structure of LDs prevents the exchange of materials with other organelles by bulk flow of bilayer vesicles. Unlike other organelles that contain an aqueous lumen, LDs comprise of a fatty core consisting of neutral lipids. Furthermore, the hydrophobic core of LDs is surrounded by a phospholipid monolayer instead of a bilayer. While, the phospholipid fatty acid tails orient towards the neutral lipid core, the hydrophilic head-groups point towards the cytosol. Thus, the structure properties of LDs are incompatible with regular fusion and fission events with bilayer bounded organelles.

Membrane contact sites (MCSs) are an alternative way for interorganelle communication that bypasses the vesicular traffic[65,84]. Contact sites are specialized regions where regulatory complexes are assembled between organelles to promote efficient and rapid transfer of lipids, ions, and other small molecules[65, 84]. At the heart of the contact sites are proteins or complex of proteins termed "tethers" that bind and maintain the interacting organelles at a defined distance (~10-70 nm)[65, 84]. Non-tethering proteins at the contact sites can help mediate adaptation or fulfill the function of the contact sites such as exchange of materials[65, 84]. Protein tethers can also function as regulators or effectors[65, 84].

Little is known about the tethers that mediate the attachment of LDs to other organelles. Several proteins have been reported to play a role in LD-mitochondrial contact sites formation, including the SNARE protein SNAP23**Error! Bookmark not defined.**. SNAP23 deletion in mouse fibroblasts resulted in a reduction LD-mitochondrial interaction and β-oxidation, but the mechanism is still unclear**Error! Bookmark not defined.**. In brown adipose tissue (BAT), perilipin 1 (PLIN1), a member of the perilipin family of LD proteins has been reported to be involved in LD-mitochondrial interactions[86]. PLIN1 was found to interact with the outer mitochondrial membrane fusion GTPase mitofusion 2 (MFN2)[86]. MFN2 deletion decreased LD-mitochondrial interactions and altered lipid metabolism[86]. However, the main role of MFN2 is in mitochondrial fusion. Thus, it is unclear whether the effects from MFN2 deletion is due to alterations in mitochondrial fusion or LD-mitochondrial tethering. To date, it is still unclear whether PLIN1 and MFN2 are true LD-mitochondrial tethers, or other proteins may be involved.

The most well-studied LD-mitochondrial interactor is perilipin 5 (also known as PLIN5 or LSDP5), a different member of the perilipin family[20,81,121-123]. PLIN5 is highly expressed in oxidative tissues, including BAT, cardiomyocytes, skeletal muscle, and liver[81,124-126]. PLIN5 stabilizes LDs by inhibiting hydrolysis and channeling fatty acids (FAs) to triacylglycerol (TAG) stores at the expense of FA oxidation, thus protecting mitochondria from a local surge in FA flux[127]. Indeed, PLIN5 was found to improve hepatic lipotoxicity and prevent hepatosteatitis by inhibiting lipolysis[128]. Unlike other perilipin proteins however, overexpressing PLIN5 has been shown to induce mitochondria recruitment to LDs in multiple cell and tissue types, including CHO cells, hepatic AML12, cardiac HL-1, primary brown adipocytes, INS1 cells, and mouse heart[87,89, 121,129]. Super-resolution microscopy also confirmed that PLIN5 localized to the LD-mitochondrial contact sites[123]. The last 20 amino acids from the C-terminus of PLIN5 was found to be necessary and sufficient for LD-

mitochondrial association[20]. However, it is unclear whether PLIN5 directly acts as a LD-mitochondrial tether, or if it affects the association between the two organelles by an indirect mechanism. Furthermore, the mitochondrial protein that is tethered to PLIN5 is currently unknown. Thus, the identification of LD-mitochondrial tethering proteins will allow experimental manipulations to understand their biological functions at the contact sites.

To identify LD-mitochondrial protein tethers, we employed a proximity-labeling technique using engineered ascorbate peroxidase (APEX)[130-135]. APEX is a 27 kDa monomeric ascorbate peroxidase that catalyzes the oxidation of biotin-phenol to a short-lived (<1 ms) biotin-phenoxyl radical in the presence of hydrogen peroxide (H_2O_2)[130-135]. This results in biotinylation of electron-rich amino acids (tyrosine, tryptophan, cysteine, and histidine) of neighboring proteins[130-135]. A more catalytically active APEX2 was developed soon after[131-133]. APEX was successfully used to map the proteome of LDs[132], mitochondrial intermembrane space[130], and primary cilia[133]. In addition to organelle profiling, was used as a tool to identify protein-protein interactions. For example, APEX2 was fused to ER-resident Ca^{2+} sensor STIM1 to map the proteome of the ER-PM junction[134]. This led to the identification of STIM-activating enhancer TMEM110 (STIMATE)[134]. APEX2 also used to identify an ER-shaping protein, reticulon 1A (RTN1A), as an ER-mitochondrial contact promoter at the contact sites[135]. Proximity-labeling techniques could be useful to discover proteins at the LD-mitochondrial junction, and further unravel their communication and function.

Proximity-Labeling Strategy using APEX2

We generated hepatocarcinoma Huh7 cells inducible expressing APEX2 genetically fused to the N-terminus of PLIN5 (APEX2-PLIN5). A mutant version of PLIN5 (APEX2-PLIN5ΔC) that lacks the last 72 amino acids was also generated to control for non-specific labeling of mitochondrial proteins (**Figure 3-1A**). To facilitate the identification of proteins labeled by APEX2 at the LD-mitochondrial interface, we adopted a quantitative LC-MS/MS approach using ratiometric stable isotope labeling with amino acids in cell culture (SILAC) to subtract non-interacting mitochondrial proteins. Huh7 cells equilibrated in SILAC media were either parental cells (SILAC-light arginine and lysine), cells expressing APEX2-PLIN5 (SILAC-medium), or APEX2-PLIN5ΔC (SILAC-heavy). Cells were grown in SILAC media for at least two weeks, and treated with oleate overnight prior to biotinylation to induce LD biogenesis. Live, intact cells were then briefly incubated with biotin-phenol and H_2O_2 (BpH).

In the presence of BpH, APEX2 catalyzes the generation of a short-lived biotin-phenoxyl radical that form covalent adducts with electron-rich amino acids in proteins located within a 10-20 nm radius (**Figure 3-1B-1D**). The conjugation of biotin is irreversible and allows the enrichment of labeled proteins for proteomic analysis. This method not only preserves organelle architecture and minimizes post-lysis artifacts, but also label proteins that may weakly interact with PLIN5. Soluble biotinylated proteins were recovered and released from streptavidin beads, followed by LC/MS-MS analysis. APEX2-PLIN5 will not only biotinylate proteins associated with the monolayer of LDs[132] , but also other organelle proteins in its proximity (i.e. mitochondrial proteins) (**Figure**

3-1C). Overexpressed PLIN5ΔC is unable to recruit the mitochondria to LDs[20]. Thus, APEX2-PLIN5ΔC should not biotinylate mitochondrial proteins. Biotinylated outer membrane mitochondrial proteins that are highly enriched in APEX2-PLIN5 that are reduced in APEX2-PLIN5ΔC will be considered as potential interactors (**Figure 3-1B-1D).**

Generation and Characterization of LD-Targeted APEX2

Cells incubated with various concentrations of doxycycline (DOX) induced APEX2 fusion protein expression, and the addition of BpH increased the levels of biotinylated proteins (**Figure 3-2A and 3-2B)**. To confirm the localization of APEX2-PLIN5 and APEX2-PLIN5ΔC, cells were preloaded with oleate to induce LD biogenesis. Both APEX2-PLIN5 and APEX2-PLIN5ΔC decorated the periphery of LDs labeled by BODIPY493/503, indicating that APEX2 is recruited to the LD monolayer (**Figure 3-2C)**. As expected mitochondria stained with MitoTracker Orange CMTMRos was recruited to LDs in cells expressing APEX2-PLIN5, but not APEX2-PLIN5ΔC (**Figure 3-2D)**. This verifies that the C-terminus of PLIN5 is necessary for LD-mitochondrial interaction. Fluorescently-labeled streptavidin stained the periphery of LDs in both APEX2 fusion proteins, further confirming the proteins are catalytically active (**Figure 3-2E).**

Purification of Proximity-Labeled Proteins

Western blotting validated the expression and biotinylation of APEX2-PLIN5 and ΔC (**Figure 3-3A)**. No biotinylated proteins were present in mock-transfected (SILAC-light). As expected, PLIN5 was identified in the proteomics analysis with equivalent heavy/medium SILAC ratios, and was high relative to SILAC-light (**Figure 3-3B)**. Various outer mitochondrial proteins were identified from our analysis, including TOM70, MAVS, and MFN2 (**Figure 3-3C)**. Interestingly, perilipin 1 was previously reported interact with MFN2, and involved in LD-mitochondrial interactions in BAT[86]. However, there is equal heavy/medium (APEX2-PLIN5ΔC / APEX2-PLIN5) SILAC ratios (**Figure 3-3C)**, suggesting that MFN2 is not a specific LD-mitochondrial interactor in Huh7 cells. In two biological replicates, TOM70 had low heavy/medium SILAC ratios (**Figure 3-3B and 3-3C)**. This indicates that PLIN5-TOM70 interaction was lost following C-terminus deletion of PLIN5. The interaction is specific as shown by the high M/L ratio (**Figure 3-3D).**

Translocase of the outer membrane (TOM) is a protein complex consisting of seven subunits[136-137]. The core TOM complex includes TOM5, TOM6, TOM7, TOM22, and TOM40[136-137]. TOM70 and TOM20 loosely associated with the core complex[136-137], suggesting additional roles within the outer mitochondrial membrane (OMM). In yeast TOM70 was identified as a critical component of ER-mitochondria contact sites, where it recruits the ER-localized sterol-transporter Ltc1[138]. More recently, TOM70 was found clustered at distinct OMM foci that overlapped with ER-mitochondrial contact sites[139]. TOM70 depletion impaired isositol trisphosphates-linked ER to mitochondria Ca^{2+} transfer[139]. Both TOM70 and TOM20 are anchored to the OMM by a N-terminal hydrophobic sequence, while the remaining portion of the proteins are cytosolic and contains tetratricopeptide-repeat (TPR) motifs[140]. TPR are not only essential for recognizing pre-

proteins but also protein-protein interactions[141], suggesting that TOM70 may play a role in LD-mitochondrial interaction or function.

TOM70 is not Required for LD-Mitochondrial Contact

We performed a co-immunoprecipitation (co-IP) using S-peptide agarose to test whether APEX2-PLIN5 and TOM70 directly interacts. However, most *in vivo* protein-protein interacts are transient and occurs only briefly to facilitate signaling or function. To stabilize any weak protein-protein interactions, we treated the cells with dithiobis (succinimidylproprionate) (DSP), an amine crosslinker prior to co-IP. Crosslink of proteins were reversible in the presence of reducing agents. Unfortunately, APEX2-PLIN5 did not co-purify with either endogenous (**Figure 3-S1A**) or overexpressed TOM70 (data not shown), suggesting the proteins do not interact.

To test if TOM70 is required for LD-mitochondrial contact, we knockdowned TOM70 using siRNAs. Knockdown was confirmed by Western blot and immunofluorescence (**Figure 3-S1B and S1C**). Unfortunately, TOM70 knockdown in overexpressed APEX2-PLIN5 Huh7 cells did not prevent LD-mitochondrial interaction (**Figure 3-S1C**). This suggests that TOM70 is not necessary for LD-mitochondrial contact.

TOM70 is not Necessary or Sufficient for PLIN5-Mediated LD Tethering

MCSs that have multiple redundant tether machineries and tend to have a higher degree of plasticity compared to contact sites replying on a single tether. Redundant machineries make it difficult to determine how much each organelle-tethering structure contribute to the functions and formation of the entire organelle contact sites. Long-term genetic ablation of tethers may allow the rest of the contact sure machinery to adapt to the perturbation and may not be the optimal approach to identify contribution of a protein as a membrane tether. However, it is possible that TOM70 is a genuine LD-mitochondrial tether protein, but PLIN5 prefers a different protein at the contact site. (**Figure 3-S2A**).

To test if TOM70 is sufficient to tether to LDs, we targeted TOM70 to the ER membrane. Here, the cytosolic domain of TOM70 that contains the TPR motifs was fused to the N-terminus of cytochrome p450 (ERM-TOM70; **Figure 3-S2A**). The N-terminal 29 amino acids of cytochrome p450 was sufficient to retain it in the ER[142-143]. If our model is correct, TOM70 targeted to the ER membrane will be sufficient to recruit LDs to the ER (**Figure 3-S2B**). We generated DOX-inducible Huh7 cells expressing ERM-TOM70 (**Figure 3-S2C**) and APEX2-PLIN5, but we did not observe LD-ER recruitment (**Figure 3-S2C**). This confirms that TOM70 is not necessary or sufficient to mediate LD-mitochondrial interaction.

Conclusion

The cell is tightly packed with organelles, macromolecules, and small molecules. Communication between organelles has to be tightly organized to maintain normal cellular homeostasis. Indeed, defects in interorganelle communication have been shown to play a role in the pathogenesis of multiple human diseases[144-147]. More specifically, ablation of LD-mitochondrial contacts was reported to impair β-oxidation and alter lipid metabolism[20, 89]. SNAP23 and PLIN1 were suggested to be important for LD-mitochondrial interaction[19, 86]. However, MCSs tend to have redundant tethering proteins that play various functions depending on the cell and tissue type. Thus, identifying the full repertoire of proteins regulating LD-mitochondrial contact and understanding molecular events occurring at the contact sites are critical to developing potential therapeutic strategies for LD related diseases, such as obesity, diabetes, lipodystrophy, and steatohepatitis.

Overexpression of PLIN5 was shown to recruit the mitochondria to LDs[20,87,89,121,123,129], suggesting that PLIN5 is a potential LD-mitochondrial protein tether. However, the OMM protein that directly interacts with PLIN5 to maintain the contact is currently unknown. In this study, we applied proximity labeling using engineered APEX2 to identify proteins that exist within LD-mitochondrial contacts. Biotin-phenoxyl radical converted by APEX2 has a short half-life (<1 ms) and small labeling radius (<20 nm), which allows the capture of proteins in close proximity in live cells[130-135]. Previous protein tethers were identified from membrane fractions that could be a result of organelle contamination. Furthermore, weak protein-protein interactors may be lost during membrane fractionation and protein purifications. One advantage of our approach is that weak protein-protein interactors are preserved during our live-cell biotinylating assay. This approach was previously used successfully to capture novel proteins associated at the ER-mitochondrial contact[134].

To capture OMM proteins associated to PLIN5, we targeted APEX2-PLIN5 to LDs in Huh7 cells. Using SILAC radiometric, we purified biotinylated proteins using streptavidin-agarose beads. Although proximity labeling by APEX2 is highly specific, a combination of SILAC labeling and biochemical purification was shown to improve the specificity of targets identified by proximity labeling[130-135], especially if APEX2 is exposed to the outside membrane-enclosed cellular compartment. Conveniently, the C-terminus of PLIN5 is critical for LD-mitochondrial contact[20]. Thus, APEX2-PLIN5ΔC is the ideal control. Candidate mitochondrial tethers that are biotinylated by full length APEX2-PLIN5 should be excluded from APEX2-PLIN5ΔC.

Out of 803 biotinylated proteins identified by LC-MS/MS, 14 proteins are known OMM proteins. MFN2 was identified from our analysis, which was previously suggested to be a LD-mitochondrial tether protein[86]. However, the SILAC ratio of APEX2-PLIN5 relative to parental Huh7 control cells was 0.33. This suggest that MFN2 does not specifically interact with APEX2-PLIN5 even though it may be highly enriched at the contact sites. An interesting protein identified from our mass spectrometry analysis from two biological replicates was TOM70, previously shown to be involved in ER-mitochondrial contact. However, we found that TOM70 was not necessary for LD recruitment to the mitochondria. It is possible that TOM70 has other functions at the LD-mitochondrial junction other than tethering that have yet to be explored. For example, LD-

associated mitochondria may be important for LD expansion[89] or fatty-acid transfer**Error! Bookmark not defined.,Error! Bookmark not defined.**.

It is also possible that LD-mitochondrial contact may involve other mechanisms other than protein-protein interaction. Studies found that LD-mitochondrial association was resistant to tryptic digestion and high salt wash, but sensitive to detergents. This suggest that membrane-membrane interactions, such as hemifusion may help stabilize the contact. This process involves a transient fusion of the phospholipid monolayer of LDs with the OMM leaflet[148]. Although the contents of the interacting organelles do not mix, this type of interaction allows the direct exchange of metabolites and enzymes[148].

One disadvantage of the APEX2 technology is its high affinity for electron-rich residues, such as tyrosines[130-135]. It is possible that we were unable to identify a PLIN5-mitochondrial tethering protein because the electron-rich residues are masked and not readily accessible by phenoxyl radical. Furthermore, if PLIN5 is interacting with a mitochondrial lipid or directly inserted into the mitochondrial membrane, these would not be identified using APEX2. PLIN5 can also translocate to the nucleus and regulate gene transcription[149], suggesting that PLIN5 may be involved in the induction of expression of the components linking PLIN5 to the OMM. Although APEX2-PLIN5 is a useful tool, further work needs to be done to identify true LD-mitochondrial protein tethers. Identifying tethers that mediate attachment of LDs to other organelles will allow experimental manipulation of LDs contact sites and will advance our understanding of their exact biological functions.

Materials and Methods

Cell Culture
Huh7 and Hek293T/17 cells were cultured in DMEM containing 4.5 g/L glucose and L-glutamine (Corning) supplemented with 10% fetal bovine serum (FBS; Thermo Fisher Scientific and Gemini Bio Products)) at 37°C and 5% CO_2.

Huh7 TetR expression lines were generated by infection with pLenti CMV TetR Blast virus (716-1 (Addgene plasmid #17492) and treated with 10 µg/mL polybrene followed by selection in media containing 4 µg/mL blasticidin. Huh7 TetR cells were subsequently infected with pLenti CMV/TO Puro DEST virus (670-1) (Addgene plasmid #17293) containing APEX2 fusion constructs and expressing cells were selected in media containing 1 µg/mL puromycin.

Proteome Labeling
For each APEX2 cell lines, twenty 15-cm plates of cells were treated with 0.5 ng/ml doxycycline of 48 hr following by incubation in 200 µM oleate for 24 hr. Cells were then treated with 500 µM biotin-phenol for 30 min. Biotinylation of proteins were subsequently catalyzed by the addition of 1 µM H_2O_2 for 1 min. The reaction was quenched by washing the cells 3X with PBS containing 10 mM sodium ascorbate and 5 mM Trolox. Cells were harvested in PBS, centrifuged for 10 min at 500 x g, and cell pellets were incubated for 10 min in cold hypotonic lysis medium (HLM, 20

mM Tris-HCL pH 7.4 and 1 mM EDTA) containing cOmplete, Mini, EDTA-free Protease inhibitor Cocktail (Sigma-Aldrich). Cells were dounced 80X strokes in a 7 mL dounce and lysates were centrifuged at 1000 x g for 10 min. A final concentration of 1 % SDS was added to the supernatant, sonicated for 15 sec, and incubated for 10 min at 65°C.

Proteomic Analysis of Biotinylated Proteins
For isolation of biotinylated proteins, soluble fractions containing 1% SDS were diluted with PBS/0.1% Tween-20 (PBST) to a final concentration of 0.1% SDS. 50 μL of streptavidin-conjugated agarose bead slurry (Thermo Fisher Scientific) was washed 3X with PBST and added to the diluted samples for 4 hr at room temperature with constant mixing. Beads were centrifuged at 600 x g and washed 5X with PBST, followed by 3X washes with PBS and 3X washes with 50 mM ammonium bicarbonate. The beads were resuspended in one bread volume of 50 mM ammonium bicarbonate containing 0.02% Rapigest (Waters) (w/v), heated at 65°C for 15 min and bound proteins were digested O/N at 37°C with 1 μg mass spectrometry grade trypsin (Promega). After protein digestion, beads were removed and the supernatant was acidified to pH < 2 by addition of 500 mM HCl and incubated at room temperature for 45 min. Any precipitated materials were removed by centrifugation at 20,000 x g for 15 min. Peptides were dried down to a final volume of ~20 μL in a vacuum centrifuge.

Peptides were analyzed by LC-MS/MS on a Thermo Scientific Q Exactive Orbitrap Mass spectrometer connected to a Proxeon Easy-nLC II HPLC (Thermo Fisher Scientific) and Proxeon nanospray source at the University of California, David Proteomics Core Facility. Peptide identify and MS/MS counts were determined by analyzing RAW output files in MaxQuant (Max Planck Institute of Biochemistry) using the reviewed human protein database obtained from Uniprot. Variable modifications were set to include N-terminal acetylation and oxidation. The FDR was set to 1% and minimum peptide length was set to 6 amino acids.

Fluorescence Microscopy
Cells grown on poly-L-lysine-coated coverslips were incubated in the presence or absence of 200 μM oleate for 16 hr. For the last 30 minutes of treatment, 100 nM of MitoTracker Orange CMTMRos or MitoTracker Green FM (Thermo Fisher Scientific) was added to the cells in the incubated at 37°C. Cells were then washed with PBS, fixed for 15 min in PBS containing 4% (wt/vol) paraformaldehyde, and permeabilized for 30 min with 0.1% triton diluted in staining buffer [PBS and 1% (wt/vol) bovine serum albumin]. Primary antibodies were incubated with staining buffer for 2 hr at room temperature. Cells were washed with staining buffer, and incubated in Alexa Fluor secondary antibodies, and stained with fluorescent streptavidin-568 or LDs (10 μg BODIPY 493/403; Thermo Fisher Scientific) by incubating in staining buffer for 1 hr at room temperature. Cells were subsequently washed with staining buffer and mounted in Fluoromount G (Southern Biotech). Stained cells were analyzed by Deltavision Elite widefield epifluorescence deconvolution microscope with either a 60× oil immersion objective.

Plasmids and Reagents
Plasmids were generated using traditional site-directed mutagenesis, restriction enzyme and ligation, or polymerase incomplete primer extension (PIPE)[120] cloning protocols. Lentiviruses

were produced in HEK293T/17 cells. Plasmid transfections were performed using Fugene 6 (Promega) or X-tremeGENE HP (Roche) transfection reagent according to the manufacturer's instruction. siRNAs were obtained from Sigma Aldrich and transfected using Lipofectamine RNAiMAX (Thermo Fisher Scientific) according to the manufacturer's instructions.

Reagents employed in this study, and their concentrations, include: 200 µM oleate (Sigma-Aldrich), 0.1% fatty-acid free BSA (Sigma-Aldrich), doxycycline (Sigma-Aldrich), 500 µM biotin-phenol (Iris Biotech GmbH), 1 µM H_2O_2 (Sigma-Aldrich), puromycin (Invitrogen).

Co-Immunoprecipitation
Cells were washed with ice-cold PBS 3X, and proteins were crosslinked with 0.5 mM dithiobis (succinimidyl propionate) (DSP) at 4°C for 1 hr with occasional mixing. The cross-linking reaction was quenched in 200 mM Tris, pH 7.5 and incubated at 4°C for an additional 15 min. To remove excess unreacted DSP, cells were washed with ice-cold PBS 3X. Cells were collected, pelleted at 500 x g for 5 min. Cells were resuspended in lysis buffer (50 mM Tris (pH 7.5), 150 mM NaCl, 1% Triton) containing cOmplete, Mini, EDTA-free Protease inhibitor Cocktail (Sigma-Aldrich) and rotated at 4°C for 30 min. Supernatant was collected after centrifugation at 20,000 x g and 1 mg of proteins were purified with S-protein agarose beads. The beads were washed with lysis buffer 5X and incubated at 65°C for 15 min in the absence or presence of reducing agents (10% β-mercaptoethanol and 0.1 M dithiothreitol).

Immunoblotting
Cells were washed in PBS and lysed in 1% SDS. Protein amounts were normalized using bicinchoninic acid (BCA) Protein Assay (Thermo Fisher Scientific). Proteins were separated on 4-20% polyacrylamide gradient gels (Bio-Rad) and transferred onto low fluorescence PVDF or nitrocellulose membranes (Bio-Rad). Membranes were washed in PBS + 0.1% Tween-20 (PBST) and blocked in 5% (wt/vol) dried nonfat milk in PBST for 30 min to reduce non-specific antibody binding. Membranes were incubated for at least 2 hr in PBST containing 1% bovine serum albumin (BSA) (Sigma Aldrich) and primary antibodies. Following washing in PBST, membranes were incubated with fluorescent secondary antibodies were diluted in 1% BSA in PBST at room temperature for 1 hr. All immunoblots were visualized on a LI-COR imager (LI-COR Biosciences).

The following antibodies were used: anti-S-tag (EMD Millipore), anti-TOM70 (A-8) (Santa Cruz), anti-GAPDH (EMD Millipore), IRDye800 conjugated streptavidin (LI-COR Biosciences). All IRDye680 and IRDye800 conjugated secondary antibodies for immunoblotting were obtained from Li-COR Biosciences.
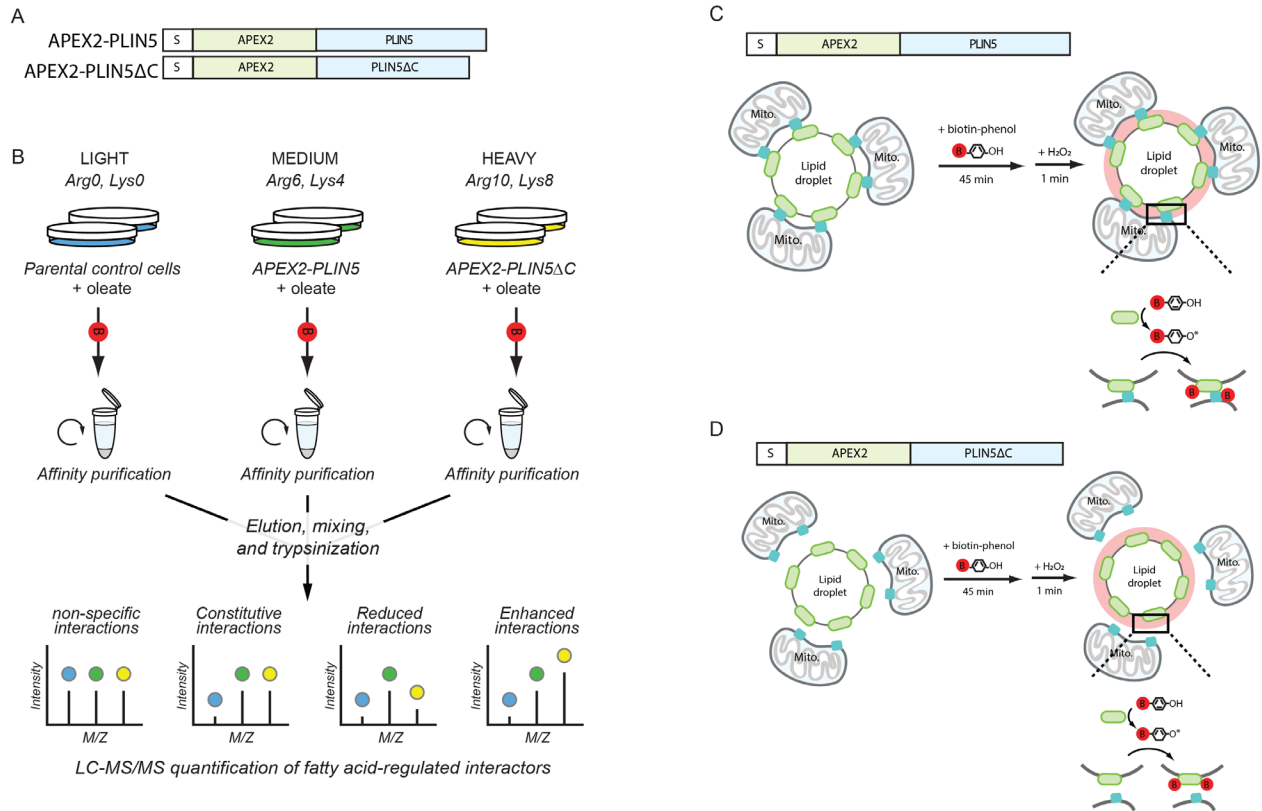
Figures

Figure 3-1. Illustration of the proximity labeling strategy to identify LD-mitochondrial tethering proteins

(A) APEX2 constructs used in this study. *(B)* Illustration of the proximity labeling strategy to identify LD-mitochondrial tether proteins. Huh7 cells expressing APEX2-PLIN5 or APEX2-PLIN5ΔC were cultured in medium or heavy lysine and arginine-containing SILAC media, and parental Huh7 cells were grown in SILAC-light. Cells were treated with doxycycline (DOX) for 48 hr to induce expression of PLIN5-targeted APEX2 proteins, and then oleate for 24 hr to induce LD formation. Upon the addition of biotin-phenol and hydrogen peroxide (H_2O_2), APEX2 covalently modifies proximal protein with biotin. Biotinylated proteins were subsequently affinity purified, eluted, mixed at equal ratios, trypsinized, and identified by mass spectrometry. *(C)* Illustration of the proximity labeling strategy to identify mitochondrial tethering proteins in proximity to full length APEX2-PLIN5, *(D)* that are not biotinylated with APEX2-PLIN5ΔC that lacks the last 72 amino acids at the C-terminus necessary for LD-mitochondrial interaction.
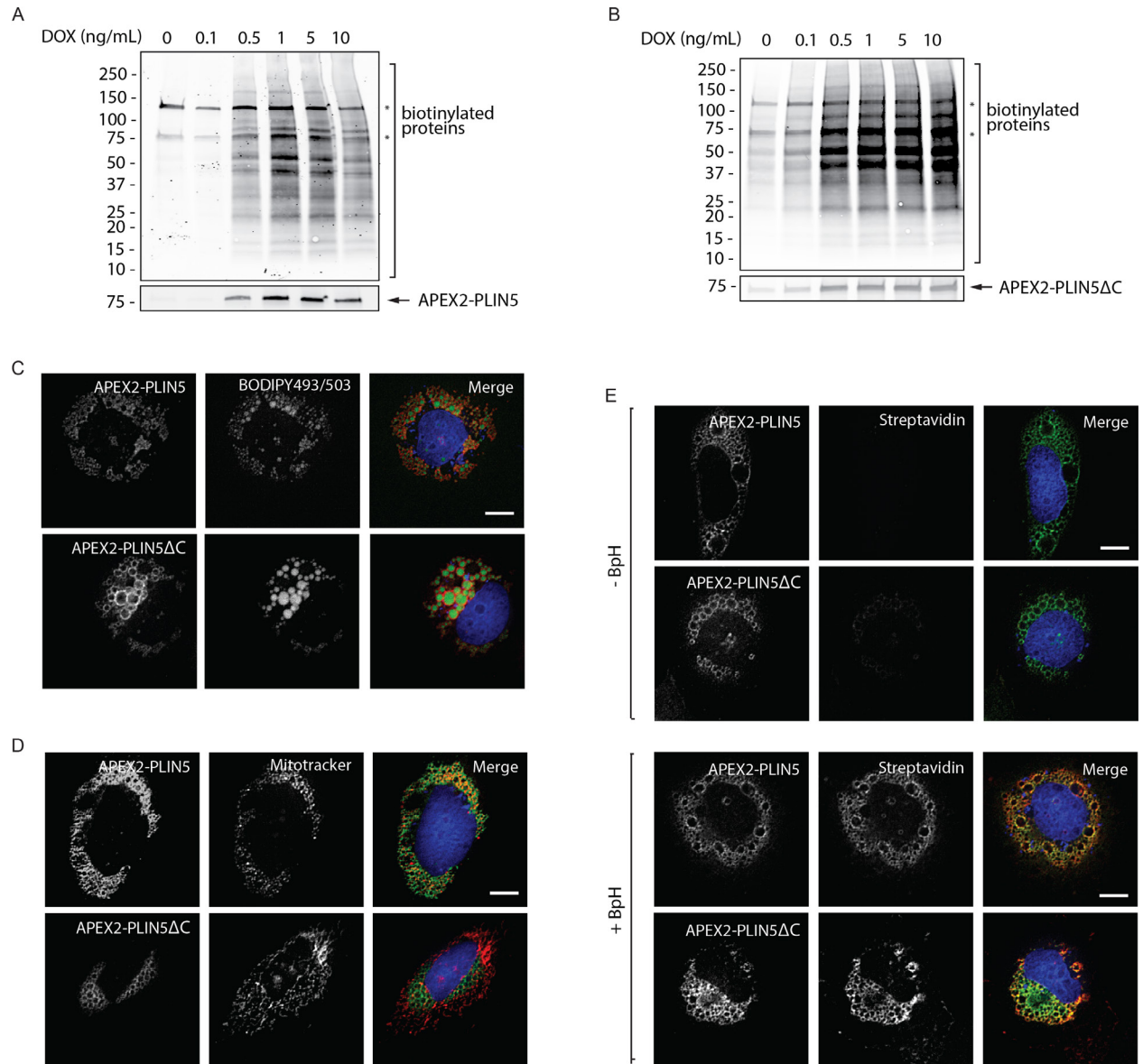
Figure 3-2. Biotinylation of proteins in proximity to PLIN5-targeted APEX2

(A-B) Huh7 cells expressing PLIN5-targeted APEX2 were treated with 0-10 ng/mL DOX for 48 hr and biotin-phenol/H_2O_2 (BpH). Total proteins from lysed cells were separated by SDS-PAGE and analyzed by blotting with fluorescently-labeled streptavidin and antibodies against the S-tag. *(C-E)* Huh7 cells expressing PLIN5-targeted APEX2 were treated with 0.5 ng/mL DOX for 48 hr and 200 µM oleate for 24 hr. *(C)* Fixed cells were imaged by fluorescence microscopy using antibodies against the S-tag (red) and BODIPY493/503 (green), or *(D)* S-tag (green), MitoTracker Orange CMTMRos (red), and DAPI (blue). *(E)* Cells were treated with BpH and imaged by fluorescence microscopy using antibodies against S-tag (green) and fluorescent streptavidin-568 (red). Scale bars represent 10 µm.
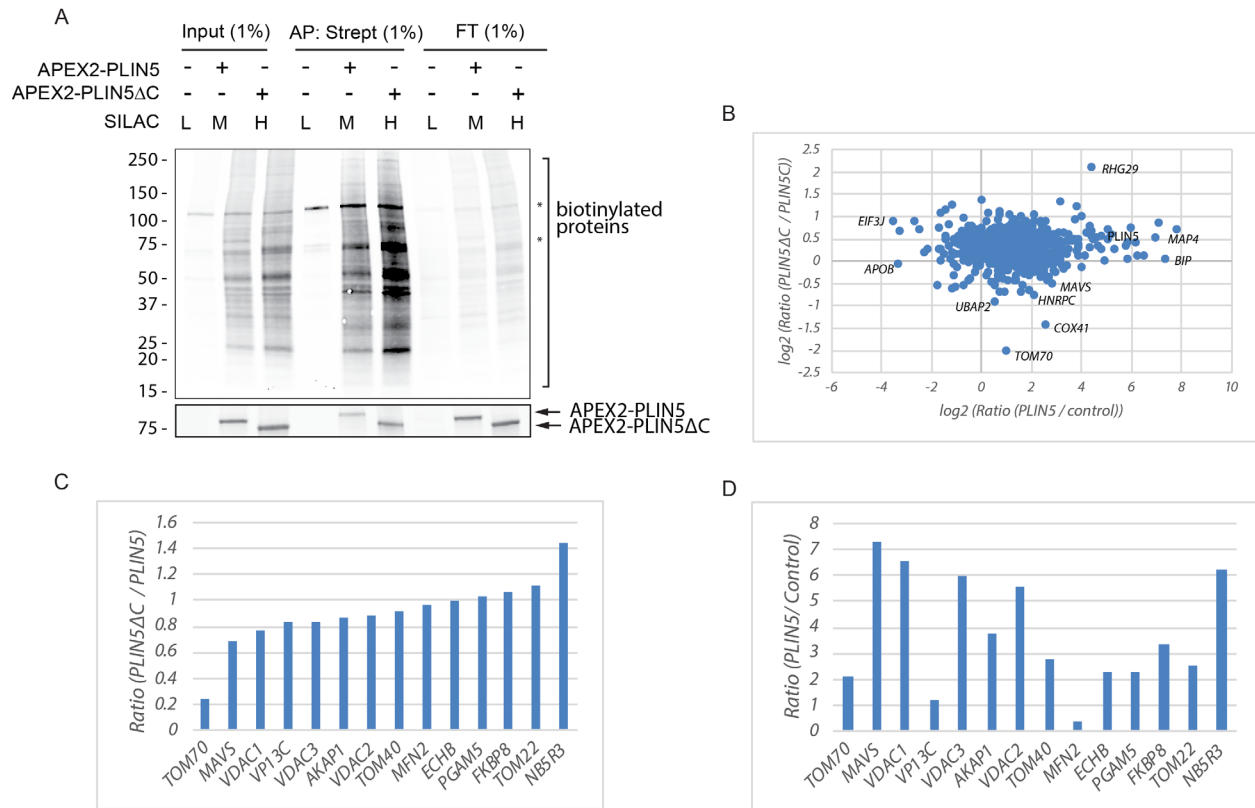
Figure 3-3. Proteomic analysis of biotinylated proteins

(A) Parental Huh7 cells, APEX2-PLIN5, and APEX-PLIN5ΔC were cultured in light, medium, or heavy lysine and arginine-containing SILAC medium. Cells were treated with 0.5 ng/mL DOX for 48 hr, and 200 μM oleate for 24 hr. Cells were incubated with biotin-phenol/H_2O_2 (BpH), and biotinylated proteins were affinity purified using streptavidin-conjugated beads. Proteins from light-, medium-, and heavy-labeled cells were combined at equal volumes and identified by mass spectrometry. *(B)* Log$_2$ graph depicting the heavy-to-medium (APEX2-PLIN5/APEX-PLIN5ΔC) SILAC ratios versus medium-to-light (APEX2-PLIN5/control). *(C)* Heavy-to-medium and *(D)* medium-to-light SILAC ratios of known outer mitochondrial proteins identified by mass spectrometry.
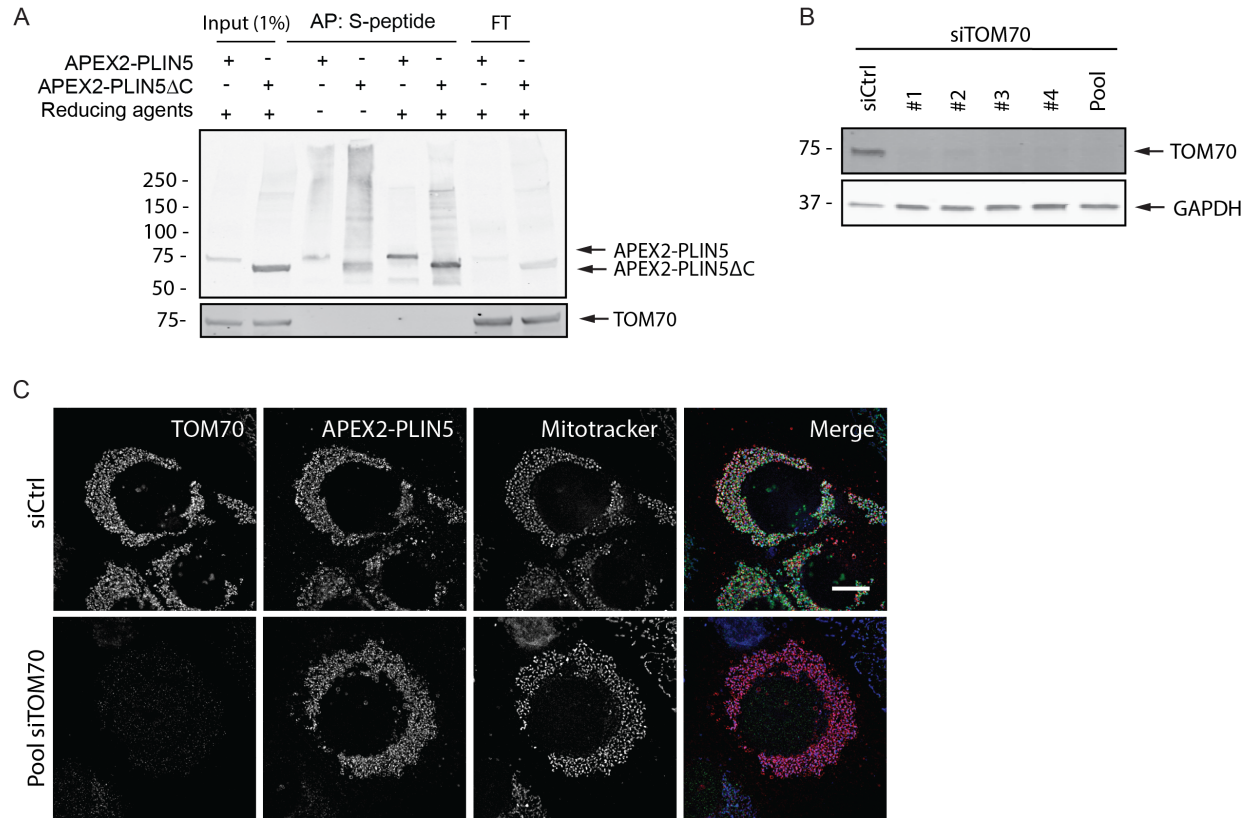
Figure 3-S1. TOM70 is not required for LD-mitochondrial interaction

(A) Co-immunoprecipitation of TOM70 and PLIN5-targerted APEX2. Huh7 cells expressing APEX2-PLIN5, and APEX-PLIN5ΔC were treated with 0.5 ng/mL DOX for 48 hr, and 200 µM oleate for 24 hr. Proteins were crosslinked with 0.5 mM dithiobis (succinimidyl propionate) (DSP) and PLIN5-targeted APEX2 proteins were purified with S-protein agarose beads. To reverse the crosslinking, purified proteins were treated with reducing agents (10% β-mercaptoethanol and 0.1 M dithiothreitol). Proteins were separated by SDS-PAGE and analyzed by blotting with antibodies against the S-tag and endogenous TOM70. *(B)* Western blot validation of siRNA-mediated knockdown of TOM70. *(C)* Pooled siRNA knockdown of TOM70 in Huh7 cells expressing APEX2-PLIN5. Cells were treated with 0.5 ng/mL DOX for 48 hr, and 200 µM oleate for 24 hr. Fixed cells were imaged by fluorescence microscopy using antibodies against TOM70 (green), S-tag (red), and MitoTracker Deep Red (blue). Scale bars represent 10 µm.
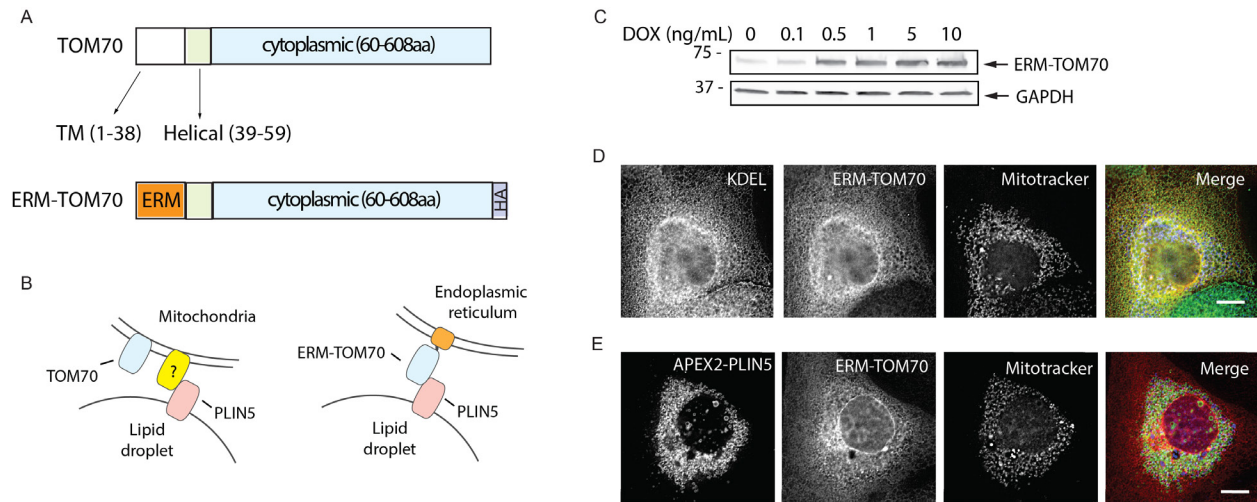
Figure 3-S2. ER-targeted TOM70 is not sufficient to recruit LDs to the ER membrane

(A) TOM70 and ERM-TOM70 constructs used in this study. *(B)* Schematic of LD-mitochondrial interaction mediated by PLIN5 and an unknown outer mitochondrial tethering protein. *(C)* Schematic of ER-targeted TOM70 (ERM-TOM70) recruiting and interacting with LD-targeted APEX2-PLIN5 at the ER membrane. *(D)* Huh7 cells expressing ERM-TOM70 were treated with 0-10 ng/mL DOX for 48 hr, and 200 µM oleate for 24 hr. Proteins from lysed cells were separated by SDS-PAGE and analyzed by blotting with antibodies against TOM70 and GAPDH. *(E-F)* Huh7 cells expressing ERM-TOM70 were treated with 0.5 ng/mL for 48 hr, and 200 µM oleate for 24 hr. *(E)* ERM-TOM70 localization analyzed by immunofluorescence microscopy using antibodies against KDEL (green), TOM70 (red) and MitoTracker Deep Red (blue). *(F)* Localization of APEX2-PLIN5 and ERM-TOM70 by immunofluorescence microscopy using antibodies against S-tag (green), TOM70 (red), and MitoTracker Deep Red (blue). Scale bars represent 10 µm.

CONCLUSION

As neutral lipid storage organelles, lipid droplets (LDs) are hubs for cellular lipid metabolism**Error! Bookmark not defined.**˙**Error! Bookmark not defined.**. Dysregulation of LD biogenesis and consumption have been implemented in various metabolic related diseases, including atherosclerosis, obesity, and neutral lipid storage disease**Error! Bookmark not defined.**. However, LDs are not a passive sink for fatty acid (FA) storage, but rather they are a highly dynamic organelle with various cellular functions that communicate with other organelles to maintain optimal cellular function and homeostasis**Error! Bookmark not defined.**˙**Error! Bookmark not defined.**.

In chapter one, we demonstrate that mTORC1-regulated autophagy is necessary and sufficient for starvation-induced LD biogenesis. We further found that the ER-resident diacyglycerol acyltransferase 1 (DGAT1) selectively channels autophagy-liberated FAs into new, clustered LDs that are in close proximity to mitochondria and are lipolytically degraded. However, LDs were not required for FA delivery to the mitochondria, but instead function to prevent acylcarnitine accumulation and lipotoxic dysregulation of the mitochondria. Thus, our data support a model in which LDs provide a lipid buffering system that sequesters FAs released during the autophagic degradation of membranous organelles, reducing lipotoxicity. These findings reveal an unrecognized aspect of the cellular adaptive response to starvation, mediated by LDs. It also demonstrates a highly coordinated relationship between autophagy, mitochondria, the endoplasmic reticulum (ER), and LDs to promote cellular energy homeostasis.

LDs have been found in contact with the mitochondria[17-18, 83-85]. However, the function of the contact site is currently controversial. In chapter two, we developed an inducible tethering of organelles with synthetic heterodimers (iTOSH) system. Here we targeted FRB and FKBP to LDs and mitochondria. In the presence of rapalog, FRB-PLIN2 and tom20ss-tdFKBP formed a dimer and the mitochondria is recruited to LDs. The iTOSH system also successfully recruited cytosolic proteins to FRB or FKBP fusion proteins. The iTOSH system is a useful tool to spatially and temporary regulate LD-mitochondrial contacts in future studies.

Organelles communicate and transfer materials at membrane contact sites (MCSs)[8,65,84,98]. At the heart of the MCSs are tethering proteins or complexes that stabilize and maintain the contact. To identify LD-mitochondrial tethering proteins, in chapter three we employed a proximity-labeling approach using ascorbate peroxidase (APEX2) to biotinylate proteins at the LD-mitochondrial junction, the biotinylated proteins were subsequently identified by mass spectrometry. APEX2 was targeted to LDs by PLIN5. PLIN5 have been implemented as a potential LD-mitochondrial tethering protein[20], but the interacting protein is current unknown. Using this approach, we identified outer mitochondrial proteins. Although we were unable to identify mitochondrial proteins required for LD recruitment in our analysis, APEX2 may still be useful to identify other interorganelle tethering proteins.

In summary, we have described several aspects of LD functions maintaining cellular lipid metabolism, including sequestering FAs to prevent lipotoxicity during acute starvation. We have also discussed and developed useful tools to further evaluate LD function in organelle

communication for future studies. These approaches can lead to the development of novel therapeutic options for the treatment of lipid related diseases.

KEY RESOURCES TABLE

REAGENT OR RESOURCE	SOURCE	IDENTIFIER
Antibodies		
Rabbit monoclonal anti-Phospho-p70 S6 Kinase (Thr389)	Cell Signaling Technology	Cat. # 9234, 108D2; RRID: AB_2269803
Rabbit polyclonal anti-p70 S6 Kinase	Cell Signaling Technology	Cat. #9202; RRID: AB_10695156
Rabbit polyclonal anti-Phospho-AMPKα (Thr172)	Cell Signaling Technology	Cat. #2531
Rabbit polyclonal anti- AMPKα	Cell Signaling Technology	Cat. # 2532; RRID: AB_330331
Mouse monoclonal anti-Glyceraldehyde-3-Phosphate Dehydrogenase	Thermo Fisher Scientific	Cat. # MAB374MI, 6C5
Rabbit polyclonal anti-α-tubulin	Cell Signaling Technology	Cat. # 2144; RRID: AB_2210548
Rabbit polyclonal anti-LC3B	Sigma-Aldrich	L7543; RRID: AB_796155
Rabbit polyclonal anti-p62	Enzo Life Sciences	BML-PW9860; RRID: AB_219009
Rabbit monoclonal anti-Phospho-ULK1 (Ser757)	Cell Signaling Technology	Cat. # 14202, D7O6U; RRID: AB_2665508
Rabbit monoclonal anti-ULK1	Cell Signaling Technology	Cat. # 8054, D8H5; RRID: AB_11178668
Rabbit polyclonal anti-ATF4	Proteintech Group, Inc.	Cat. # 10835-1-AP; RRID: AB_2058600
Mouse monoclonal anti-V5 tag	Invitrogen	Cat. # 46-0705l RRID: AB_2556564
Mouse monoclonal anti-S-tag	EMD Millipore	Cat. # 71549-3; RRID: AB_10806301

Chemicals, Peptides, and Recombinant Proteins		
Bafilomycin A1 (250 nM)	Sigma-Aldrich	Cat. # B1793
TCV-3166 (1 µM)	3-V Biosciences	Obtained from 3-V Biosciences through MTA
AICAR (250 µM)	Cell Signaling Technology	Cat. #9944
Compound C (10 µM)	Tocris	Cat. # 3093
Torin1 (250 nM)	Tocris	Cat. # 4247
T863 (20 µM)	Sigma-Aldrich	Cat. # SML0539

PF-06424439 (10 μM)	Sigma-Aldrich	Cat. # PZ0233
GSK2606414 (1 μM)	EMD Millipore Corporation	Cat. # 516535
Oleate (200 μM)	Sigma-Aldrich	Cat. # O1383
Tunicamycin (5 μg/mL)	Cayman Chemical Co.	Cat. # 11445
Etomoxir (100 μM)	Cayman Chemical Co.	Cat. # 11969
Orlistat (50 μM)	Sigma-Aldrich	Cat. #O4139
ATGListatin (20 μM)	EMD Millipore Corporation	Cat. # 5.30151.0001
BODIPY 493/503 (4,4-Difluoro-1,3,5,7,8-Pentamethyl-4-Bora-3a,4a-Diaza-s-Indacene)	Life Technologies Co.	Cat. # D3922
BODIPY 558/568 C12 (4,4-Difluoro-5-(2-Thienyl)-4-Bora-3a,4a-Diaza-s-Indacene-3-Dodecanoic Acid)	Life Technologies Co.	Cat. # D3835
MitoTracker Orange CMTMRos	Life Technologies Co.	Cat. # M7510
MitoTracker Green FM	Life Technologies Co.	Cat. # M7514
MitoTracker Deep Red FM	Life Technologies Co.	Cat. # M22426
MitoSOX Red Mitochondrial Superoxide Indicator (5 μM)	Life Technologies Co.	Cat. # M36008
CellROX Deep Red Reagent, for oxidative stress detection	Life Technologies Co.	Cat. # C10422
BODIPY 581/591 C11 (Lipid Peroxidation Sensor)	Life Technologies Co.	Cat. # D3861
JC-9 Dye (Mitochondrial Membrane Potential Probe)	Fisher Scientific	Cat. # D22421
Valinomycin (12 μM)	Sigma-Aldrich	Cat. # V0627
Rapalog (250 nM)		
Doxycycline	Sigma-Aldrich	Cat. # D9891
Blasticidin S HCL	Thermo Fisher Scientific	Cat. # A1113903
Puromycin Dihydrochloride	Thermo Fisher Scientific	Cat. # A1113803
Hygromycin B	Thermo Fisher Scientific	Cat. # 10687010
Biotin-phenol	Iris Biotech GmbH	Cat. # LS-3500.0250
Trolox	Sigma-Aldrich	Cat. # 238813
L-Lysine	Cambridge Isotope Laboratories	Cat. # ULM-8766-0.1
L-Arginine	Cambridge Isotope Laboratories	Cat. # ULM-8347-PK
4,4,5,5-D_4-L-Lysine	Cambridge Isotope Laboratories	Cat. # DLM-2640-PK
$^{13}C_6$-L-arginine	Cambridge Isotope Laboratories	Cat. # CLM-2265-H-PK
$^{13}C_6$-$^{15}N_2$-Lysine	Cambridge Isotope Laboratories	Cat. # CNLM-3454-PK

$^{13}C_6$-$^{15}N_4$-L-arginine	Cambridge Isotope Laboratories	Cat. # CNLM-9007-CA-0.1MG
Pierce Protease Inhibitor Mini Tablets, EDTA-free	Thermo Fisher Scientific	Cat. # A32955
Pierce Streptavidin Agarose	Thermo Fisher Scientific	Cat. # 20347
S-protein agarose	EMD Millipore	Cat. # 69704
Rapigest SF Surfactant	Waters	Cat. # 186001861
Pierce Trypsin Protease, MS Grade	Thermo Fisher Scientific	Cat. # 9057
Fugene 6	Promega	Cat. # E2691
X-tremeGENE HP	Roche	Cat. # 6366244001
Lipofectamine RNAiMAX	Thermo Fisher Scientific	Cat. # 13778-075

Critical Commercial Assays

Seahorse XF24 FluxPak (includes necessary reagents – oligomycin, rotenone/antimycin, FCCP)	Agilent Technologies	Cat. # 100850-001
FITC Annexin V Apoptosis Detection Kit I	BD Biosciences / BD Pharmingen	Cat. # 556547
High Capacity cDNA Reverse Transcription Kits	Applied Biosystems	Cat. # 4368814
SsoAdvanced Universal SYBR® Green Supermix	Bio-Rad Laboratories, Inc.	Cat. # 1725272

Experimental Models: Cell Lines

Mouse embryonic fibroblasts (MEFs) isolated from C57 mice	Kind gift from Dr. Joseph Napoli (University of California, Berkeley)	N/A
U2OS	Kind gift from Dr. Ron Kopito (Stanford University)	N/A
HeLa	ATCC	Cat. # CCL-2
HEK 293T/17	ATCC	Cat. # CRL-11268
Huh7	Kind gift from Dr. Holly Ramage (University of Pennsylvania)	N/A

Oligonucleotides

Nprl2 gRNA #1, Exon 2-1 *CACCG*GGAGCAGCTTTGTATCCAACG	This paper, http://crispr.mit.edu	N/A
Nprl2 gRNA #1, Exon 2-2 *AAAC*CGTTGGATACAAAGCTGCTCC	This paper, http://crispr.mit.edu	N/A
Nprl2 gRNA #2, Exon 3-1 *CACCG*ATGGCGAAACCCGTCAATGT	This paper, http://crispr.mit.edu	N/A

Nprl2 gRNA #2, Exon 3, 2   This paper,   N/A
*AAAC*ACATTGACGGGTTTCGCCATC   http://crispr.mit.edu

Recombinant DNA

pMRX-IP-GFP-LC3-RFP-LC3ΔG	Kaizuka et al., 2016	Addgene plasmid # 84572
Str-KDEL_SBP-EGFP-E-cadherin plasmid	Boncompain et al., 2012	Kind gift from Dr. Boncompain (Institut Curie)
LentiCRISPR-V2	Sanjana et al., 2014	Addgene Plasmid # 52961

Software and Algorithms

FlowJo Software	Schneider et al., 2012	https://imagej.nih.gov/ij
ImageJ	FlowJo	https://www.flowjo.com
GraphPad Prism	GraphPad Software	https://www.graphpad.com/scientific-software/prism
MaxQuant	Max Planck Institute of Biochemistry	http://www. Biochem.mpg.de/5111795/maxquant

REFERENCES

1. Hashemi, H.F., and Goodman, J.M. (2015). The life cycle of lipid droplets. Curr. Opin. Cell Biol. *33*, 119–124.

2. Pol, A., Gross, S.P., and Parton, R.G. (2014). Review: biogenesis of the multifunctional lipid droplet: lipids, proteins, and sites. J. Cell Biol. *204*, 635–646.

3. Walther, T.C., and Farese, R.V. (2012). Lipid droplets and cellular lipid metabolism. Annu. Rev. Biochem. *81*, 687–714.

4. Galluzzi, L., Pietrocola, F., Levine, B., and Kroemer, G. (2014). Metabolic control of autophagy. Cell *159*, 1263–1276.

5. Yang, Z., and Klionsky, D.J. (2010). Mammalian autophagy: core molecular machinery and signaling regulation. Curr. Opin. Cell Biol. *22*, 124–131.

6. Nguyen, B.T., Louie, M.S., Daniele, R. J., Tran, Q., Dillin, A., Zoncu, R., Nomura, K. D., and Olzmann, A. J. (2017). DGAT1-dependent lipid droplet biogenesis protects mitochondrial function during starvation-induced autophagy. Dev. Cell 42, 9-21.

7. Rambold, A.S., Cohen, S., and Lippincott-Schwartz, J. (2015). Fatty acid trafficking in starved cells: regulation by lipid droplet lipolysis, autophagy, and mitochondrial fusion dynamics. Dev. Cell *32*, 678–692.

8. Scorrano, L., De Matteis, M.A., Emr, S., Giordano, F., Hajanóczky, G., Jornmann, B., Lackner, L.L. Levine, T.P., Pellegrini, L., Reinisch, K., Rizzulo, R., Simmen, T., Stenmark, H., Ungermann, C., and Schuldiner, M. (2019). Coming together to define membrane contact sites. Nat. Commun. *10*, 1287.

9. Bailey, A.P., Koster, G., Guillermier, C., Hirst, E.M.A., MacRae, J.I., Lechene, C.P., Postle, A.D., and Gould, A.P. (2015). Antioxidant Role for Lipid Droplets in a Stem Cell Niche of Drosophila. Cell *163*, 340–353.

10. Garbarino, J., Padamsee, M., Wilcox, L., Oelkers, P.M., Ambrosio, D. D', Ruggles, K.V., Ramsey, N., Jabado, O., Turkish, A., and Sturley, S.L. (2009). Sterol and diacylglycerol acyltransferase deficiency triggers fatty acid-mediated cell death. J. Biol. Chem. *284*, 30994–31005.

11. Listenberger, L.L., Han, X., Lewis, S.E., Cases, S., Farese, R.V., Ory, D.S., and Schaffer, J.E. (2003). Triglyceride accumulation protects against fatty acid-induced lipotoxicity. Proc. Natl. Acad. Sci. U.S.A. *100*, 3077–3082.

12. Petschnigg, J., Wolinski, H., Kolb, D., Zellnig, G., Kurat, C.F., Natter, K., and Kohlwein, S.D. (2009). Good fat, essential cellular requirements for triacylglycerol synthesis to maintain membrane homeostasis in yeast. J. Biol. Chem. *284*, 30981–30993.

13. Velázquez, A.P., Tatsuta, T., Ghillebert, R., Drescher, I., and Graef, M. (2016). Lipid droplet-mediated ER homeostasis regulates autophagy and cell survival during starvation. J. Cell Biol. *212*, 621–631.

14. Martinez-Lopez, N., and Singh, R. (2015). Autophagy and Lipid Droplets in Liver. Annu. Rev. Nutr. *25*, 215-37.

15. Singh, R., Kaushik, S., Wang, Y., Xiang, Y., Novak, I., Komatsu, M., Tanaka, K., Cuervo, A.M., and Czaja, M.J. (2009). Autophagy regulates lipid metabolism. Nature *458*, 1131–1135.

16. Xu, S., Zhang, X., and Liu, P. (2018). Lipid droplet proteins and metabolic disease. Biochim Biophys Acta Mol. Basis Dis. *1864*, 1968-1983.

17. Barbosa, A.D., and Siniossoglou, S. (2017). Function of lipid droplet-organelle interactions in lipid homeostasis. Biochim. Biophys. Acta Mol. Cell Res. *1864*, 1459-1468.

18. Cohen, S. (2018). Lipid droplets as organelles. Int. Rev. Cell Mol. Biol. *337*, 83-110.

19. Jagerstrom, S., Polesie, S., Wickstrom, Y., Johansson, B.R., Schroder, H.D., Hojlund, K., and Bostrom, P. (2009). Lipid droplets interact with mitochondria using SNAP23. Cell Biol. Int. *33*, 934-940.

20. Wang, H., Sreenivasan, U., Hu, H., Saladino, A., Polster, B.M., Lund, L.M., Gong, D.W., Stanley, W.C., and Sztalryd, C. (2011). Perilipin 5, a lipid droplet-associated protein, provides physical and metabolic linkage to mitochondria. J. Lipid Res. *52*, 2159-2168.

21. Chantranupong, L., Wolfson, R.L., and Sabatini, D.M. (2015). Nutrient-sensing mechanisms across evolution. Cell *161*, 67–83.

22. Efeyan, A., Comb, W.C., and Sabatini, D.M. (2015). Nutrient-sensing mechanisms and pathways. Nature *517*, 302–310.

23. Finn, P.F., and Dice, J.F. (2006). Proteolytic and lipolytic responses to starvation. Nutrition *22*, 830–844.

24. Cabodevilla, A.G., Sánchez-Caballero, L., Nintou, E., Boiadjieva, V.G., Picatoste, F., Gubern, A., and Claro, E. (2013). Cell survival during complete nutrient deprivation depends on lipid droplet-fueled β-oxidation of fatty acids. J. Biol. Chem. *288*, 27777–27788.

25. Herms, A., Bosch, M., Reddy, B.J.N., Schieber, N.L., Fajardo, A., Rupérez, C., Fernández-Vidal, A., Ferguson, C., Rentero, C., Tebar, F., Enrich, C., Parton, R.G., Gross, S.P., and Pol, A. (2015). AMPK activation promotes lipid droplet dispersion on detyrosinated microtubules to increase mitochondrial fatty acid oxidation. Nat. Commun. *6*, 7176.

26. Lass, A., Zimmermann, R., Oberer, M., and Zechner, R. (2011). Lipolysis - a highly regulated multi-enzyme complex mediates the catabolism of cellular fat stores. Prog. Lipid Res. *50*, 14–27.

27. Gomes, L.C., Di Benedetto, G., and Scorrano, L. (2011). During autophagy mitochondria elongate, are spared from degradation and sustain cell viability. Nat. Cell. Biol. *13*, 589–598.

28. Rambold, A.S., Kostelecky, B., Elia, N., and Lippincott-Schwartz, J. (2011). Tubular network formation protects mitochondria from autophagosomal degradation during nutrient starvation. Proc. Natl. Acad. Sci. U.S.A. *108*, 10190–10195.

29. Kaizuka T., Morishita H., Hama, Y., Tsukamoto, S., Matsui, T., Toyota, Y., Kodama, A., Ishihara, T., Mizushima, T., and Mizushima, N. (2016). An autophagic flux probe that releases an internal control. Mol. Cell *64*, 835-849.

30. Zoncu, R., Efeyan, A., and Sabatini, D.M. (2011). mTOR: from growth signal integration to cancer, diabetes and ageing. Nat. Rev. Mol. Cell Biol. *12*, 21–35.

31. Alers, S., Löffler, A.S., Wesselborg, S., and Stork, B. (2012). Role of AMPK-mTOR-Ulk1/2 in the regulation of autophagy: cross talk, shortcuts, and feedbacks. Mol. Cell Biol. *32*, 2–11.

32. Kim, J., Kundu, M., Viollet, B., and Guan, K.L. (2011). AMPK and mTOR regulate autophagy through direct phosphorylation of Ulk1. Nat. Cell Biol. *13*, 132–141.

33. Nada, S., Hondo, A., Kasai, A., Koike, M., Saito, K., Uchiyama, Y., and Okada, M. (2009). The novel lipid raft adaptor p18 controls endosome dynamics by anchoring the MEK-ERK pathway to late endosomes. EMBO J. *28*, 477–489.

34. Sancak, Y., Bar-Peled, L., Zoncu, R., Markhard, A.L., Nada, S., and Sabatini, D.M. (2010). Ragulator-Rag complex targets mTORC1 to the lysosomal surface and is necessary for its activation by amino acids. Cell *141*, 290–303.

35. Bar-Peled, L., Chantranupong, L., Cherniack, A.D., Chen, W.W., Ottina, K.A., Grabiner, B.C., Spear, E.D., Carter, S.L., Meyerson, M., and Sabatini, D.M. (2013). A Tumor suppressor complex with GAP activity for the Rag GTPases that signal amino acid sufficiency to mTORC1. Science *340*, 1100–1106.

36. Harris, C.A., Haas, J.T., Streeper, R.S., Stone, S.J., Kumari, M., Yang, K., Han, X., Brownell, N., Gross, R.W., Zechner, R., and Farese, R.V. Jr. (2011). DGAT enzymes are required for

triacylglycerol synthesis and lipid droplets in adipocytes. J. Lipid Res. *52*, 657–667.

37. To, M., Peterson, C.W., Roberts, M.A., Counihan, J.L., Wu, T.T., Forster, M.S., Nomura, D.K., and Olzmann, J.A. (2016). Lipid disequilibrium disrupts ER proteostasis by impairing ERAD substrate glycan trimming and dislocation. Mol. Biol. Cell. *28*, 270-284.

38. Li, D., Song, J.Z., Li, H., Shan, M.H., Liang, Y., Zhu, J., and Xie, Z. (2015). Storage lipid synthesis is necessary for autophagy induced by nitrogen starvation. FEBS Lett. *589*, 269–276.

39. Shpilka, T., Welter, E., Borovsky, N., Amar, N., Mari, M., Reggiori, F., and Elazar, Z. (2015). Lipid droplets and their component triglycerides and steryl esters regulate autophagosome biogenesis. EMBO J. *34*, 2117–2131.

40. Dupont, N., Chauhan, S., Arko-Mensah, J., Castillo, E.F., Masedunskas, A., Weigert, R., Robenek, H., Proikas-Cezanne, T., and Deretic, V. (2014). Neutral lipid stores and lipase PNPLA5 contribute to autophagosome biogenesis. Curr. Biol. *24*, 609–620.

41. Mayer, N., Schweiger, M., Romauch, M., Grabner, G.F., Eichmann, T.O., Fuchs, E., Ivkovic, J., Heier, C., Mrak, I., Lass, A., Höfler, G., Fledelius, C., Zechner, R., Zimmermann, R., and Breinbauer, R. (2013). Development of small-molecule inhibitors targeting adipose triglyceride lipase. Nat. Chem. Biol. *12*, 785-7.

42. Harding, H.P., Novoa, I., Zhang, Y., Zeng, H., Wek, R., Schapira, M., and Ron, D. (2000). Regulated translation initiation controls stress-induced gene expression in mammalian cells. Mol. Cell *6*, 1099–1108.

43. Boncompain, G., Divoux, S., Gareil, N., de Forges, H., Lescure, A., Latreche, L., Mercanti, V., Jollivet, F., Raposo, G., and Perez, F. (2012). Synchronization of secretory protein traffic in populations of cells. Nat. Methods *9*, 493-498.

44. McCoin, C.S., Knotts, T.A., and Adams, S.H. (2015). Acylcarnitines--old actors auditioning for new roles in metabolic physiology. Nat. Rev. Endocrinol. *11*, 617–625.

45. Son, N.-H., Yu, S., Tuinei, J., Arai, K., Hamai, H., Homma, S., Shulman, G.I., Abel, E.D., and Goldberg, I.J. (2010). PPARγ-induced cardiolipotoxicity in mice is ameliorated by PPARα deficiency despite increases in fatty acid oxidation. J. Clin. Invest. *120*, 3443–3454.

46. Wajner, M., and Amaral, A.U. (2015). Mitochondrial dysfunction in fatty acid oxidation disorders: insights from human and animal studies. Biosci. Rep. *36*, e00281.

47. Ravikumar, B., Sarkar, S., Davies, J.E., Futter, M., Garcia-Arencibia, M., Green-Thompson, Z.W., Jimenez-Sanchez, M., Korolchuk, V.I., Lichtenberg, M., Luo, S., Massey, D.C., Menzies, F.M., Moreau, K., Narayanan, U., Renna, M., Siddiqi, F.H., Underwood, B.R., Winslow, A.R., and Rubinsztein, D.C. (2010). Regulation of mammalian autophagy in physiology and

pathophysiology. Physiol. Rev. *90*, 1383–1435.

48. Xu, G., Sztalryd, C., Lu, X., Tansey, J.T., Gan, J., Dorward, H., Kimmel, A.R., and Londos, C. (2005). Post-translational regulation of adipose differentiation-related protein by the ubiquitin/proteasome pathway. J. Biol. Chem. *280*, 42841–42847.

49. Gubern, A., Barceló-Torns, M., Casas, J., Barneda, D., Masgrau, R., Picatoste, F., Balsinde, J., Balboa, M.A., and Claro, E. (2009). Lipid droplet biogenesis induced by stress involves triacylglycerol synthesis that depends on group VIA phospholipase A2. J. Biol. Chem. *284*, 5697–5708.

50. Lee, J., Mendez, R., Heng, H., Yang, Z., and Zhang, K. (2012). Pharmacological ER stress promotes hepatic lipogenesis and lipid droplet formation. Am. J. Transl. Res. *4*, 102-13.

51. Parmigiani, A., Nourbakhsh, A., Ding, B., Wang, W., Kim, Y.C., Akopiants, K., Guan, K.L., Karin, M., and Budanov, A.V. (2014). Sestrins inhibit mTORC1 kinase activation through the GATOR complex. Cell Rep. *9*, 1281–1291.

52. Wilfling, F., Wang, H., Haas, J.T., Krahmer, N., Gould, T.J., Uchida, A., Cheng, J.-X., Graham, M., Christiano, R., Fröhlich, F., Liu, X., Buhman, K.K., Coleman, R.A., Bewersdorf, J., Farese, R.V. Jr., and Walther, T.C. (2013). Triacylglycerol synthesis enzymes mediate lipid droplet growth by relocalizing from the ER to lipid droplets. Dev. Cell *24*, 384–399.

53. Yen, C.-L.E., Stone, S.J., Koliwad, S., Harris, C., and Farese, R.V. (2008). Thematic review series: glycerolipids. DGAT enzymes and triacylglycerol biosynthesis. J. Lipid Res. *49*, 2283–2301.

54. Koliwad, S.K., Streeper, R.S., Monetti, M., Cornelissen, I., Chan, L., Terayama, K., Naylor, S., Rao, M., Hubbard, B., and Farese, R.V. (2010). DGAT1-dependent triacylglycerol storage by macrophages protects mice from diet-induced insulin resistance and inflammation. J. Clin. Invest. *120*, 756–767.

55. Liu, L., Shi, X., Bharadwaj, K.G., Ikeda, S., Yamashita, H., Yagyu, H., Schaffer, J.E., Yu, Y.-H., and Goldberg, I.J. (2009). DGAT1 expression increases heart triglyceride content but ameliorates lipotoxicity. J. Biol. Chem. *284*, 36312–36323.

56. Liu, L., Yu, S., Khan, R.S., Homma, S., Schulze, P.C., Blaner, W.S., Yin, Y., and Goldberg, I.J. (2012). Diacylglycerol acyl transferase 1 overexpression detoxifies cardiac lipids in PPARγ transgenic mice. J. Lipid Res. *53*, 1482–1492.

57. Liu, L., Trent, C.M., Fang, X., Son, N.-H., Jiang, H., Blaner, W.S., Hu, Y., Yin, Y.-X., Farese, R.V., Homma, S., Turnbull, A.V., Eriksson, J.W., Hu, S.L., Ginsberg, H.N., Huang, L.S., Goldberg, I.J. (2014). Cardiomyocyte-specific loss of diacylglycerol acyltransferase 1 (DGAT1) reproduces the abnormalities in lipids found in severe heart failure. J. Biol. Chem. *289*, 29881–29891.

58. Robblee, M.M., Kim, C.C., Porter Abate, J., Valdearcos, M., Sandlund, K.L.M., Shenoy, M.K., Volmer, R., Iwawaki, T., and Koliwad, S.K. (2016). Saturated inflammasome in myeloid cells. Cell Rep. *14*, 2611-2623.

59. McCoin, C.S., Knotts, T.A., and Adams, S.H. (2015). Acylcarnitines--old actors auditioning for new roles in metabolic physiology. Nat. Rev. Endocrinol. *11*, 617–625.

60. Son, N.-H., Yu, S., Tuinei, J., Arai, K., Hamai, H., Homma, S., Shulman, G.I., Abel, E.D., and Goldberg, I.J. (2010). PPARγ-induced cardiolipotoxicity in mice is ameliorated by PPARα deficiency despite increases in fatty acid oxidation. J. Clin. Invest. *120*, 3443–3454.

61. Wajner, M., and Amaral, A.U. (2015). Mitochondrial dysfunction in fatty acid oxidation disorders: insights from human and animal studies. Biosci. Rep. *36*, e00281.

62. Long, J.Z., Svensson, K.J., Bateman, L.A., Lin, H., Kamenecka, T., Lokurkar, I.A., Lou, J., Rao, R.R., Chang, M.R., Jedrychowski, M.P., Paulo, J.A., Gygi, S.P., Griffin, P.R., Nomura, D.K., and Spiegalman, B.M. (2016). The secreted enzyme PM20D1 regulates lipidated amino acid uncouplers of mitochondria. Cell *166*, 424–435.

63. Requero, M.A., Goñi, F.M., and Alonso, A. (1995a). The membrane-perturbing properties of palmitoyl-coenzyme A and palmitoylcarnitine. A comparative study. Biochemistry *34*, 10400–10405.

64. Requero, M.A., González, M., Goñi, F.M., Alonso, A., and Fidelio, G. (1995b). Differential penetration of fatty acyl-coenzyme A and fatty acylcarnitines into phospholipid monolayers. FEBS Lett. *357*, 75–78.

65. Prinz, W.A. (2014). Bridging the gap: membrane contact sites in signaling, metabolism, and organelle dynamics. J. Cell Biol. *205*, 759–769.

66. Toulmay, A., and Prinz, W.A. (2011). Lipid transfer and signaling at organelle contact sites: the tip of the iceberg. Curr. Opin. Cell Biol. *23*, 458–463.

67. Friedman, J.R., Lackner, L.L., West, M., DiBenedetto, J.R., Nunnari, J., and Voeltz, G.K. (2011). ER tubules mark sites of mitochondrial division. Science *334*, 358–362.

68. Rowland, A.A., Chitwood, P.J., Phillips, M.J., and Voeltz, G.K. (2014). ER contact sites define the position and timing of endosome fission. Cell *159*, 1027–1041.

69. Salo, V.T., Belevich, I., Li, S., Karhinen, L., Vihinen, H., Vigouroux, C., Magré, J., Thiele, C., Hölttä-Vuori, M., Jokitalo, E., and Ikonen, E. (2016). Seipin regulates ER-lipid droplet contacts and cargo delivery. EMBO J. *35*, 2699–2716.

70. Wang, H., Becuwe, M., Housden, B.E., Chitraju, C., Porras, A.J., Graham, M.M., Liu, X.N., Thiam, A.R., Savage, D.B., Agarwal, A.K., Garg, A., Olarte, M.J., Lin, Q., Fröhlich, F., Hannibal-

Bach, H.K., Upadhyayula, S., Perrimon, N., Kirchhausen, T., Ejsing, C.S., Walther, T.C., and Farese, R.V. (2016). Seipin is required for converting nascent to mature lipid droplets. Elife *5*.

71. Vance, J.E. (2014). MAM (mitochondria-associated membranes) in mammalian cells: lipids and beyond. Biochim. Biophys. Acta *1841*, 595–609.

72. Benjamin, E.I., Li, D.S., Lowe, W., Heuer, T., Kembie, G., and Nomura, D.K. (2015). Diacylglycerol metabolism and signaling is a driving force underlying FASN inhibitor sensitivity in cancer cells. ACS Chem. Biol. *10, 1616-1623.*

73. Louie, S.M., Roberts, L.S., Mulvhill, M.M., Luo, K., and Nomura, D.K. (2013). Cancer cells incorporate and remodel exogenous palmitate into structural and oncogenic signaling lipids. Biochim. Biophys. Acta *1831*, 1566-1572.

74. Louie, S.M., Grossman, E.A., Crawford, L.A., Ding, L., Camarda, R., Huffman, T.R., Miyamoto, D.K., Goga, A., Weerapana, E., and Nomura, D.K. (2016). GSTP1 is a driver of triple-negative breast cancer cell metabolism and pathogenicity. Cell Chem. Biol. *23*, 567-578.

75. Daniele, J.R., Heydari, K., Arriaga, E.A., and Dillin, A., (2016). Identification and characterization of mitochondrial subtypes in *Caenorhabditis elegans* via analysis of individual mitochondria by flow cytometry. Anal. Chem. *88*, 6309-6316.

76. Cossarizza, A., Baccaranicontri, M., Kalashnikova, G., and Franceschi, C. (1993). A new method for the cytofluorometric analysis of mitochondrial membrane potential using the J-aggregate forming lipophilic cation 5,5',6,6'-tetrachloro-1,1',3,3'-tetraethylbenzimidazolcarbocyanine Iodide (JC-1). Biochem. Biophys. Res. Commun. *197*, 40-45.

77. Reers, M., Smith, T.W., and Chen, L.B. (1991). J-aggregate formation of a carbocyanine as a quantitative fluorescent indicator of membrane potential. Biochemistry *30*, 4480-4486.

78. Wolken, G.G., and Arriaga, E.A. (2014). Simultaneous measurement of individual mitochondrial membrane potential and electrophoretic mobility by capillary electrophoresis. Anal. Chem. *86*, 4217-4226.

79. Beavis, A.D., Brannan, R.D., and Garlid, K.D. (1985). Swelling and contraction of the mitochondrial matrix. I. A structural interpretation of the relationship between light scattering and matrix volume. J. Biol. Chem. *260*, 13424-13433.

80. Knight, V.A., Wiggins, P.M., Harvey, J.D., and O'Brien, J.A. (1981). The relationship between the size of mitochondria and the intensity of light that they scatter in different energetic states. Biochim. Biophys. Acta *637*, 146-151.

81. Petit, P.X. (1992). Flow cytometric analysis of rhodamine 123 fluorescence during modulation of the membrane potential in plant mitochondria. Plant Physiol. *98*, 279-286.

82. Schneider, C.A., Rasband, W.S., and Eliceiri, K.W. (2012). NIH image to ImageJ: 25 years of image analysis. Nat. Methods *9*, 671-675.

83. Olzmann, J.A. and Carvalho, P. (2019). Dynamics and functions of lipid droplets. Nat. Rev. Mol. Cell Biol. *3*, 137-155.

84. Eisenberg-Bord M., Shai, N., Schuldiner, M., and Bohnert, M. (2016) A tether is a tether is a tether: Tethering at membrane contact sites. Dev. Cell *39*, 395-409.

85. Schuldiner, M., and Bohnert, M. (2017). A different kind of love – lipid droplet contact sites. Biochim Biophys. Acta Mol. Cell Biol. Lipids *1862*, 1188-1196.

86. Boutant, M., Kulkarni, S.S., Joffraud, M., Ratajczak, J., Valera-Albernia, M., Combe, R., Zorzano, A., and Canto, C. (2017). Mfn2 is critical for brown adipose tissue thermogenic function. EMBO J. *36*, 1543-1558.

87. Wang, H., Sreenivassan, U., Gong, D.W., O'Connell, K.A., Dabkowski, E.R., Hecker, P.A, Ionica, N., Konig, M., Mahurkar, A., Sun, Y., Stanley, W.C., and Sztalryd, C. (2013). Cardiomyocyte-specific perilipin 5 overexpression leads to myocardial steatosis and modest cardiac dysfunction. J. Lipid Res. *54*, 953-65.

88. Tarnopolsky, M.A., Rennie, C.D., Robertshaw, H.A., Fedak-Tarnopolsky, F., Devries, M.C., and Hamadeh, M.J. (2007). Influence of endurance exercise training and sex on intramyocellular lipid and mitochondrial ultrastructure, substrate use, and mitochondrial enzyme activity. J. Phys. Regul. Integr. Comp. Phys. *292*, R1271-R1278.

89. Benador, I.Y., Veliova, M., Mahdaviani, K., Petcherski, A., Wikstrom, J.D., Assali, E.A., Acin-Pérez, R., Shum, M., Oliveira, M.F., Cinti, S., Sztalryd, C., Barshop, W.D., Wohlschlegal, J.A., Corkey, B.E., Liesa, M., and Shirihai, O.S. (2018). Mitochondria bound to lipid droplets have unique bioenergetics, composition, and dynamics that support lipid droplet expansion. Cell Metab. *27*, 869-885.

90. DeRose, R., Miyamoto, T., and Inoue, T. (2013). Manipulating signaling at will: chemically-inducible dimerization (CID) techniques resolve problems in cell biology. Pflugers Arch. *465*, 409-417.

91. Inoue, T., Heo, W.D., Grimley, J.S., Wandless, T.J., and Meyer, T. (2005). An inducible translocation strategy to rapidly activate and inhibit small GTPase signaling pathways. Nat. Methods *2,* 415-8.

92. Putyrski, M. and Schultz, C. (2012) Protein translocation as a tool: The current rapamycin story. FEBS Lett. *15*, 2097-105.

93. Ballou, L.M. and Lin, R.Z. (2008). Rapamycin and mTOR kinase inhibitors. J. Chem. Biol. *1*, 27-36.

94. Csordás, G., Várnai, P., Golenár, T., Roy, S., Purkins, G., Schneider, T.G., Balla, T., and Hajinóczky, G. (2010). Imaging interorganelle contacts and local calcium dynamics at the ER-mitochondrial interface. Mol. Cell *1*, 121-32.

95. Liberti, M.V. and Locassale, J.W. (2016). The Warburg Effect: How does it benefit cancer cells? Trends Biochem. Sci. *41*, 211-218.

96. Itabe, H., Yamaguchi, T., Nimura, S., and Sasabe, N. (2017). Perilipins: a diversity of intracellular lipid droplet proteins. Lipids Health Dis. *16*, 18.

97. Kory, N., Thiam, A.R., Farese, R.V. Jr., amd Walther, T.C. (2015). Protein crowding is a determinant of lipid droplet protein composition. Dev. Cell *34*, 351-63.

98. Lahiri, S., Toulmay, A., and Prinz, W. A. (2015) Membrane contact sites, gateways for lipid homeostasis. Curr. Opin. Cell Biol. *33*, 82–87.

99. Tatsuta, T., Scharwey, M., and Langer, T. Mitochondrial lipid trafficking. (2014) Trends Cell Biol. *24*, 44–52.

100. Burgoyne, T., Patel, S. and Eden, E. R. (2015) Calcium signaling at ER membrane contact sites. Biochim Biophys Acta *1853*, 2012–2017.

101. Friedman, J. R., Lackner, L.L. West, M., DiBenedetto, J.R., Nunnari, J., and Voeltz, G.K. (2011). ER tubules mark sites of mitochondrial division. Science *334*, 358–362.

102. Knoblach, B. and Rachubinski, R. A. (2015). Transport and retention mechanisms govern lipid droplet inheritance in *Saccharomyces cerevisiae*. Traffic *16*, 298–309.

103. Hariri, H., Rogers, S., Ugrankar, R., Liu, Y.L., Feathers, J.R., and Henne, W.M. (2018). Lipid droplet biogenesis is spatially coordinated at ER–vacuole contacts under nutritional stress. EMBO Rep. *19*, 57–72.

104. Raiborg, C., Wenzel, E.M., Pedersen, N.M., Olsvik, H., Schink, K.O., Schultz, S.W., Vietri, M., Nisi, V., Bucci, C., Brech, A., Johansen, T., and Stenmark, H. (2015). Repeated ER-endosome contacts promote endosome translocation and neurite outgrowth. Nature *520*, 234–238.

105. Eden, E. R., White, I. J., Tsapara, A., and Futter, C.E. (2010). Membrane contacts between endosomes and ER provide sites for PTP1B–epidermal growth factor receptor interaction. Nat. Cell Biol. *12*, 267–272.

106. Hamasaki, M., Furuta, N., Matsuda, A., Nezu, A., Yamamoto, A., Fujita, N., Oomori, H., Noda, T., Haraguchi, T., Hiraoka, Y., Amano, A., and Yoshimori, T. (2013). Autophagosomes form at ER–mitochondria contact sites. Nature *495*, 389–39

107. Stefan, C. J., Manford, A.G., Baird, D., Yamada-Hanff, J., Mao, Y., and Emr, S.D. (2011). Osh proteins regulate phosphoinositide metabolism at ER–plasma membrane contact sites. Cell *144*, 389–401.

108. Dickson, E. J., Jensen, J.B., Vivas, o., Kruse, M., Traynor-Kaplan, A.E., and Hille, B. (2016). Dynamic formation of ER–PM junctions presents a lipid phosphatase to regulate phosphoinositides. J. Cell Biol*. 213*, 33–48.

109. Barbosa, A.D., Sembongi, H., Su, W.M., Abreu, S., Reggiori, F., Carman, G.M., and Siniossoglou, S. (2015). Lipid partitioning at the nuclear envelope controls membrane biogenesis. Mol. Biol. Cell *26*, 3641-57.

110. Gao, Q. and Goodman, J.M. (2015). The lipid droplet-a well-connected organelle. Front Cell Dev. Biol. *3*, 49.

111. Beller, M., Thiel, K., and Jäckle, H. (2010). Lipid droplets: a dynamic organelle moves into focus. FEBS Lett. *584*, 2176-82.

112. Murphy, S., Martin, S., and Parton, R.G. (2009). Lipid droplet-organelle interactions; sharing the fats. Biochim. Biophys. Acta *2791*, 441-447.

113. Welte, A. M. (2016). Expanding roles for lipid droplets. Curr. Biol. *25*, R470-R481.

114. Filipe, A. and McLauchlan, J. (2015). Hepatitis C virus and lipid droplets: finding a niche. Trends Mol. Med *21*:34–42.

115. Palade, G. (1959). Subcellular particles (The Ronald Press Company).

116. Csorás, G., Várnai, P., Golenár, T., Roy, S., Purkins, G., Schneider, T.G., Balla, T., and Hajinóczky, G. (2010). Imaging interorganelle contacts and local calcium dynamics at the ER-mitochondrial interface. Mol. Cell *39*, 121-32.

117. Várnai, P., Balázs, T., Tóth, J.D., Hunyady, L., and Balla, T. (2007). Visualization and manipulation of plasma membrane-endoplasmic reticulum contact sites indicates the presence of additional molecular components within the STIM1-Orai1 complex. J. Biol. Chem. *282*, 29678-90.

118. Kakimoto, Y., Tashiro, S., Kojima, R., Morozumi, Y., Endo, T., and Tamura, Y. (2018). Visualizing multiple inter-organelle contact sites using the organelle-targeted split-GFP system. Sci Rep *8*, 6175.

119. Kudla, J. and Bock, R. (2016). Lighting the way to protein-protein interactions: Recommendations on best practices for bimolecular fluorescence complementation analyses. Plant Cell *28*, 1002-8.

120. Stevenson, J., Krycer, R.J., Phan, L., and Brown, J.A. (2013). A practical comparison of ligation-independent cloning techniques. PLoS ONE *8*, e83888.

121. Wang, H., Sreenivasan, U., Hu, H., Saladino, A., Polster, B.M., Lund, L.M., Gong, D.W., Stanley, W.C., and Sztalryd, C. (2011) Perilipin 5, a lipid droplet-associated protein, provides physical and metabolic linkage to mitochondria. J. Lipid Res. *52*, 2159-68.

122. Bosma, M., Minnaard, R., Sparks, L.M., Schaart, G., Losen, M., de Baets, M.H., Duimel, H., Kersten, S., Bickel, P.E., Schrauwen, P., and Hesselink, M.K. (2012). The lipid droplet coat protein perilipin 5 also localizes to muscle mitochondria. Histochem. Cell Biol. *137*, 205-15.

123. Gemmink, A., Daeman, S., Brouwers, B., Huntjens, P.R., Schaart, G., Moonen-Kornips, E., Jörgensen, J., Hoeks, J., Schrauwen, P., and Hesselink, M.K.C. (2018). Dissociation of intramyocellular lipid storage and insulin resistance in trained athletes and type 2 diabetes patients; involvement of perilipin 5?. J. Physiol. *596*, 857-868.

124. Wolins, N.E., Quaynor, B.K., Skinner, J.R., Tzekov, A., Croce, M.A., Gropler, M.C., Varma, V., Yao-Borengasser, A., Rasouli, N., Kern, P.A., Finck, B.N., and Bickel, P.E. (2006) OXPAT/PAT-1 is a PPAR-induced lipid droplet protein that promotes fatty acid utilization. Diabetes *55*, 3418-3428.

125. Dalen, K.T., Dahl, T., Holter, E., Arntsen, B., Londos, C., Sztalryd, C., and Nebb, H.I. (2007). LSDP5 is a PAT protein specifically expressed in fatty acid oxidizing tissues. Biochim. Biophys. Acta *1771*, 210–227.

126. Yamaguchi, T., Matsushita, S., Motojima, K., Hirose, F., and Osumi, T. (2006). MLDP, a novel PAT family protein localized to lipid droplets and enriched in the heart, is regulated by peroxisome proliferator-activated receptor alpha. J. Biol. Chem. *281*, 14232–14240.

127. Keenan, S.N., Meex, R.C., Lo, C.Y.J., Ryan, A., Nie, S., and Montgomery, K.M. (2019). Perilipin 5 deletion in hepatocytes remodels lipid metabolism and causes hepatic insulin resistance in mice. Diabetes *68*, 543-555.

128. Wang, C., Zhao, Y., Gao, X., Li, Y., Liu, F., Zhang, L., Wu, J., Hu, P., Zhang, X., Gu, Y., Xu, Y., Wang, Z., Li, Z., Zhang, H., and Ye, J. (2015). Perilipin 5 improves hepatic lipotoxicity by inhibiting lipolysis. Hepatology *61*, 870-82.

129. Kimmel, A.R. and Sztalryd, C. (2014). Perilipin 5, a lipid droplet protein adapted to mitochondrial energy utilization. Curr. Opin. Lipidol. *25*, 110-7.

130. Hung, V., Zou, P., Rhee, H.-W., Udeshi, N.D., Cracan, V., Svinkina, T., Carr, S.A., Mootha, V.K., and Ting, A.Y. (2014) Proteomic mapping of the human mitochondrial intermembrane space in live cells via ratiometric APEX tagging. Mol. Cell *55*, 332-341.

131. Lam, S.S., Martell, J.D., Kamer, K.J., Deerinck, T.J., Ellisman, M.H., Mootha, V.K., and Ting, A.Y. (2015) Directed evolution of APEX2 for electron microscopy and proximity labeling. Nat. Methods *12*, 51-54

132. Bersuker, K., Peterson, W.H.C., To, M., Sahl, J.S., Savikhin, V., Grossman, A.E., Nomura, K.D., and Olzmann, A.J. (2018). A proximity labeling strategy provides insights into the composition and dynamics of lipid droplet proteomes. Dev. Cell *44*, 97-122.

133. Hwang, J. and Espenshade, P.J. (2016). Proximity-dependent biotin labelling in yeast using the engineered ascorbate peroxidase APEX2. Biochem. J. *473*, 2463-9.

134. Jing, J., He, L., Sun, A., Quintana, A., Ding, Y., Ma, G., Tan, P., Liang, X., Zheng, X., Chen, L., Shi, X., Zhang, S.L., Zhong, L., Huang, Y., Dong, M.Q., Walker, C.L., Hogan, P.G., Wang, Y., and Zhou, Y. (2015). Proteomic mapping of ER-PM junctions identifies STIMATE as a regulator of Ca2+ influx. Nat. Cell Biol. *17*, 1339–1347.

135. Cho, I. Adelmant, G., Lim, Y., Marto, A.J., Cho, G., and Golden, A.J. (2017). Ascorbate peroxidase proximity labeling coupled with biochemical fractionation identifies promoters of endoplasmic reticulum-mitochondrial contacts. J. Biol. Chem. *292*, 16382-16392.

136. Ahting, U., Thun, C., Hegerl, R., Typke, D., Nargang, F.E., Neupert, W., and Nussberger, S. (1999). The TOM core complex: The general protein import pore of the outer membrane of mitochondria. J. Cell Biol. *147*, 959-968.

137. Rapaport, D. (2002). Biogenesis of the mitochondrial TOM complex. Trends Biochem. Sci. *27,* 191-197.

138. Murley, A., Sarsam, R.D., Toulmay, J., Yamada, J., Prinz, W.A., and Nunnari, J. (2015). Ltc1 is an ER-localized sterol transporter and a component of ER-mitochondria and ER-vacuole contacts. J. Cell Biol. *209*, 539-548.

139. Filadi, R., Leal, N.S., Schreiner, B., Rossi, A., Dentoni, G., Pinho, M.C., Wiehager, B., Cieri, D., Calì, T., Pizzo, P., and Ankarcrona, M. (2018). TOM70 sustains cell bioenergetics by promoting IP3R3-mediated ER to mitochondria Ca2+ transfer. Current Biology *28*, 369-382.

140. Kulawiak, B., Höpker, J., Gebert, M., Guiard B., Wiedemann, N., and Gebert, N. (2013). The mitochondrial protein import machinery has multiple connections to the respiratory chain. Biochim. Biophys. Acta *1827*, 612-626.

141. Grove, T.Z., Cortajarena, A.L., and Regan, L. (2008). Ligand binding by repeat proteins: Natural and designed. Curr. Opin. Struct. Biol. *18*, 507-515.

142. Ahn, K., Szczesna-Skorupa, E., and Kemper, B. (1993). The amino-terminal 29 amino acids of cytochrome p450 2C1 are sufficient for retention in the endoplasmic reticulum. J. Biol. Chem. *268*, 18726-33.

143. Hung, V., Lam, S.S., Udeski, N.D., Svinkina, T., Guzman, G., Mootha, K.V., Carr, A.S., and Ying, A.Y. (2017). Proteomic mapping of cytosol-facing outer mitochondrial and ER membranes in living human cells by proximity biotinylation. eLife *6*, e24463.

144. Paillusson, S., Stoica, R., Gomez-Suaga, R., Lau, D.H., Mueller, S., Miller, T., and Miller, C.C. (2016). There's something wrong with my MAM; the ER-mitochondria axis and neurodegenerative diseases. Trends Neurosi. *39*, 146-157.

145. Filadi, R., Theurey, P., and Pizzo, P. (2017). The endoplasmic reticulum-mitochondria coupling in health and disease: molecules, functions and significance. Cell Calcium *62*, 1-15.

146. Bravo-Sagua, R., Torrealba, N., Paredes, F., Morales, P.E., Pennanen, C., López-Crisosto, C., Troncoso, R., Criollo, A., Chiong, M., Hill, J.A., Simmen, T., Quest, A.F., and Lavandero, S. (2014). Organelle communication: signaling crossroads between homeostasis and disease. Int. J. Biochem. Cell Biol. *50*, 55-59.

147. Hariri, H., Ugrankar, R., Liu, Y., and Henne, W.M. (2016). Inter-organelle ER-endolysosomal contact sites in metabolism and disease across evolution. Commun. Integr. Biol. *9*, e1156278.

148. ChernL.V. and Kozlov, N.M. (2005). Membrane hemifusion: crossing a chasm in two leaps. Cell *123*, 375-82.

149. Gallardo-Montejan, V.I., Sexena, G., Kusminski, C.M., Yang, C., McAfee, J.L., Hahner, L., Hoch, K., Dubinsky, W., Narkar, V.A., and Bickel, P.E. (2016). Nuclear perilipin 5 integrates lipid droplet lipolysis with PGC-1α/SIRT1-dependent transcriptional regulation of mitochondrial function. Nat. Commun. *7*, 12721.